COLLISIONLESS BEAM-RADIATION PROCESSES IN THE LABORATORY AND ASTROPHYSICS

A Dissertation

Presented to the Faculty of the Graduate School

of Cornell University

in Partial Fulfillment of the Requirements for the Degree of

Doctor of Philosophy

by

Bjoern Sebastian Schmekel

August 2005

COLLISIONLESS BEAM-RADIATION PROCESSES IN THE LABORATORY AND ASTROPHYSICS

Bjoern Sebastian Schmekel, Ph.D.

Cornell University 2005

Plasma instabilities can be encountered in many branches of physics. This work focuses on relativistic plasmas with applications in theoretical astrophysics and particle accelerator physics. Even though these fields seem to be unrelated the underlying plasma physics processes are often very similar. Two plasma instabilities - the beam-beam instability and the coherent synchrotron radiation instability - are analyzed. The former severely limits the achievable luminosity in storage rings and is related to the two-stream instability which has been proposed as a candidate for the radiation mechanism of radio pulsars. The main emphasis is on coherent synchrotron radiation which can lead to prohibitive energy losses in bunch compressors. Coherent synchrotron radiation also makes up the intense emission of radio waves by pulsars. Simple models based on the linearized Vlasov equation and relativistic magnetohydrodynamics which allow to compute detailed spectra of the emitted radiation are developed.

BIOGRAPHICAL SKETCH

Bjoern S. Schmekel was born in West Berlin on June 14th, 1977. With his parents he moved to Elmshorn (a suburb located 30km north of Hamburg) where he graduated from high school in 1997. As a high school student he was mainly interested in optimizing photomultiplier based scintillation detectors and designing high voltage power supplies for the operation thereof. While still in high school he started to work at Fermi National Accelerator Laboratory in Batavia, Illinois with Ryuji Yamada on the decays of the top quark in the 6-jet channel. He continued his work at Fermilab during his summer vacations in college. In 1997 he had to work in a hospital in Bayreuth as a contentious objector for a year. Not possessing any useful skills he had to serve in a "champagne unit", so he could enroll at the Open University in Hagen in mathematics. One year later he transferred to the University of Hamburg and received his "Vordiplom" in physics in late 1999. In 2000 he came to Cornell as a graduate student in the department of physics. He has been working on a variety of problems in theoretical physics, most notably in plasma physics (with applications in astrophysics and particle accelerator physics) and gravity. In 1998 the German National Academic Foundation (Studienstiftung des deutschen Volkes) elected him a fellow. He is also a member of the American Physical Society.

To the memory of Joe Rogers

ACKNOWLEDGEMENTS

This is a book about facts. If for some reasons you object to facts I have to ask you to close this book immediately and ask the librarian to reshelve it for you. Some people may experience severe health and mental problems when exposed to facts. I strongly recommend that those people seek a fact free environment as soon as possible - and there exist plenty.

Congratulations! You decided to keep reading. Well then, I warned you, but let me begin by thanking those who contributed to the success and to the content of my research. First of all I would like to thank the American taxpayers (represented by the National Science Foundation and my longtime sponsor - the U.S. Department of Energy) who understand the importance and the potential of fundamental research in theoretical physics. Without their financial contributions this book would not have been written. More specifically I would like to thank the Laboratory for Nuclear Studies (now called Laboratory for Elementary Particle Physics) and David Hammer from the Cornell Laboratory for Plasma Studies who graciously allocated the necessary resources to me. Thanks are also due to Ira M. Wasserman who agreed to serve as the chair of my special committee even though I had no formal qualifications as an astrophysicist whatsoever. This must have made him very suspicious and it demonstrates that there are still people who have patience and endless trust in me. Maybe he started to regret his decision, but now it is too late. Being a very stubborn character it is very hard to teach me anything, but hopefully I have learnt something. The same is of course true for Richard V.E. Lovelace with whom I did most of the calculations in parallel. His patience, knowledge and skills made working with him extremely enjoyable. Richard's vast amount of experience always convinced and reassured me that everything I did

was actually worth doing.

It is with regret that one of my teachers could not see the completion of this work. Joseph T. Roger's untimely death came as a surprise to many of us. In the obituary for Joe I wrote:

" ... I was reminded of his cheerful personality, his endless patience and of course his knowledge of physics. The former was the reason undergrads in our department used to call him "Happy Joe" (I doubt he was actually aware of this, though) ...

Unfortunately, there is not much I can do except express my sincere condolences to Joe's family once again.

I was rather fortunate to have met Georg H. Hoffstaetter who helped me finish a paper on the beam-beam interaction in storage rings which I started writing together with Joe before he was diagnosed with terminal cancer. Georg's passion and enthusiasm for particle accelerators can become contagious and it simply will not stop - even when rowing across a / the Lost Lake somewhere in Oregon during heavy snowfall.

There is a huge number of support staff that struggled with my problems and they deserve being mentioned: Lori Beyea-Powers (accounting), Cora Jackson (travel arrangements), Joyce Oliver (accounting), Rosemary French (support for teaching), Tom Shannon (IT), Chuck Jessop (licensing) and many more. There is one person though I have to list separately. Of course I am talking about Debra Hatfield. The list of services she provided me with is so long that I will not even attempt to mention all the things she has done for me. I am just stunned by Deb's ability to solve my everyday problems and I will miss her.

There is yet another person missing who deserves a lot of credit and this person is James W. York, Jr.! I have been extremely lucky and privileged to have met Jimmy. His insight into general relativity is almost impossible to match. Our private conversations about general relativity, quantum gravity and other (sometimes more trivial) aspects of life encouraged me to keep working on my ideas.

Finally, I would like to apologize. I have never really worked with other people together on a project so closely before. The problem with me is that I have my own ideas and ways of doing certain things. I feel very strongly about them and about how physics ought to be done. Ultimately, this makes me at odds with almost everybody, and I can only hope Cornell will find better graduate students than me who are easier to work with in the future.

Bjoern S. Schmekel

Ithaca, New York

July 2005

TABLE OF CONTENTS

LIST OF FIGURES

PREFACE

Plasma physics effects are ubiquitous. Most of space is made of plasma and many devices on earth (including household appliances) generate plasmas, e.g. fluorescent bulbs, klystrons in microwave ovens, electron beams in CRTs, particle accelerators or electron microscopes etc. There are two recurring main questions which arise in plasma physics: How do plasmas evolve in time and are there equilibria which are stable under the influence of small perturbations? How much energy is lost due to radiation? Even though the mentioned applications do not seem to have much in common, plasma instabilities and radiation are often caused by the same few well-known (and some not so well-known) processes. This opens up possibilities for testing astrophysical processes in the laboratory.

After covering a few basics, the beam-beam instability (a rather unpleasant instability encountered in storage rings which severely limits the achievable luminosity) is reviewed. In some aspects this instability resembles the two-stream instability which is currently considered to be responsible for the radio emission of spinning neutron stars (radio pulsars). Chapter 5 deals with the Coherent Synchrotron Radiation instability as an alternative to the two-stream instability in radio pulsars. According to the preceding paragraph it may not come as a surprise that this instability also plays a crucial role in particle accelerators. In chapter 7 a simplified approach is presented which is based on magnetohydrodynamics and the results of a computer simulation thereof can be found in chapter 6.

It is hoped that one day a gifted experimenter will exploit these similarities and come up with particle accelerator experiments which might greatly benefit the astrophysics community.

Chapter 1

Plasma Physics

1.1 Statistical Mechanics of Plasmas

In classical mechanics the trajectory of a particle $\mathbf{x}(t)$ is completely determined if the forces acting on the particle are known and if the position $\mathbf{x}_0$ and the velocity $\dot{\mathbf{x}}_0$ (or alternatively the momentum $\mathbf{p}_0$) at an arbitrary initial time are known. One needs two initial conditions because the equations of motion are second order differential equations excluding some peculiar special cases. For a huge number of particles, e.g. gas molecules in a steel cylinder, it is obviously not very practical to compute the trajectories of all those particles, and it is not even necessary. Since for all practical purposes the gas molecules are indistinguishable even for a "classical" observer one can ask instead how many particles $f(\mathbf{x}, \mathbf{p}, t)d^3xd^3p$ one could encounter at time t, position $\mathbf{x}$ and momentum $\mathbf{p}$ inside a phase space interval of size d^3xd^3p assuming the normalization

$$\int d^3x \int d^3p f(\mathbf{x}, \mathbf{p}, t) = N \tag{1.1}$$

where N is the total number of particles. Of course any other normalization is equally good. If all the forces acting on this collection of particles are known it should be possible to find an operator acting on the distribution function f which describes its time evolution. Such an "operator" does exist and the resulting equation is known as the Vlasov equation. Note that a statistical treatment based on a smooth distribution function [1] eliminates certain features known as discrete particle effects which can have a rather big impact on the distribution function.

[1] In simple models of shock formation the distribution function may tend to a discontinuous limit.

Recovering these effects is usually rather difficult but nevertheless important. In plasma physics for instance, continuous charge distributions like a rotating ring with completely uniform charge density do not radiate, i.e. even synchrotron radiation (both coherent and incoherent) is due to the discreteness of electric charge.

1.2 Vlasov Equation

Consider the following "microscopic distribution function"

$$F(\mathbf{x},\mathbf{p},t)=\sum_{j=1}^{N}\delta[\mathbf{x}-\mathbf{x}_j(t)]\delta[\mathbf{p}-\mathbf{p}_j(t)] \tag{1.2}$$

which contains all the information about each individual particle. It satisfies the following equation of motion

$$\sum_{j=1}^{N}\left\{\frac{\partial}{\partial t}+\mathbf{v}_j\cdot\frac{\partial}{\partial\mathbf{x}}+\frac{d}{dt}\mathbf{p}_j\cdot\frac{\partial}{\partial\mathbf{p}}\right\}\delta[\mathbf{x}-\mathbf{x}_j(t)]\delta[\mathbf{p}-\mathbf{p}_j(t)]=0 \tag{1.3}$$

(Klimontovich equation). In a plasma the average force exerted on a particle by all other particles (which acts like an external force) is bigger than the force exerted by the nearest neighbors. With

$$\begin{aligned}\langle F\rangle &= f\\ \langle\dot{\mathbf{x}}_j\rangle &= \mathbf{v}\\ \langle\dot{\mathbf{p}}_j\rangle &= \dot{\mathbf{p}}\ .\end{aligned} \tag{1.4}$$

averaging the Klimontovich equation gives the Vlasov equation

$$\left\{\frac{\partial}{\partial t}+\mathbf{v}\cdot\frac{\partial}{\partial\mathbf{x}}+\frac{d}{dt}\mathbf{p}\cdot\frac{\partial}{\partial\mathbf{p}}\right\}f=0\ . \tag{1.5}$$

The last equation in (1.4) is justified if binary correlations are assumed small. Thus, all discrete particle effects like binary collisions have been removed. They

can be recovered by writing Eq. (1.4) as a sum of an average (external) part and an internal part due to nearest neighbor interactions. In section 1.8 this will lead us to the Fokker-Planck equation. For astrophysical plasmas the densities are usually so low that the plasma can be assumed to be collisionless.

1.3 Solving the Vlasov Equation

For particles interacting electromagnetically one replaces $\frac{d}{dt}\mathbf{p}$ in Eq. (1.5) with the Lorentz force

$$\frac{d}{dt}\mathbf{p} = q\left(\mathbf{E} + \mathbf{v} \times \mathbf{B}\right) \tag{1.6}$$

The fields are related to the sources by the Maxwell equations

$$\nabla \cdot \mathbf{B} = 0 \tag{1.7}$$

$$\nabla \cdot \mathbf{E} = 4\pi\rho \tag{1.8}$$

$$\nabla \times \mathbf{E} = -\frac{\partial}{\partial t}\mathbf{B} \tag{1.9}$$

$$\nabla \times \mathbf{B} = 4\pi\mathbf{j} + \frac{\partial}{\partial t}\mathbf{E} \tag{1.10}$$

where

$$\rho = q\int d^3p f(\mathbf{x}, \mathbf{p}, t) \tag{1.11}$$

$$\mathbf{j} = q\int d^3p \mathbf{v} f(\mathbf{x}, \mathbf{p}, t) \tag{1.12}$$

Furthermore, velocities and momenta are related by

$$\mathbf{v} = \frac{\mathbf{p}/m}{\sqrt{1 + \mathbf{p}^2/m^2}} \tag{1.13}$$

where m is the rest mass of the particles. This system of equations is referred to as the relativistic Vlasov-Maxwell system of equations. In the purely electrostatic case

the Maxwell equations simplify to the Poisson equation and the resulting system is known as the Vlasov-Poisson system. The system of equations is nonlinear in f and is therefore hard to solve analytically. Eq. (1.12) can usually be linearized either in the non-relativistic or in the ultrarelativistic case. Finding an equilibrium distribution, i.e. a distribution with $\partial f/\partial t = 0$, simplifies the system and this task is often doable under more or less realistic assumptions. It can be shown that any distribution function f which only depends on the constants of motion represents an equilibrium. Typically, the constants of motion are the Hamiltonian and the canonical angular momentum. However, rewriting f as a function of $\mathbf{x}$ and $\mathbf{p}$ still requires solving a nonlinear equation. Once an equilibrium is found one can ask whether this equilibrium is stable to small amplitude perturbations. This question can be answered by linearizing the Vlasov equation about the equilibrium distribution. A variety of instabilities has been analyzed this way.

1.4 Solving the Linearized Vlasov Equation Using the Method of Characteristics

As was pointed out earlier the nonlinear nature of the Vlasov equation makes it hard to find analytical solutions for it, but looking for equilibrium solutions may be a successful endeavour in many simplified situations. Once an equilibrium has been found it is possible to linearize the Vlasov equation about the equilibrium. This provides valuable information about the stability properties of the found equilibrium. Writing the distribution function and the fields as a sum of the

equilibrium part and a perturbation

$$f = f^0 + \delta f$$

$$\mathbf{E} = \mathbf{E}^0 + \delta\mathbf{E}$$

$$\mathbf{B} = \mathbf{B}^0 + \delta\mathbf{B} \tag{1.14}$$

and neglecting second order terms one obtains the linearized Vlasov equation

$$\left\{ \frac{\partial}{\partial t} + \mathbf{v} \cdot \frac{\partial}{\partial \mathbf{x}} - e\left(\mathbf{E}^0 + \mathbf{v} \times \mathbf{B}^0\right) \cdot \frac{\partial}{\partial \mathbf{p}} \right\} \delta f = -e\left(\delta\mathbf{E} + \mathbf{v} \times \mathbf{B}\right) \cdot \frac{\partial}{\partial \mathbf{p}} f^0 \tag{1.15}$$

The linearized Vlasov equation can be rewritten by following a particle on an equilibrium orbit $(\mathbf{x}', \mathbf{p}')$ which passes through $(\mathbf{x}, \mathbf{p})$ at time $t' = t$. The equilibrium orbits have to satisfy the equations of motion

$$\frac{d}{dt'}\mathbf{x}'(t') = \mathbf{v}'(t') \tag{1.16}$$

$$\frac{d}{dt'}\mathbf{p}'(t') = -e\left\{\mathbf{E}^0(\mathbf{x}'(t')) + \mathbf{v}'(t') \times \mathbf{B}^0(\mathbf{x}'(t'))\right\} \tag{1.17}$$

Thus,

$$\frac{d}{dt'}\delta f(\mathbf{x}'(t'), \mathbf{p}'(t'), t') = -e\left(\delta\mathbf{E}(\mathbf{x}', t') + \mathbf{v}' \times \delta\mathbf{B}(\mathbf{x}', t')\right) \cdot \frac{\partial}{\partial \mathbf{p}'} f^0(\mathbf{x}', \mathbf{p}') \tag{1.18}$$

Integrating the last equation an expression for δf can now be obtained easily.

1.5 Mathematical Properties of the Vlasov-Maxwell System

Since it is hard to develop an intuition for how solutions of the Vlasov-Maxwell system look like for a particular set of initial data it is desirable to find theorems regarding general properties of the system. Will the solution remain smooth at all times for smooth initial data, i.e. will the momentum space carrier of the distribution function remain compact in finite time? Will the solution remain symmetric

for symmetric initial data? For the three dimensional relativistic Vlasov-Maxwell equations the answer to the first question is still unknown, but lots of incremental progress has been made. A very good review article on this subject is [1]. Glassey and Schaeffer [2] have shown that the answer is "yes" in two spatial and three momentum dimensions. The answer is important for deciding whether shocks can form spontaneously or not. The answer to the second question is "yes" for spherically symmetric initial data [1].

1.6 Magnetohydrodynamics

The distribution function f contains all the meaningful information one could possibly ask for in a statistical treatment and it is determined by either the Vlasov equation in the absence of discrete particle effects or by the Boltzmann or Fokker-Planck equation in the presence of discrete particle effects. These equations are usually difficult to solve and solving them numerically is usually not an option either - at least not in three dimensions where one would have to deal with seven-dimensional PDEs. Even though numerical solutions are being obtained by Ellison and collaborators [3] for lower dimensional problems (one spatial dimension, two dimensions in phase space) this is usually not a viable method.

The underlying problem is that the distribution function still contains a lot of information and one may wonder whether the problem simplifies if one is content with less information. For many practical purposes it may be enough to compute certain macroscopic quantities like

the number density

$$n(\mathbf{x},t) = \int f(\mathbf{x},\mathbf{p},t)d^3p \ , \tag{1.19}$$

the mean velocity

$$\mathbf{u}(\mathbf{x},t) = n^{-1} \int \mathbf{v} f(\mathbf{x},\mathbf{p},t) d^3p \ , \tag{1.20}$$

the mean momentum

$$\bar{\mathbf{p}}(\mathbf{x},t) = n^{-1} \int \mathbf{p} f(\mathbf{x},\mathbf{p},t) d^3p \ , \tag{1.21}$$

and the three dimensional stress tensor

$$\mathbf{P} = m \int (\mathbf{v}-\mathbf{u}) \otimes (\mathbf{v}-\mathbf{u}) f(\mathbf{x},\mathbf{p},t) d^3p \ , \tag{1.22}$$

i.e. moments of the distribution function. The definition of the stress tensor depends on the previous definition of the mean velocity.

More macroscopic quantities can be obtained by multiplying the integrand by an arbitrary power of momentum and / or velocity components. Starting from the Vlasov equation one can find equations determining those moments easily. Integrating Eq. (1.5) over all momenta gives the continuity equation.

$$\frac{\partial}{\partial t} n + \nabla \cdot (n\mathbf{u}) = 0 \tag{1.23}$$

Multiplying Eq. (1.5) by $\mathbf{v}$ and integrating over all momenta results in the "Euler equation"

$$\left(\frac{\partial}{\partial t} + \mathbf{u} \cdot \nabla \right) \bar{\mathbf{p}} = -n^{-1} \nabla \cdot \mathbf{P} + \mathbf{F}(\mathbf{x},t) \tag{1.24}$$

These are exactly the same equations one encounters in fluid dynamics if the higher order moments, i.e. the stress tensor, is neglected. Therefore, this approach

is known as magnetohydrodynamics (MHD). An arbitrary number of equations can be found this way. There is one serious problem, though. The moment expansion does not close in the absence of collisions, i.e. each equation will couple to the next higher moment. In fluid dynamics the equation of state can be used to close the system, but in plasma physics such an equation is generally unavailable - at least in the absence of collisions. However, under certain conditions it may be possible to guess an equation of state or it may be possible to neglect the higher order moments, e.g. for a cold plasma in the absence of a pressure gradient and heat flux. Magnetohydrodynamics will usually give good results if the frequency which is characteristic for the evolution of the distribution is much smaller than the plasma frequency and the cyclotron frequency.

1.7 Some Plasma and Fluid Instabilities

1.7.1 Negative Mass Instability

A longitudinal bunching can occur in a beam executing circular motion if the effective mass of the particles is negative, i.e. if an increase in energy leads to a decrease in angular velocity ($d\dot{\phi}/dE < 0$ where $\dot{\phi} = |\dot{\phi}|$). The energy at which the sign of $d\dot{\phi}/dE$ changes is called transition energy. In a weak focusing machine (e.g. charged particles moving perpendicular to an external magnetic field without gradient) this condition is always satisfied. Assume that due to an arbitrary initial perturbation the charge density is higher at a certain point on the circle. The electrostatic potential tries to repel particles away from the center of higher density. Particles in front of the region of higher density gain energy, but their angular velocity decreases. Similarly, particles behind the region of higher den-

sity lose energy and increase their angular velocity. Thus, neighboring particles are attracted to the region of higher density. The negative mass instability can be compensated by a sufficiently large energy spread. In the limit of zero energy spread the dispersion relation is [4]

$$1 = \frac{N r_e}{2\pi r_0} \frac{\eta}{\gamma^3} \frac{1}{(\Delta\tilde{\omega})^2} \tag{1.25}$$

where

$$\eta \equiv \frac{p}{\dot{\phi}} \frac{d\dot{\phi}}{dp} \tag{1.26}$$

and

$$\Delta\tilde{\omega} \equiv \frac{\omega - m\dot{\phi}}{m\dot{\phi}} \tag{1.27}$$

N is the number of electrons, r_0 is the radius of the orbit, r_e is the classical electron radius, and the azimuthal mode number is denoted by m. Classical references are [5, 6, 4].

1.7.2 Rayleigh-Taylor Instability

The Rayleigh Taylor instability is a fluid instability which can develop if a less dense fluid with density ρ_1 propagates in a denser fluid with density ρ_2. Clumps of gas observed in supernova remnants are often due to this instability.

1.7.3 Kelvin-Helmholtz Instability

The Kelvin-Helmholtz instability is a non-relativistic fluid instability which can form at the interface of two flows with different velocities u_1 and u_2. The ubiquitous water waves caused by wind blowing over the surface of a pond are a typical

example. The Kelvin-Helmholtz instability may also be important to understand the observed patterns of astrophysical jets surrounded by the interstellar medium.

The complex frequency ω of a perturbation in a system unstable to both the Rayleigh-Taylor instability and the Kelvin-Helmholtz instability is given by [7]

$$\frac{\omega}{k} = \frac{\rho_1 u_1 + \rho_2 u_2}{\rho_1 + \rho_2} \pm \sqrt{\frac{g}{k}\left(\frac{\rho_1 - \rho_2}{\rho_1 + \rho_2}\right) - \frac{\rho_1 \rho_2 (u_1 - u_2)^2}{(\rho_1 + \rho_2)^2}} \tag{1.28}$$

where k is the wavenumber of the perturbation and g is the gravitational acceleration.

1.7.4 Diocotron Instability

The Diocotron instability is ubiquitous in the circular motion of a low density non-neutral plasma with $d\dot{\phi}/dr \neq 0$ and can be found in common microwave generating devices. This electrostatic instability resembles the Kelvin-Helmholtz instability in the sense that it forms in the presence of shear. For equilibrium configurations with $\partial/\partial z = 0$ a sufficient condition for stability is that the number density $n(r)$ is a monotonically decreasing function, i.e. the maximum number density occurs at $r = 0$.

1.7.5 Cyclotron Maser Instability

A relativistic beam moving along a guiding magnetic field may be subject to the cyclotron maser instability. Unlike the classical Diocotron or the negative mass instability it is a transverse electromagnetic instability which is capable of producing coherent electromagnetic waves. The instability is driven by an inverted population in the transverse (i.e. parallel to the magnetic field) momentum distribution, i.e. the momentum distribution is sharp and its mean is non-zero. The cyclotron

maser instability is exploited in microwave generating devices.

1.7.6 Two-stream Instability

The two-stream instability is an electrostatic instability which occurs for a plasma consisting of two (or more streams) of (not necessarily the same species of) particles with different velocities. Its development requires a region in phase space with $\partial f/\partial p > 0$ and the momentum of the particles satisfying the latter inequality have to be large compared with the momenta of the remaining particles. This instability is of importance for the understanding of problems associated with the solar wind. In particle accelerators secondary emission of electrons from the beam pipe may provide a background of electrons which can trigger a two-stream instability.

1.8 The Fokker-Planck equation

The averaging employed in section 1.2 was rather crude and removed all discrete particle effects. In this section it is attempted to recover the effect of statistical processes like radiation damping and quantum excitation occurring at random times t_i. Instead of Eqs. (1.4) one now uses

$$\dot{x} = g(x,p,t) + \sum_i \Delta x_i \delta(t - t_i) \tag{1.29}$$

$$\dot{p} = h(x,p,t) + \sum_i \Delta p_i \delta(t - t_i) \tag{1.30}$$

The probability for the occurrence of a perturbation in momentum space with Δx_i and Δp_i is given by the probability densities $P_x(\Delta x_i)$ and $P_p(\Delta p_i)$, respectively. P_x and P_p are taken to be normalized to unity and symmetric in their

arguments. Without the former condition the distribution function would not remain normalized. After a timestep Δt the phase space element $\Delta x \Delta p$ changes by the factor

$$1 + \left(\frac{\partial g}{\partial x} + \frac{\partial h}{\partial p} \right) \Delta t \tag{1.31}$$

as can be seen by expanding the evolution of $\Delta x \Delta p$ to first order in Δt using Eq. (1.29) and (1.30). Assuming the number of particles is conserved one obtains

$$f(x + g\Delta t, p + h\Delta t, t + \Delta t)\Delta x \Delta p \left[1 + \left(\frac{\partial g}{\partial x} + \frac{\partial h}{\partial p} \right) \Delta t \right] =$$
$$\Delta x \Delta p \int_{-\infty}^{\infty} \int_{-\infty}^{\infty} d(\Delta x) d(\Delta p) P_x(\Delta x) P_p(\Delta p) f(x - \Delta x, p - \Delta p, t) \tag{1.32}$$

Expanding the distribution function inside the integral to second order in Δx and Δp allows one to evaluate the integral. Making use of the properties of P_x and P_p mentioned above

$$\frac{\partial f}{\partial t} + g \frac{\partial f}{\partial x} + h \frac{\partial f}{\partial p} - \left(\frac{\partial g}{\partial x} + \frac{\partial h}{\partial p} \right) f + \frac{1}{2} \Xi_x \frac{\partial^2 f}{\partial x^2} + \frac{1}{2} \Xi_p \frac{\partial^2 f}{\partial p^2} \tag{1.33}$$

where the coefficients Ξ_x and Ξ_p are related to the second order moments of P_x and P_p, respectively. Eq. (1.33) is known as the Fokker-Planck equation. It describes the evolution of a plasma under the additional influences of radiation damping due to incoherent synchrotron radiation (in this case the parenthesis in Eq. (1.33) differs from unity) and quantum excitation due to the statistical nature of the radiation process (the plasma emits "discrete" photons). The former tends to increase the phase space density whereas the latter tends to decrease it. Setting the parenthesis to unity and neglecting the excitation coefficients Ξ_x and Ξ_p the Vlasov equation is recovered.

1.9 A Simple Solution of the Fokker-Planck Equation in Beam Physics

Since radiation damping and quantum excitation counteract each other equilibria may exist, i.e. distribution functions with $\partial f/\partial t = 0$. In action angle variables (cf. §2.4) one can find the following ϕ-independent equilibrium

$$f = \frac{1}{2\pi\epsilon} e^{-\frac{J}{\epsilon}} \tag{1.34}$$

Beams whose equilibrium distribution is given by Eq. (1.34) are called Gaussian beams. They can be encountered in electron-positron rings with significant synchrotron radiation.

Chapter 2

Physics of Particle Accelerators

2.1 Applications and Limitations

Particle accelerators have become an invaluable tool for high energy physics experiments. Due to the increasing complexity of such machines particle accelerators themselves have become the subject of detailed theoretical studies. Current machines can reach center of mass energies of up to 2 TeV (Tevatron / Fermilab, as of 2001) and luminosities of up to 6350 pb^{-1} per year (CESR / Cornell, as of 2000). Such parameters give rise to all kinds of instabilities. One can divide accelerators into circular and linear machines. The best known linear accelerator (LINAC) is probably the Cathode Ray Tube which accelerates electrons emitted from a filament by a large electrical potential difference between the filament and a plate with a hole in it. Due to the large potential differences needed for a high energy beam such accelerators become technically unfeasible beyond 10MV. In a Wideroe LINAC alternating current instead of direct current is used to accelerate the particles. Charged particles travel through an array of conducting tubes with alternating polarity. Negatively charged particles in a gap between two tubes which leave a tube at negative potential are attracted by the next tube at positive potential. When the AC source reverses the polarity the particles are inside a tube and are shielded from the fields exerted by neighbouring tubes. To account for the increasing velocity of the particles the tubes have to increase in length. Linear accelerators like the proposed Linear Collider tend to be rather long if high energies are desired. In a synchrotron the particles execute circular motion and can pass the accelerating structure multiple times before reaching the desired energy and

being injected into a storage ring, for instance. The increasing energy of particles passing through the accelerating structure can be taken into account by adjusting the frequency of the voltage applied to the structure. As the name suggests the purpose of a storage ring is to store the accelerated particles. Usually there is a rotating and a counter-rotating beam consisting of particles and antiparticles, respectively [1]. At the interaction point (there may be multiple ones) the beams cross each other and colliding particles may annihilate and produce new particles which can be detected by a huge detector surrounding the interacting point. However, the probability for such an event to happen is small and huge amounts of energy would be wasted if the remaining particles were just dumped. The idea of the storage ring is to keep the particles circulating in the ring (possibly for many hours) until they finally collide. There are two main problems with circular machines, though. Accelerated charges (in this case the acceleration stems from forcing the particles onto a circular orbit) emit synchrotron radiation. The energy loss due to synchrotron radiation can make the operation of such machines prohibitive at high energies. At ultra-relativistic energies the radiated power is given by

$$P_\gamma = \frac{c}{2\pi} C_\gamma \frac{E^4}{R} \tag{2.1}$$

where C_γ is Sand's radiation constant for electrons

$$C_\gamma = \frac{4\pi}{3} \frac{r_c}{(m_e c^2)^3} = 8.8575 \cdot 10^{-5} \mathrm{mGeV}^{-3} \ , \tag{2.2}$$

r_c is the classical radius of the electron, R is the radius of the ring and E is the energy of the electron. Thus, for high energies very large radii are needed which makes accelerators expensive to build. Even if the energy loss is not a concern the

[1] The never-completed SSC was supposed to collide protons onto protons (instead of antiprotons)

highest achievable energy is limited by the magnet technology. Currently, the highest fields are provided by superconducting magnets, but superconductivity breaks down at sufficiently high magnetic field strengths. The current record for a continuous field is 45.1 Tesla measured at the National High Magnetic Field Laboratory at Florida State University [8]. The simplest conceivable circular accelerators consists only of dipole magnets which bend the beam and two plates with a potential difference which accelerate the beam. Such an accelerator is known as a weak-focusing machine. Its drawback is the beam size which increases with increasing radius. Bigger and bigger machines were built until the apertures of the magnets became prohibitively big and expensive to produce.

2.2 Strong Focusing

The beam size was drastically reduced once strong-focusing machines were invented. These machines contain quadrupole magnets with alternating gradients (in addition to the dipole magnets). Therefore, the beam size and the force due to the quadrupole magnets depends on the position s in the ring which is a number between zero and the circumference $2\pi R$ of the ring. The focusing force in the horizontal and vertical plane, respectively, is

$$x'' = -K_x(s)x \qquad y'' = -K_y(s)y \tag{2.3}$$

with

$$\begin{aligned} K_x(s) &= \frac{1}{R^2} + \frac{1}{B_{0y}R}\frac{\partial B_y}{\partial x} \\ K_y(s) &= -\frac{1}{B_{0x}R}\frac{\partial B_x}{\partial y} \end{aligned} \tag{2.4}$$

where x and y are the horizontal and vertical displacement from the design orbit, respectively. Derivatives with respect to s are denoted by a prime. Let us focus

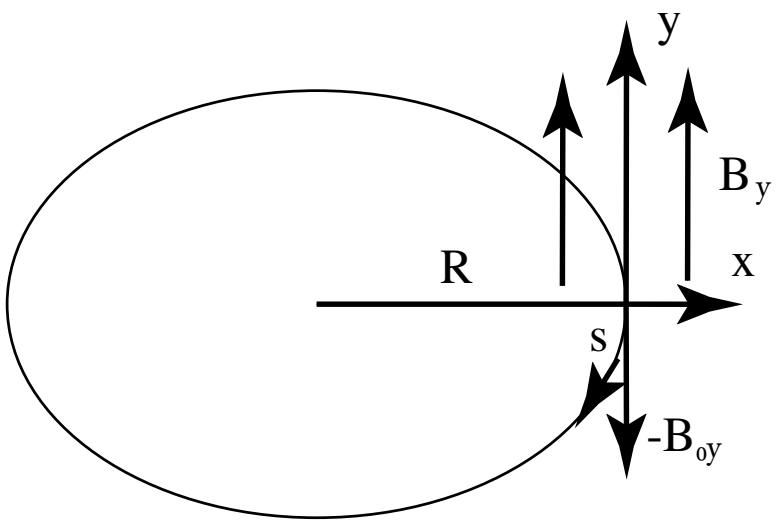

Figure 2.1: Geometry of the strong focusing machine

on the equation for the horizontal motion. A solution which satisfies the initial conditions $x(0) = x_0$, $x'(0) = x_0'$, $w(0) = w_0$, $w'(0) = w_0'$ and $\psi(0) = \psi_0$ is given by [9, 10]

$$x = \left[\left(w_0' \sin\psi_0 + w_0^{-1}\cos\psi_0\right) x_0 - w_0 x_0' \sin\psi_0\right] w(s)\cos\psi(s) + \left[-\left(w_0' \cos\psi_0 - w_0^{-1}\sin\psi_0\right) x_0 + x_0' w_0 \cos\psi_0\right] w(s)\sin\psi(s) \tag{2.5}$$

where the width $w(s)$ of the beam is determined by the envelope equation

$$w(s)'' + K(s)w(s) + \frac{1}{w(s)^3} = 0\ . \tag{2.6}$$

Furthermore,

$$\psi'(s) = w(s)^{-2}\ . \tag{2.7}$$

Individual particles oscillate ("betatron oscillations") about the design trajectory ν times, but all particle orbits are contained in the "envelope" whose width is given by $w(s)$. The w^{-3} term in Eq. (2.6) acts like a "centrifugal barrier" and gives the

beam envelope a non-zero width. ν is called the (machine) tune which is defined as

$$\nu \equiv \frac{1}{2\pi} \oint \beta(s) K(s) ds \tag{2.8}$$

where

$$\beta(s) = w^2(s) \tag{2.9}$$

is called the betatron function and $\oint$ denotes the integration from zero to $2\pi R$.

2.3 Weak Focusing

In the case of weak focusing, i.e. $K(s) = K$, the above equations simplify dramatically. One obtains

$$K = \beta^{-2} \qquad \nu = 1 \ , \tag{2.10}$$

i.e. even in the absence of quadrupole magnets the beam executes one betatron oscillation per revolution.

2.4 Emittance

The forces exerted by dipoles, quadrupole and higher order magnets which may be needed to correct for certain "optical errors" are conservative, i.e. the phase space density occupied by the particles in a beam is constant. The phase space area in (x, x') space is $\pi\epsilon$ where ϵ is called the emittance. Rewriting Eq. (2.5) as

$$x(s) = \sqrt{\epsilon \beta(s)} \cos \mu_0 \tag{2.11}$$

the emittance is determined by

$$\epsilon = \gamma_0 x_0^2 + 2\alpha_0 x_0 x_0' + \beta_0 {x_0'}^2 \tag{2.12}$$

where

$$\alpha = -\frac{1}{2}\beta' \tag{2.13}$$

$$\gamma = \beta^{-1}(1+\alpha^2) \tag{2.14}$$

$$\mu = \psi - \psi_0 \tag{2.15}$$

Similarly, for $x'(s)$

$$x'(s) = \sqrt{\frac{\epsilon}{\beta}}\,(\sin\mu_0 - \alpha\cos\mu_0) \tag{2.16}$$

Instead of using x and x' to describe the motion of a particle trajectory it is very often advantageous to use the so-called "action angle variables" ψ and $J = \epsilon/2$ because the latter is a constant of motion if the system is conservative. Note that particles in an accelerator are subject to many non-conservative forces like synchrotron radiation damping and acceleration.

2.5 Beam-Beam Interaction

All the limitations mentioned in section 2.1 are well known, but there is a myriad of less obvious issues that arise from the collective behavior of the particles which interact electromagnetically among themselves. The most severe limit on the achievable luminosity is due to the beam-beam interaction. If two oppositely charged beams which are slightly off-axis collide head-on the rotating beam is deflected by the electromagnetic field of the counter-rotating beam and vice versa. The beam-beam force is highly non-linear. Its presence causes a tune shift ξ at the interaction point. It is customary to estimate ξ using the linear part of the beam-beam force. ξ is proportional to the number density of the beam and therefore ξ is frequently used to parametrize the strength of a beam. In e^+e^- colliders

the observed beam-beam limit is in the range $0.02 \leq \xi \leq 0.1$ [11, 12]. A further increase in ξ increases the vertical emittance and leads to particle loss. Attempts to cancel the beam-beam force have failed so far. In the DCI experiment at SAL, Orsay, France, pairs of electron and positron beams were made to collide, i.e. both beams had zero net charge [13]. The result was disappointing. No significant improvement of the beam-beam limit was observed. This outcome was explained by Derbenev in terms of a collective instability of the four-beam system [14]. Therefore, it is reasonable to assume that a collective instability is responsible for the beam-beam instability in the two-beam system as well. Indeed, collective oscillations are seen in computer simulations [14, 15, 16]. The linearized Vlasov equation has been used to study the stability of colliding beams [14, 15, 16]. In [16] Chao and Ruth analyzed the stability properties of beams that are confined to motion in the vertical direction ("flat beams"). They perturbed a "water-bag" equilibrium which has a uniform density within an ellipse in the phase-space (y, y'). However, electron and positron beams tend to have a "Gaussian" distribution (cf. section 1.9). Very roughly speaking there are more particles in the inner region of the ellipse than in the outer region. In chapter 4 the stability properties of an electron beam colliding head-on with a positron beam are investigated. They beams are assumed to be flat and have a "Gaussian" equilibrium distribution. Both angular and radial modes are considered. Radial modes are modes which change the size of the ellipse. It is found that the radial modes have a profound influence on the stability of the system.

2.6 Coherent Synchrotron Radiation

The beam-beam interaction is ubiquitous in storage rings when beams collide, but it is by no means the only significant instability. More recently an instability due to coherent synchrotron radiation (CSR) is being thoroughly investigated which has been identified as a potential problem for the design of the proposed linear collider. Since the particles in the beams have only one chance to collide one would like to decrease their emittances as much as possible in order to achieve high luminosity. Such low emittance beams can only be produced in damping rings where the emittance is reduced by emitting synchrotron radiation. The linear collider needs very short bunches to operate, but beams in a damping rings are subject to other instabilities if their bunch length is too short. The solution is to reduce the bunch length in a device known as a bunch compressor before the beam is injected into the linear collider. Bunch compressors consist of an accelerating section and an arc section. In the arc the beam emits synchrotron radiation whose wavelength may be close to the bunch length. In this scenario the electromagnetic waves can modulate the beam in such a way that the bunches are equidistant. The radiation from individual bunches can now interfere constructively and the incoherent radiation becomes coherent. For coherent radiation the total radiated power scales as N^2 instead of N where N is the number of particles. The beam would lose all its energy almost instantly. Therefore, it is important to know under which operating conditions one can avoid this effect. CSR has been observed already in a couple of accelerator labs [17, 18]. In chapter 5 a simple model of a collisionless, relativistic, finite-strength, cylindrical layer of charged particles is presented which is capable of emitting coherent radiation. The particles interact with their retarded electromagnetic self-fields in a way that allows them to clump together. Including

the radial dynamics is difficult, and a small energy spread (which translates into a small non-zero thickness of the rotating layer) is one of the main requirements. It is shown that the betatron oscillations can lead to a significant decoherence which is responsible for the emission of a very characteristic spectrum. The stability properties are analyzed by solving the linearized Vlasov-Maxwell system of equations. The treatment resembles work by Uhm, Davidson and Petillo [19] who examined the stability of a thin relativistic electron ring. However, their interest is in the negative mass instability and their approximations are not suitable for electromagnetic effects like CSR. A simpler model in which all particles were constrained to move on a circle with fixed radius was presented in 1971 by Goldreich and Keeley [20]. In this model the particles initially move at constant speed, but they can gain or lose energy by interacting with the azimuthal component of the electric field. However, no mechanism for fixing the radial degree of freedom is provided. It is unclear whether (or under which conditions) the radial degree of freedom can be neglected. If, for instance, the circular motion is due to an external magnetic field without gradient ("weak focusing") an increase in energy translates into an increase of the orbit radius whereas the velocity remains almost constant in the case of ultra-relativistic motion. This may not be very favorable for the development of a bunching instability. A more realistic model was investigated by Heifets and Stupakov. In [21, 22] they analyze the stability of electrons executing circular motion. The radius of the individual particle orbit is determined by the energy of that particle, i.e. the radial motion and the relative longitudinal motion are coupled such that the problem has effectively only one degree of freedom. It is not entirely obvious under which conditions such an approach is valid. The model was extended by Byrd [23] to include the effect of a conducting beam pipe which

can serve as a cut-off of the allowed wavelengths. A conducting beam pipe can severely attenuate the CSR instability.

Chapter 3

Physics of Rotating Neutron Stars

3.1 Stellar Evolution

A living star is supported against its own weight by the pressure it builds up as a result of heat generated in fusion reactions inside the star. A young star generates its heat from the conversion of hydrogen into helium by nuclear fusion. Once the supply of hydrogen is exhausted in the core the star starts to shrink increasing its temperature. This allows the star to burn the remaining hydrogen in its shell. One has to distinguish two cases.

3.1.1 $M < 8M_{\odot}$

In the red giant stage the shell expands leaving behind the core which continues to shrink until a white dwarf is formed. Fluid instabilities destroy the shell turning it into a nebula. This stage can be regarded as the end point of the evolution of a light star. The white dwarf continues to emit thermal radiation until it has completely cooled down.

3.1.2 $M > 8M_{\odot}$

Heavier stars become hotter during contraction triggering fusion reactions of heavier elements. Fusion stops once all material in the core has been converted into iron [1]. Like in the previous case burning continues in the outer shell. Instead of a red giant a super red giant is formed with a radius bigger than 100 million kilome-

[1]The element with the highest binding energy is ^{62}Ni and not ^{56}Fe. Cf. an article by Fewell [24] on why iron is more abundant than nickel.

ters. The core is supported by the degeneracy pressure of non-relativistic electrons and - as the star continues to contract - the electrons become relativistic and the increase in pressure slows down. Furthermore, at relativistic electron energies the protons can capture electrons which turns them into neutrons, thus reducing the degeneracy pressure of degenerate electrons. Photodissociation of iron leads to a polytropic index smaller than 4/3 rendering the core unstable to collapse [25]. The iron core implodes which generates a shock wave propagating outward. The shock wave comes to a stop before it can leave the super red giant. However, under certain conditions a bubble can form between the core and the shock front. A small fraction of the binding energy of the star is used to eject all the material of the star except the core in a supernova explosion. Its mechanism is complicated, but it is believed to be caused by convection and neutrinos transporting energy. The remnant is called a neutron star because it is only supported by the degeneracy pressure of degenerate neutrons. Sometimes the conditions under which a supernova explosion takes place are not satisfied or an insufficient amount of matter is released. In this case even the degenerate neutrons cannot prevent the star from collapsing even further and a black hole is formed.

3.2 Properties of Rotating Neutron Stars

The radius of a typical neutron star is in the order of $R \sim 10$ km while its mass is in the order of $M_\odot$. In addition to a strong gravitational field on their surface they also posses a strong magnetic field which can be as strong as 10^8 Tesla. The field can be described by a magnetic dipole to a good approximation (cf. section 3.3). Like on earth the magnetic field may be created by the dynamo effect. Since charged particles are necessary to create a magnetic field a neutron

star cannot consist entirely of neutrons. Indeed, it is believed that a neutron star contains a small fraction of electrons and protons in its core [26]. Neutron stars born with a large amount of angular momentum are capable of emitting intense electromagnetic radiation in the radio frequency range. Such radio pulsars have rotation periods ranging from 1s down to 33ms for the Crab pulsar. In general the axis of rotation does not coincide with the alignment of the magnetic dipole moment. Therefore, the radiation sweeps out a cone about the axis of rotation. Every time the observer's line of sight coincides with the magnetic axis a pulse of intense electromagnetic radiation is observed with a period equal to the period of the rotation of the star $T = 2\pi/\Omega$ (lighthouse model).

The discovery of millisecond pulsars ruled out white dwarfs as possible candidates for radio pulsars as can be seen from the following simple argument. For a stable star the centrifugal force exerted on particles at the surface of the star cannot exceed the force due to gravity. Thus,

$$\Omega^2 R \leq GMR^{-2} \tag{3.1}$$

White dwarfs are not sufficiently dense to satisfy the inequality above.

Due to its large mass and angular momentum the star posses a huge amount of kinetic energy which powers the emission of the intense radiation. Therefore, as the pulsar continues to lose energy its angular velocity has to decrease ("spin-down"). The details of the process converting kinetic energy to electromagnetic radiation are not completely understood yet. However, an argument based on conservation of energy suffices to relate some fundamental parameters of a pulsar. Assuming the energy loss is due to magnetic dipole radiation

$$I\Omega\dot{\Omega} = \frac{dW}{dt} = P = \frac{1}{3}\Omega^4 R^6 B_0^2 \ , \tag{3.2}$$

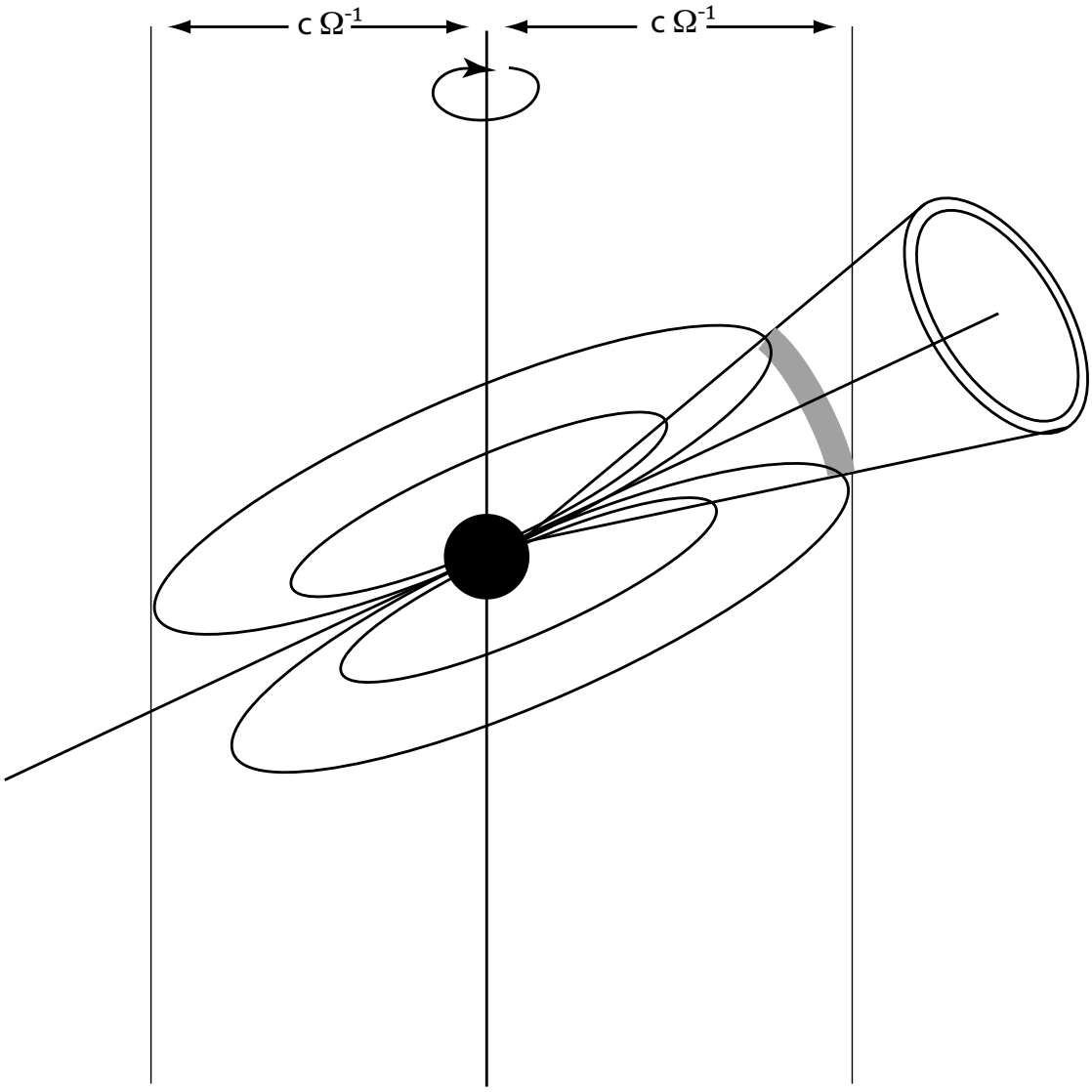

Figure 3.1: Radio pulsars are spinning neutron stars with strong magnetic fields. At the magnetic poles their radiation follows the magnetic field lines. Since the field lines and the axis of rotation are misaligned the radiation sweeps out a cone. The region in which the radiation is believed to be generated is shown in gray. A similar cone could be drawn on the other side of the star.

i.e. measuring the spin-down $\dot{\Omega}$ and equating the energy lost by a magnetic dipole to the loss of kinetic energy one can solve for the normal component B_0 of the magnetic field at the magnetic pole if the angular velocity Ω, the radius R and the moment of inertia I are given. The spin-down can be measured very precisely.

3.3 Braking Index

Eq. (3.2) relates Ω to $\dot{\Omega}$

$$\dot{\Omega} \propto \Omega^n \tag{3.3}$$

where the so-called braking index is denoted by n. According to Eq. (3.2) the braking index is 3 if the emission is due to dipole radiation. Deviations from $n = 3$ would suggest that the simple model leading to Eq. (3.2) is not completely accurate. Indeed, braking indices as low as $n = 1.4$ have been measured. The determination of the braking index is very simple if $\ddot{\Omega}$ is known. Differentiation of Eq. (3.3) and making use of the same equation again to eliminate the proportionality constant one obtains

$$n = \frac{\ddot{\Omega}\Omega}{\dot{\Omega}^2} \tag{3.4}$$

3.4 Some Fundamental Parameters of the Crab Pulsar

We start by estimating how many charged particles could be present in the magnetosphere. In a model by Goldreich and Julian [27] the axis of rotation is assumed to coincide with the orientation of the magnetic dipole moment. Assuming the neutron star and its surrounding magnetosphere along the magnetic field lines are perfect conductors one obtains

$$\mathbf{E} + (\mathbf{\Omega} \times \mathbf{r}) \times \mathbf{B} = 0 \tag{3.5}$$

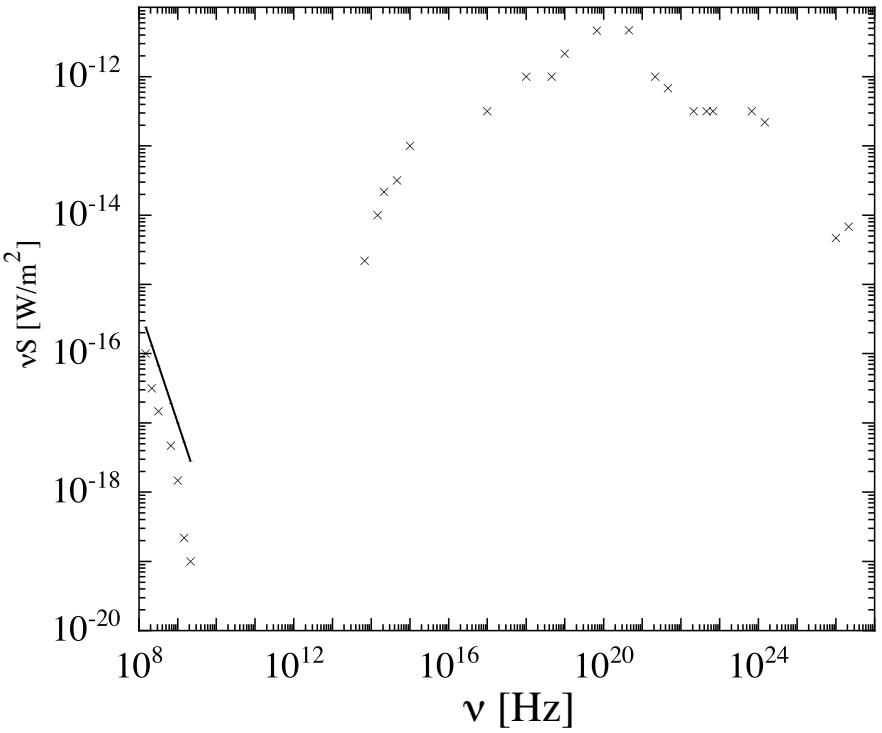

Figure 3.2: The observed spectrum of the Crab pulsar extends from the radio regime to frequencies up to 10^{27}Hz [28].The straight line in the radio regime is proportional to $\nu^{-5/3}$

Thus, the magnetosphere must have the Goldreich-Julian charge density

$$n_{GJ} = (4\pi)^{-1}\nabla \cdot \mathbf{E} = \frac{\mathbf{\Omega} \cdot \mathbf{B}}{2\pi e} \sim 10^{11} cm^{-3}(B/10^{12}G)(R/r)^3[T/1s]^{-1} \qquad (3.6)$$

at radius $r > R$ where $T = 2\pi/|\mathbf{\Omega}|$.

The energy loss can be determined from Eq. (3.2) by measuring Ω and $\dot{\Omega}$.

$$P = 4\pi^2 I\dot{T}/T^3 \qquad (3.7)$$

It is in the order of 10^{39}erg s^{-1} for the Crab pulsar where [29]

$$M \sim 10^{31}\text{kg} \qquad R \sim 10^{4}\text{m} \qquad I \sim 10^{33}\text{kg m}^2$$
$$T = 33\text{ms} \quad \dot{T} = 4.22 \cdot 10^{-13} \quad B = 5.2 \cdot 10^{12} G \tag{3.8}$$

The highest detected frequency of the Crab pulsar is in the order of 10^{27}Hz, but the spectrum in Fig. 3.2 starts to drop off significantly at 10^{24}Hz.

Integrating the Goldreich-Julian charge density from the surface of the surface to the velocity of light cylinder (Fig. 3.3) gives

$$\begin{aligned} N &= 10^{11} cm^{-3} (B/10^{12}G)[T/1s]^{-1} R^3 \int_R^{c\Omega^{-1}} 4\pi \cdot r^2 dr r^{-3} \\ &= 10^{11} cm^{-3} (B/10^{12}G)[T/1s]^{-1} \cdot 4\pi R^3 \ln \frac{cT}{2\pi R} \qquad (3.9) \\ &\sim 10^{33} \ . \qquad (3.10) \end{aligned}$$

3.5 Emission Mechanism

Obviously, one would like to have a better understanding of how the rotational energy is converted into radiation and in particular how the radiation mechanism works. In this paragraph it is shown that incoherent synchrotron radiation cannot account for the observed brightness of the radio signal. The synchrotron radiation is partly reabsorbed by the inverse Compton effect (cf. section 3.11). The ratio of the brightness temperature (cf. section 5.10) due to inverse Compton radiation to the brightness temperature due to synchrotron radiation is given by [30]

$$L_{iC}/L_s \sim \frac{1}{2}(T_{max}/10^{12}\text{K})^5 (f_c/1\text{MHz}) \left[1 + \frac{1}{2}(T_{max}/10^{12}\text{K})^5 (f_c/1\text{MHz})\right] \tag{3.11}$$

For $T_{max} < 10^{11}$K and an upper cutoff frequency $f_c \sim 10^5$MHz in the radio regime this ratio is smaller than one, but for $T_{max} > 10^{12}$K

$$L_{iC}/L_s \sim (T_{max}/10^{11}\mathrm{K})^{10} \tag{3.12}$$

Therefore, brightness temperatures exceeding 10^{12}K are impossible to achieve with incoherent synchrotron radiation ($P \propto N$) and some sort of coherent radiation mechanism ($P \propto N^2$) is required. The brightness temperature of the Crab pulsar is roughly 10^{31}K.

3.6 Secondary Electron-Positron Plasma

The strong magnetic field forces the electrons to move parallel to the field. Since magnetic fields cannot do any work a strong electric field with $\mathbf{E}\cdot\mathbf{B} \neq 0$ is necessary. Because Eq. (3.5) implies $\mathbf{E}\cdot\mathbf{B} = 0$ the accelerating field must be due to a deviation from the Goldreich-Julian charge density [31]. Several effects accomplishing this have been suggested, e.g. general relativistic effects [32] or the bending of the magnetic field lines [33].

Some photons emitted by the accelerated charges create secondary electron-positron pairs which screen the electric field except in compact regions called "gaps". The particles are accelerated in those gaps. The plasma consisting of secondary particles has a distribution which differs significantly from the distribution of primary particles. Instabilities of the primary plasma lead to the coherent emission of radio waves whereas instabilities of the secondary plasma lead to a non-thermal emission in the high frequency regime from IR to γ-rays. This work focuses on instabilities found in the primary plasma (which may be induced by the interaction with the secondary plasma).

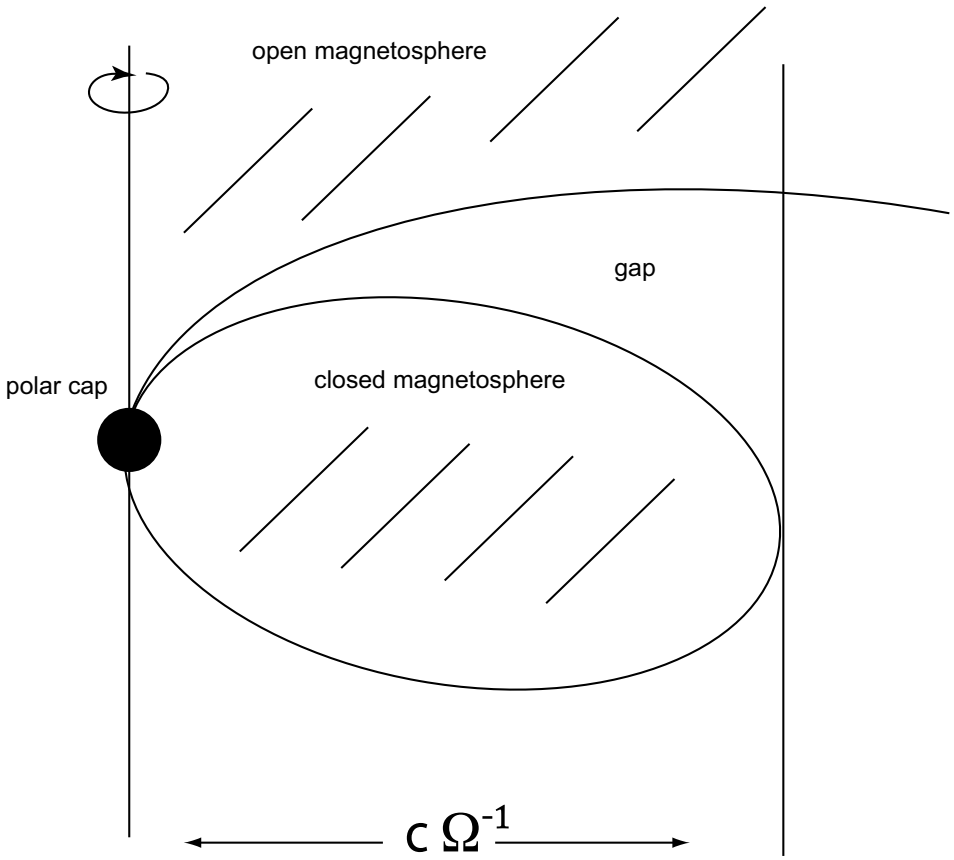

Figure 3.3: Geometry of the regions surrounding a neutron star. The closed magnetosphere is followed by a gap in which strong electric fields accelerate charged particles. The star is surrounded by a co-rotating magnetosphere which cannot extend beyond the velocity-of-light cylinder, i.e. the radius at which the velocity of the particles would exceed the speed of light at angular velocity Ω where Ω is the angular velocity of the star (and the co-rotating magnetosphere).

3.7 Free Electron Maser Emission

Several mechanism were proposed to explain the emission of electromagnetic waves by the primary plasma. This paragraph deals with the so-called free electron maser emission. It requires a strongly modulated electric field parallel to the magnetic field. How such an electric field could be generated in space is unknown. Rowe [34] found that such a set-up is capable of self-amplification if the distribution is inversely populated, i.e. there is a region in phase space where the particle density increases as the energy increases. The electric field accelerates the particles which therefore emit electromagnetic radiation. This radiation then modulates the beam until bunches of particles radiate in phase (Actual free electron lasers which are built in labs use a magnetic field from an undulator instead of an initially modulated electric field. The undulator causes the particles to move on a helical path which then emit synchrotron radiation.). Unfortunately, the growth rate as a function of energy decreases too rapidly to explain the high brightness temperatures that are observed.

3.8 Two-stream Instability

Particles of the secondary plasma might interact with those from the primary plasma and (due to their very different distributions in phase space) trigger a two-stream instability. All conditions for the development of a two-stream instability are met. However, detailed calculations [35] show that the expected growth rates are too low. Again, the high Lorentz factors and the low density of the involved beams are the offending parameters. Another problem is posed by the inability of the waves generated by the two-stream instability to escape from the neutron

star, i.e. they have to be converted into different waves which can actually escape. This may involve some yet unknown non-linear effects. Despite these shortcomings the two-stream instability is considered to be the most promising candidate for an explanation of the observed brightness temperatures by many authors [36]. Two-stream instabilities due to electrons streaming against positrons in the secondary plasma were also considered by several authors, e.g [37]. Again the reader is referred to the review article by Usov [36].

3.9 Curvature Radiation

Curvature radiation was the first emission process which was studied in the context of radio pulsars. The radiation is due to the synchrotron radiation emitted by accelerated charged particles where the acceleration originates from forcing the particles to move along an arc. Since the observed radio waves are polarized it is natural to attribute them to synchrotron radiation. The coherence was explained by a maser-like mechanism by many authors. Most approaches based on maser curvature emission ran into trouble because the conditions for a self-amplifying maser instability were not satisfied. On the other hand non maser-like mechanisms which started out with a bunched distribution were heavily criticised because it was unclear how the bunches could form and because of a lack of detailed models which took the velocity spread of the distribution into account.

In chapter 5 one such model is presented. It is assumed that the radio emission is due to coherent curvature radiation which is produced by small bunches of particles whose radiation interferes constructively. For this approach the linear stability properties of a cylindrical, collisionless, relativistic layer made of charged particles whose axis of rotation is aligned with an external magnetic field are

analyzed using the linearized Vlasov-Maxwell system. The particles are allowed to interact with their own electromagnetic self-fields. The bunches are seeded by arbitrarily small initial perturbations which grow exponentially in time until the perturbations saturate. Knowledge of the saturation amplitude is a prerequisite for calculating the intensity of the electromagnetic radiation and it can be estimated considering the trapping of particles in the "potential well of the wave".

3.10 Beaming

If an isotropic emitter moves at relativistic speed an observer at rest observes the radiation as if it was radiated into a narrow cone pointing into the forward direction. Its opening angle is approximately Γ^{-1} where Γ is the Lorentz factor of the moving source. This effectively increases the power measured by an observer who can sample only a small solid angle.

$$\Delta\Omega' = \Gamma^2 \Delta\Omega \tag{3.13}$$

where a prime denotes quantities measured by the observer.

Furthermore, the emitted frequency undergoes a relativistic Doppler shift. For a source moving towards the observer [38]

$$\frac{\omega'}{\omega} = \sqrt{\frac{1+\beta}{1-\beta}} \,. \tag{3.14}$$

3.11 Inverse Compton Radiation

It has been suggested that the radiation of the Crab pulsar is caused by the inverse Compton effect. Low energy photons can be scattered by high energy electrons

transferring energy from the electron to the photon. No uniform magnetic field is needed to initiate this process. However, the cross section for sufficiently high energy transfers is too low to account for the observed brightness temperature ruling out this radiation mechanism.

3.12 Self-absorption

It is conceivable that the radiation emitted by a plasma is partly reabsorbed. Indeed, this so-called "synchrotron self-absorption" is well known [38] and can be derived for any source using Einstein coefficients. Below the transition frequency which corresponds to the mean particle energy the intensity of the observed spectrum scales as $\nu^{5/2}$ regardless of the particular power law obeyed by the source. Because in the radio regime the brightness temperature is many orders of magnitude bigger than the associated particle energy this effect is irrelevant for the understanding of the radio spectrum of a pulsar.

Chapter 4

Beam-Beam Interaction in Storage Rings[†]

4.1 Introduction

Colliding particle bunches in a storage ring exert an electromagnetic force on each other. The beam-beam parameter ξ is the tune shift exerted by one bunch on a particle near the center of the opposing bunch. It is a useful measure of the strength of the beam-beam interaction. A limiting value of ξ_y is reached in an e^+e^- collider when further increases in beam intensity lead to particle loss or to an increase in the vertical emittance of the beam. In e^+e^- colliders, where the action of radiation excitation and damping produces a flat beam, the observed vertical beam-beam parameter limit is in the approximate range $0.02 \leq \xi_y \leq 0.1$ [11, 12]. At present it is not known whether the emittance increase is due to an incoherent, single-particle effect or to a coherent, collective instability of the colliding beams. The DCI storage rings at LAL, Orsay, France, used a pair of e^+ and e^- beams to collide with another pair, in an attempt to cancel the beam-beam force [13]. It was found, however, that the beam-beam limit in DCI was not significantly improved by the charge cancellation. Derbenev [14] explained this result in terms of a collective instability of the four-beam system and in [40] the performance of DCI was analyzed numerically. This suggests that the beam-beam limit for two-beam e^+e^- colliders may also be due to a collective instability. Simulations in

[†]This chapter appeared as a journal article [39]. Reprinted in modified form with kind permission from the American Physical Society.

[41, 42, 43] show collective oscillations of the beam at the beam-beam limit.

In references [14, 15, 16] the stability of the colliding beams was examined by solving the Vlasov equation for an equilibrium distribution with small perturbations. Chao and Ruth [16] considered a beam-beam model in which motion was confined to the vertical plane, and in which the beam has a "water-bag" equilibrium distribution (uniform within an ellipse in phase space). Synchrotron radiation damping and excitation were not considered. When the Vlasov equation was solved for a linearized beam-beam force, coherent beam modes were found to be unstable near each resonance. In [15] the stability of a Gaussian equilibrium distribution was analyzed with the Vlasov equation for round beams where the beam-beam force can be expanded in Bessel functions. A flat beam model with a Gaussian distribution and synchrotron radiation was studied in [44, 45] under the assumption that the distribution always remains Gaussian. A similar approach was chosen in [46] for a purely linear beam-beam force. The findings of these models, e.g. flipflop solutions and period-n solutions are verified numerically in [47] where the behavior of flat and round beams is considered as well.

In this paper we extend the model of Chao and Ruth to a Gaussian equilibrium distribution. In Section 4.2 we set up the equations of motion for the phase space distribution and its perturbations, and linearize the beam-beam force. In Section 4.3 we solve the equations of motion for radial and angular modes up to first order in the displacement from the design trajectory and discuss the implications of our results.

4.2 Beam Evolution

We model the flat beam as a current sheet which is uniform in the horizontal direction, x, and consider only motion in the vertical direction, y. Consider one-dimensional phase space distributions $\psi_1(y, y', s)$ and $\psi_2(y, y', s)$ of the two beams which are normalized to unity. Then the deflection from the second (first) beam on a particle in the first (second) beam is

$$\Delta y'_{1,2} = -I_{\psi_{2,1}}(y, s), \tag{4.1}$$

where we define

$$I_\psi(y, s) \equiv \frac{4\pi N r_e}{\gamma} \int_{-\infty}^{\infty} d\overline{y}\, \mathrm{sgn}(y - \overline{y}) \int_{-\infty}^{\infty} d\overline{y}' \psi(\overline{y}, \overline{y}', s) \tag{4.2}$$

and N is the number of particles per unit width in x and r_e is the classical radius of the electron. Both beams are assumed to have the same number of particles per unit width. The equations describing the motion of $\psi_{1,2}$ are given by the two Vlasov equations

$$\frac{\partial \psi_{1,2}}{\partial s} + y' \frac{\partial \psi_{1,2}}{\partial y} - K(s) y \frac{\partial \psi_{1,2}}{\partial y'} - \frac{\partial \psi_{1,2}}{\partial y'} \delta_p(s) I_{\psi_{2,1}}(y, s) = 0 \tag{4.3}$$

where the periodic delta function and the unperturbed focusing function are denoted by $\delta_p(s)$ and $K(s)$, respectively. We want to determine whether the beam is stable. That is, we want to know if small perturbations of the phase space density grow. Thus, we choose a perturbative ansatz

$$\psi_{1,2} = \psi_0 + \Delta\psi_{1,2} \tag{4.4}$$

where ψ_0 is the equilibrium distribution, i.e. a solution of Eq. (4.3) with $\psi_1(y, y', s) = \psi_2(y, y', s) = \psi_0(y, y', s) = \psi_0(y, y', s + C)$, where the circumference of the ring is denoted by C. Substituting Eq. (4.4) into Eq. (4.3), subtracting Eq. (4.3) written

for the equilibrium distribution, and neglecting the term which contains a product of two perturbations we find

$$\frac{\partial \Delta\psi_{1,2}}{\partial s} + y' \frac{\partial \Delta\psi_{1,2}}{\partial y} - \frac{\partial \Delta\psi_{1,2}}{\partial y'} F(y,s) - \delta_p(s) \frac{\partial \psi_0}{\partial y'} I_{\Delta\psi_{2,1}} = 0, \tag{4.5}$$

where

$$F(y,s) = K(s)y + \delta_p(s) I_{\psi_0}(y). \tag{4.6}$$

If we approximate the beam-beam force as linear in y

$$F(y,s) \approx F(s)y = K(s)y + \delta_p(s) I^1_{\psi_0} \tag{4.7}$$

with

$$I^1_{\psi_0} = I_{\psi_0}(0) + \frac{\partial}{\partial y} I_{\psi_0}(y)\bigg|_{y=0} \cdot y \tag{4.8}$$

we can replace $K(s)$ by the perturbed focusing function $F(s)$ to compute the perturbed Twiss parameters. In the next step we transform Eq. (4.5) to action-angle coordinates

$$y = \sqrt{2\beta J}\cos\phi \qquad y' = -\sqrt{\tfrac{2J}{\beta}}\left(\sin\phi + \alpha\cos\phi\right). \tag{4.9}$$

The betatron function is perturbed by the linearized beam-beam kick from ψ_0. We form the linear combinations for the σ- and the π-mode

$$f_\pm = \Delta\psi_1 \pm \Delta\psi_2. \tag{4.10}$$

Then Eq. (4.5) can be decoupled and rewritten in action-angle coordinates as

$$\frac{\partial f_\pm}{\partial s} + \frac{1}{\beta}\frac{\partial f_\pm}{\partial \phi} \mp \delta_p(s) \frac{\partial \psi_0}{\partial y'} I^1_{f_\pm} = 0. \tag{4.11}$$

The quantity $\frac{\partial \psi_0}{\partial y'} = -\sqrt{2\beta J}\left(\sin\phi \frac{\partial}{\partial J}\psi_0 + \frac{\cos\phi}{2J}\frac{\partial}{\partial \phi}\psi_0\right)$ simplifies since the linearization of the beam-beam force in Eq. (4.7) leads to $\psi_0 = \psi_0(J)$ and we are left

with

$$\frac{\partial f_{\pm}}{\partial s} + \frac{1}{\beta}\frac{\partial f_{\pm}}{\partial \phi} \pm \sqrt{2\beta J}\sin\phi\delta_p(s)\frac{\partial \psi_0}{\partial J} I^1_{f_{\pm}} = 0. \tag{4.12}$$

In the following discussion we omit the label $\pm$.

4.3 Solving the Equations of Motion

When the interaction term in Eq. (4.3) is not considered, any differentiable distribution which depends solely on J is an equilibrium distribution. In general, ψ_0 will be a function of both J and ϕ. Fortunately, an arbitrary differentiable function of J is an equilibrium distribution, at least to linear order in y after introducing the perturbed betatron function. We choose a Gaussian equilibrium distribution

$$\psi_0(J) = \frac{1}{2\pi\epsilon} e^{-\frac{J}{\epsilon}} \tag{4.13}$$

since in the presence of damping and quantum excitation the beam distribution naturally tends to a Gaussian distribution. The deflection of a particle due to the presence of a Gaussian beam can be obtained from Eq. (4.2),

$$I_{\psi_0}(y) = \frac{4\pi N r_e}{\gamma}\,\mathrm{erf}\left(\frac{y}{\sqrt{2\beta\epsilon}}\right). \tag{4.14}$$

We expand the linearized version of Eq. (4.12) using the ansatz

$$f(J,\phi,s) = \sum_{n'=0}^{\infty}\sum_{l'=-\infty}^{\infty} g_{n'l'}(s) e^{-\frac{J}{\epsilon}} L_{n'}\left(\frac{J}{\epsilon}\right) e^{il'\phi}. \tag{4.15}$$

Since the perturbation must be periodic in ϕ we can express the ϕ - dependence in terms of a Fourier series. The orthogonality relation for the Laguerre polynomials comes with the convenient weight factor $e^{-\frac{J}{\epsilon}}$ which simplifies working with expressions that contain the Gaussian equilibrium distribution. Furthermore, using the weight factor in the set of basis functions, guarantees that the perturbation falls

off as $J \longrightarrow \infty$. We will refer to the modes represented by the first and second index in g_{nl} as "radial" modes and "angular" modes, respectively, i.e. these words refer to the two-dimensional phase space described by action-angle variables. With Eq. (4.15) the linearization in Eq. (4.8) leads to

$$I_f \propto \int_{-\infty}^{\infty} d\overline{y}' \left[\int_{-\infty}^{y} d\overline{y} f(\overline{y}, \overline{y}', s) - \int_{y}^{\infty} d\overline{y} f(\overline{y}, \overline{y}', s) \right] \tag{4.16}$$

$$I_f^1 \propto \int_{-\infty}^{\infty} d\overline{y}' \left[\int_{-\infty}^{0} d\overline{y} f(\overline{y}, \overline{y}', s) - \int_{0}^{\infty} d\overline{y} f(\overline{y}, \overline{y}', s) + 2y f(0, \overline{y}', s) \right] \tag{4.17}$$

Using $\int_0^\infty e^{-x} L_n(x) dx = \delta_{n0}$ the first part of I_f^1 is given by

$$\int_0^\infty dJ \int_{-\pi/2}^{\pi/2} d\phi \left[f(J, \phi + \pi, s) - f(J, \phi, s) \right] = -4\epsilon \sum_{l'=-\infty}^{\infty} g_{0(2l'+1)} \frac{(-1)^{l'}}{2l'+1}. \tag{4.18}$$

The second part is given by

$$2 \int_{-\infty}^{\infty} d\overline{y}' f(0, \overline{y}', s) = 2 \int_0^\infty dJ \frac{1}{\sqrt{2\beta J}} [f(J, \pi/2, s) + f(J, -\pi/2, s)] = \sqrt{4\pi} \sqrt{\frac{2\epsilon}{\beta}} \sum_{n'=0}^{\infty} \sum_{l'=-\infty}^{\infty} g_{n'2l'} (-1)^{l'} \frac{(2n')!}{(2^{n'} n'!)^2}. \tag{4.19}$$

Here we have made use of

$$\int_0^\infty \frac{1}{\sqrt{x}} e^{-x} L_n(x) dx = \frac{(2n)!}{(2^n n!)^2} \equiv \sqrt{\pi} P_n. \tag{4.20}$$

Inserting I_f^1 into Eq. (4.12), projecting this equation onto our chosen set of basis functions by means of the orthogonality relation of the Laguerre polynomials

$$\int_0^\infty e^{-x} L_n(x) L_m(x) dx = \delta_{nm} \tag{4.21}$$

and using

$$\int_0^\infty \sqrt{x} e^{-x} L_n(x) dx = -\frac{(2n)! \sqrt{\pi}}{2(2n-1)(2^n n!)^2} = -\frac{\sqrt{\pi}}{2(2n-1)} P_n \tag{4.22}$$

and

$$\int_0^\infty x e^{-x} L_n(x) dx = \delta_{n0} - \delta_{n1} \tag{4.23}$$

we obtain

$$\frac{\partial g_{nl}}{\partial s} + \frac{il}{\beta} g_{nl} = \mp \delta_p(s) \xi \sum_{n'=0}^{\infty} \sum_{l'=-\infty}^{\infty} M_{nl,n'l'} g_{n'l'} \ , \quad \xi = \frac{N r_e}{\gamma} \sqrt{\frac{2\beta^*}{\pi \epsilon}} \ , \tag{4.24}$$

where

$$\frac{1}{2n-1} P_n (\delta_{l,1} - \delta_{l,-1}) \delta_{n',0} (-1)^{\frac{l'-1}{2}} \frac{1}{l'} a_{l'} + (\delta_{n,0} - \delta_{n,1})(\delta_{l,2} - \delta_{l,-2}) P_{n'} (-1)^{\frac{l'}{2}} b_{l'}$$
$$\equiv (2\pi i)^{-1} M_{nl,n'l'} \tag{4.25}$$

The coefficients a_l are 1 for odd l and 0 for even l and vice versa for the coefficients b_l. Each column and each row of the matrix M refers to one particular combination of an n and an l value.

4.4 Dynamic Tune

We calculate the tune ν in terms of the unperturbed tune ν_0 by means of Eq. (4.26).

$$\nu - \nu_0 = \frac{1}{4\pi} \oint \beta(s)(F(s) - K(s)) ds \ . \tag{4.26}$$

In order to obtain $F(s) - K(s)$ the deflection in Eq. (4.14) is linearized. This gives

$$\nu - \nu_0 = \frac{N r_e}{\gamma} \sqrt{\frac{2\beta^*}{\pi \epsilon}} \equiv \xi \ , \tag{4.27}$$

where β^* denotes the beta function at the interaction point.

4.5 Coherent Beam-Beam Instability

We solve the ODE (4.24) and rewrite the solution in matrix form such that the beam transport after one turn is described by a matrix T which acts on a column

vector G that contains all g_{nl}, i.e. $G(C) = TG(0)$. We parametrize the beam-current by the linear tune shift parameter ξ. One obtains the following relation for the g_{nl}'s immediately before and immediately after the interaction point by integrating through the interaction point:

$$G(0^+) - G(0^-) = \pm \xi M G(0^-) \tag{4.28}$$

There is no coupling among different Fourier components between collisions. In this case Eq. (4.24) simplifies to

$$\frac{\partial g_{nl}}{\partial s} + \frac{il}{\beta(s)} g_{nl} = 0, \tag{4.29}$$

which is solved by

$$g_{nl}(C^-) = g_{nl}(0^+) e^{-il \int_0^C \frac{1}{\beta(s)} ds} = g_{nl}(0^+) e^{-2\pi i l \nu}. \tag{4.30}$$

The one-turn transfer matrix becomes

$$T_\pm = R\,(\mathbb{1} \pm \xi M) \tag{4.31}$$

where R is a diagonal matrix which has the elements $e^{-2\pi i l \nu}$ on its diagonal. The matrix M has the following properties which follow immediately from Eq. (4.25),

$$\begin{aligned} M_{nl,n'l'} &= 0 \text{ for } l + l' = \text{odd} \\ M_{nl,n'-l'} &= M_{nl,n'l'} \\ M_{n-l,n'l'} &= -M_{nl,n'l'} \\ M^*_{nl,n'l'} &= -M_{nl,n'l'} \end{aligned} \tag{4.32}$$

In order to decide whether the system is stable or not we have to find out what happens to an arbitrary initial perturbation after a large number of turns, i.e. one needs to consider the limit T^N where $N \longrightarrow \infty$. Every matrix norm of the latter

quantity tends to infinity if the absolute value of one eigenvalue of T is bigger than 1. To analyze the stability for a given tune ν and a beam-beam parameter ξ, we therefore compute the eigenvalue λ_{max} that has the largest modulus. In case of instability we compute the corresponding eigenvector G and find its component g_{nl} which has the largest modulus. This indicates that the instability mainly drives the radial mode n and angular mode l, causing f to be dominated by $L_n(\frac{J}{\epsilon})e^{il\phi}$. Since the perturbation f must be real taking its complex conjugate must leave f invariant which gives the constraint $g_{nl} = g^*_{n-l}$. Indeed Eq. (4.24) is invariant under complex conjugation and replacing $l \longrightarrow -l$. It follows that the coefficients of T have the property $T_{n-l,n'-l'} = T_{nl,n'l'}$, which also follows from Eq. (4.32). This requires that eigenvalues of T are either real or come in a pair with their complex conjugate: Let S be a matrix performing the transformation $l \longrightarrow -l$ then we have $STSSG = \lambda SG$ and finally $T(SG^*) = \lambda^*(SG^*)$. Therefore, the l-mode and the $-l$ mode are always excited simultaneously with equal strength.

4.6 Results and Discussion

In Fig. 4.1 and 4.2 we varied the tune ν between 0 and 1 and the beam-beam parameter ξ between 0 and 0.12. A point has been plotted if the absolute value of all eigenvalues of T is smaller than or equal to 1 for both the σ- and the π-mode. We truncated T to the indicated modes. In Fig. 4.1 only the 5 modes $l = -2 \ldots 2$ for $n = 0$ were considered. In Fig. 4.2 we included the same angular modes for $n = 0 \ldots 2$. The first and second order resonances can be recognized clearly. Resonances of orders higher than 2 cannot be expected in our linearized model. It is interesting to note that the inclusion of radial modes stabilizes the motion of the beam so that a larger ξ can be tolerated.

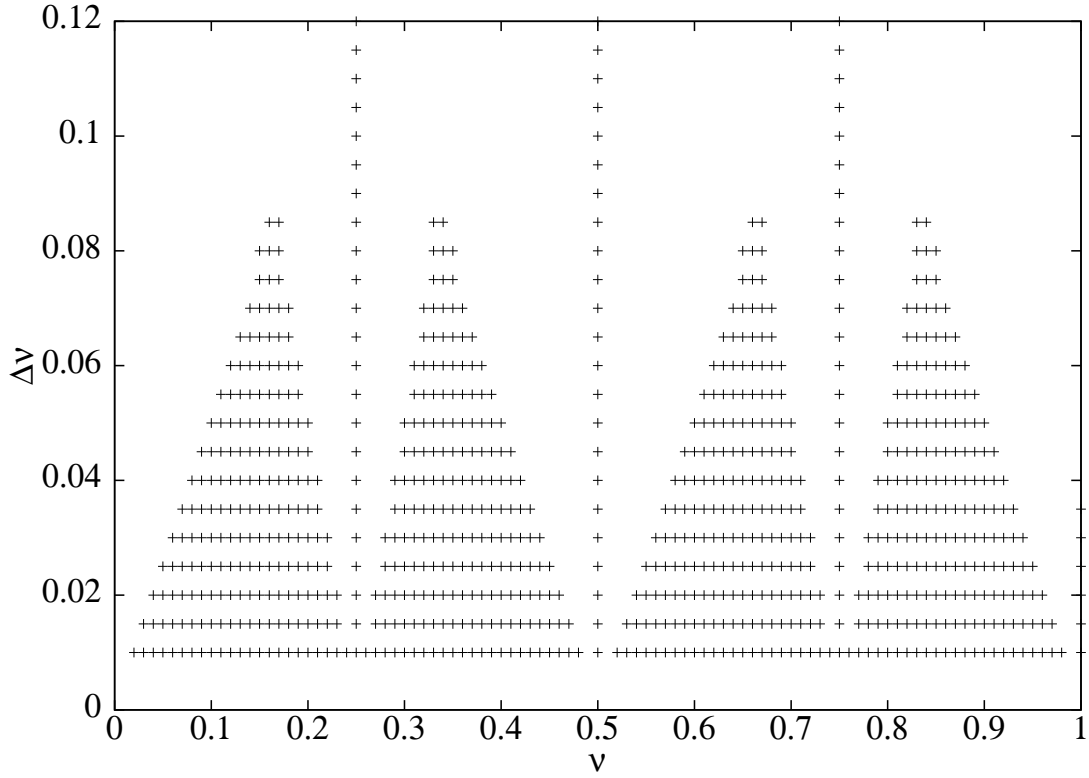

Figure 4.1: Stability diagram for $n = 0$, $l = -2 \ldots 2$

In Fig. 4.3 and 4.4 we again varied ν and ξ and plotted the largest eigenvalue $|\lambda_{max}|$ vs. ν and determined which mode becomes unstable by selecting the biggest component of the eigenvector which is associated with the largest eigenvalue. The plot shows that in the absence of dynamics in the radial direction $l = \pm 1$ and $l = \pm 2$ modes become unstable in the vicinity of $\nu = 0.5$, but in Fig. 4.4 only $l = \pm 1$ modes are excited around $\nu = 0.5$. Furthermore, the unstable $l = \pm 2$ modes which accumulate in the vicinity of $\nu = 0.25$ and $\nu = 0.75$ are attenuated if the $n = 1$ mode is included. Therefore, the radial motion leads to a damping of the $l = \pm 2$ modes.

In Fig. 4.5 we computed the phase of the largest eigenvalue of $l = \pm 2$ instabilities, corresponding to quadrupole oscillations (π-mode only), versus the perturbed tune for various $\Delta\nu$. The slope of the two lower lines is 2 which indicates that the

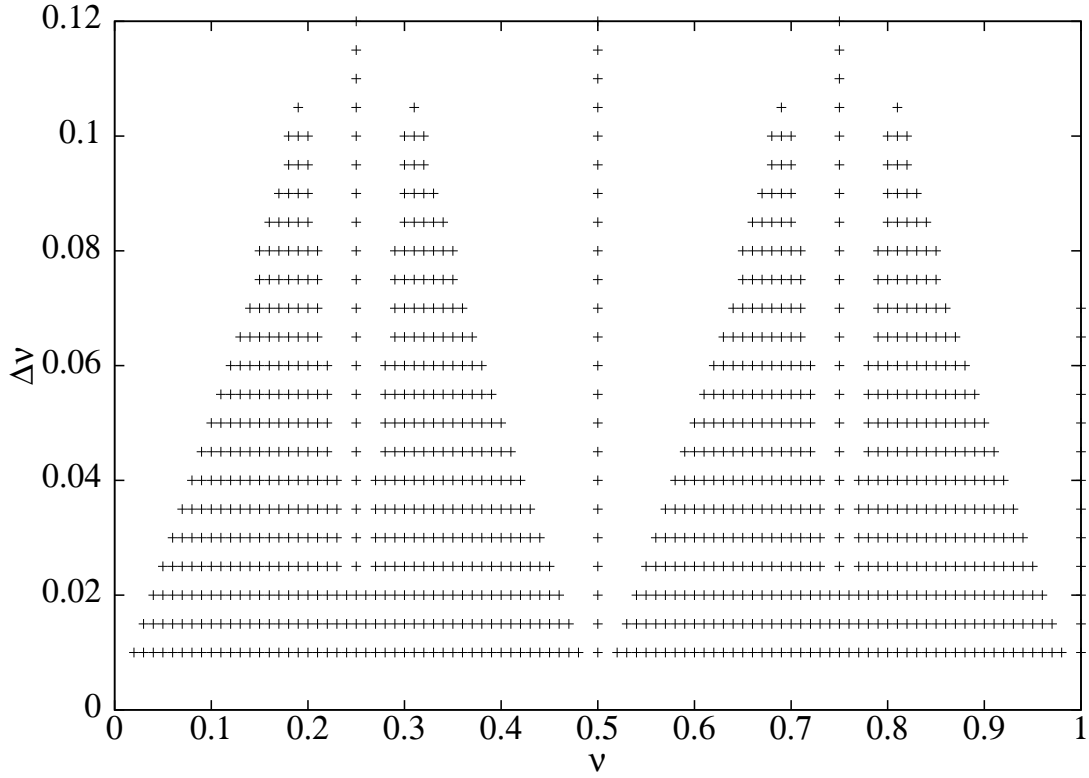

Figure 4.2: Stability diagram for $n = 0 \ldots 2$, $l = -2 \ldots 2$

collective oscillation frequency of the quadrupole mode is twice the single particle oscillation frequency for small ξ. The spread of the points for fixed ν shows how strongly the beam-beam parameter ξ influences the frequency of quadrupole oscillations. In Fig. 4.6 this spread is significantly lower which again shows that radial modes have a stabilizing effect.

The dependence of this spread on ν can be understood analytically. For simplicity we consider only the $n = 0$ modes. Close to a resonance where $l\nu$ is integer, g_{0l} and g_{0-l} perturb the beams the most. Thus, we content ourselves with the following 2x2 matrix [16]

$$T = \begin{pmatrix} e^{-2\pi i l \Delta} & 0 \\ 0 & e^{2\pi i l \Delta} \end{pmatrix} \left[\mathbb{1} \pm i\alpha \begin{pmatrix} 1 & 1 \\ -1 & -1 \end{pmatrix} \right] , \tag{4.33}$$

which satisfies all properties listed in Eq. (4.32) for $i\alpha = \xi M_{0l,0l}$. The imaginary

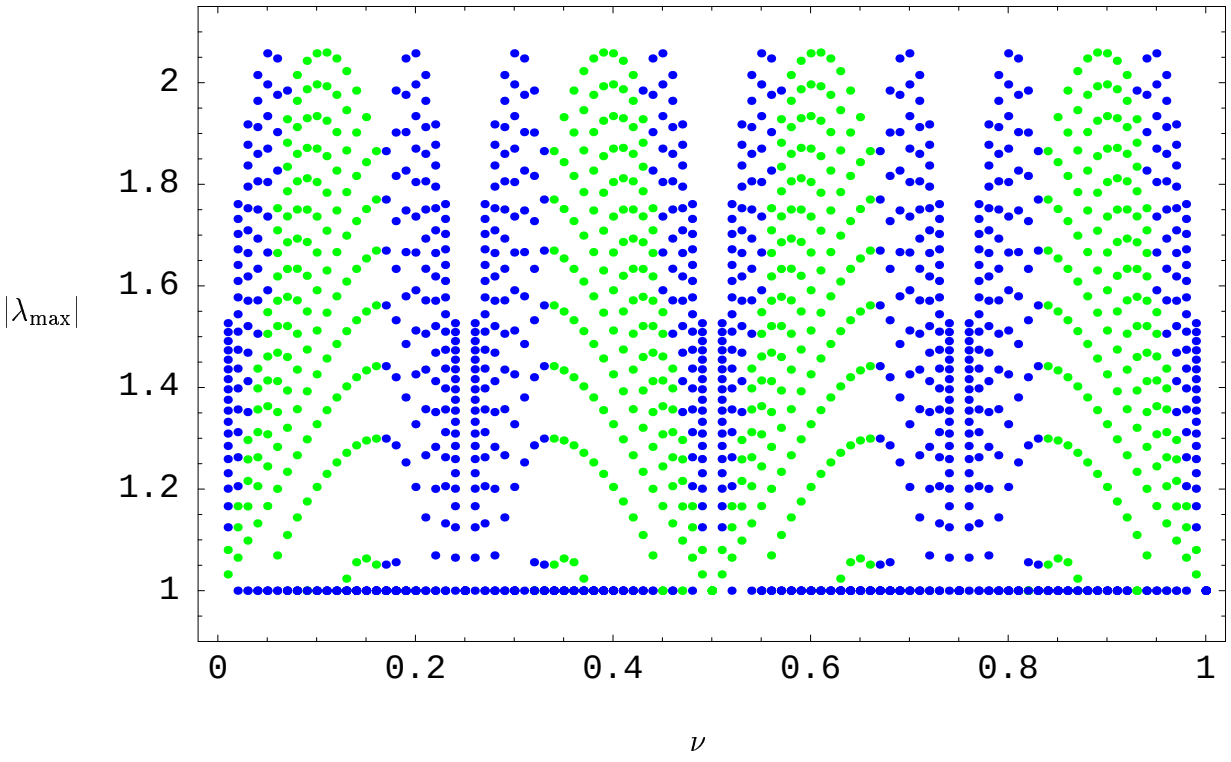

Figure 4.3: Absolute value of the largest eigenvalue λ_{max} vs. tune. Gray points indicate unstable $l = \pm 1$ modes and black points indicate unstable $l = \pm 2$ modes. The following modes were included: $n = 0$, $l = -2 \ldots 2$

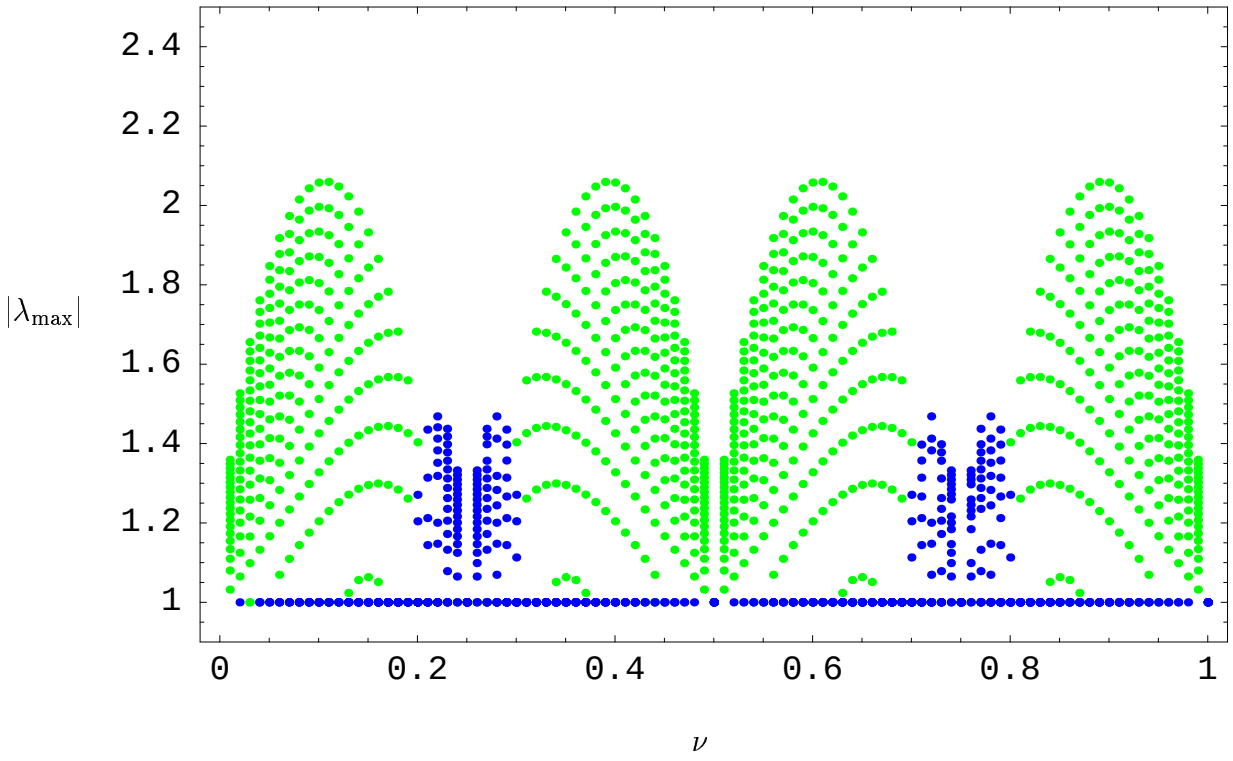

Figure 4.4: Same as Fig. 4.3, but for $n = 0 \ldots 1$, $l = -2 \ldots 2$

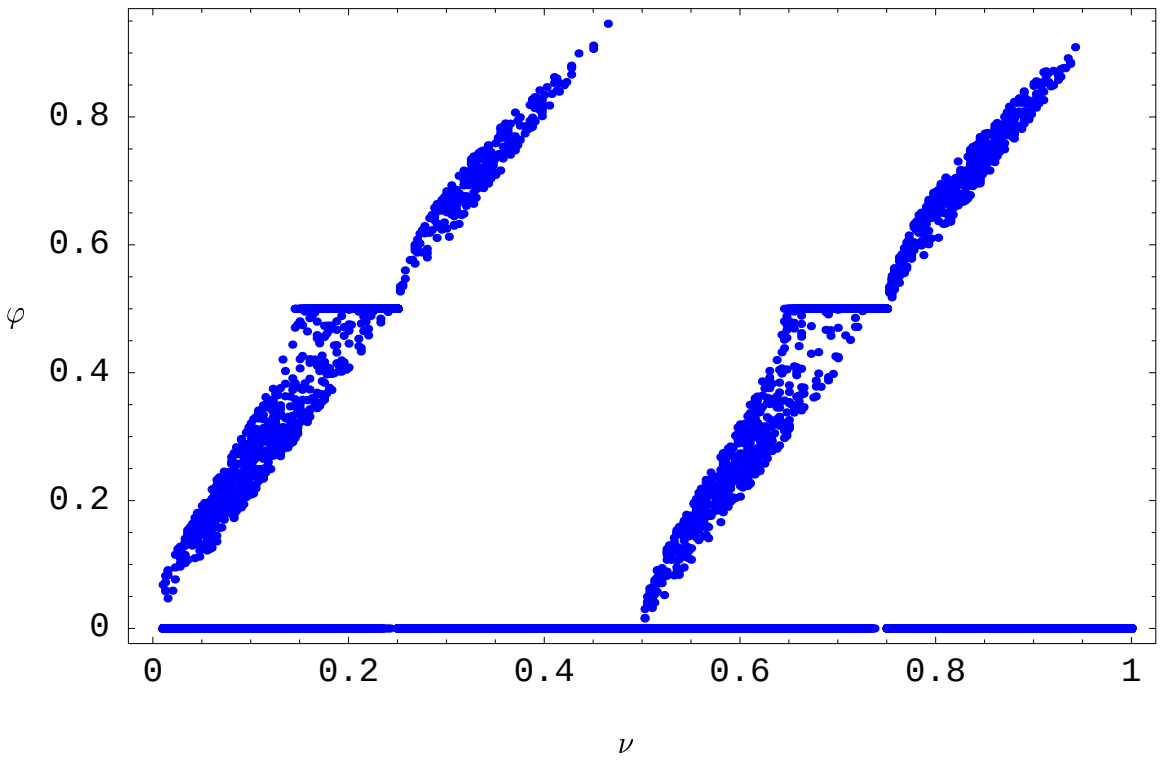

Figure 4.5: Phase vs. perturbed tune for $n = 0$, $l = \pm 2$ modes (π-mode only).

parts of the eigenvalues of the matrix T vanish for eigenvalues whose absolute value is bigger than 1. This leads to the plateaus at 0 and 0.5 in Fig. 4.5 and 4.6 at tunes ν where the $l = \pm 2$ mode becomes unstable in the Fig. 4.3 and 4.4. The difference between the dipole oscillation frequencies ν_π plotted in Fig. 4.7 gray and ν_σ plotted black of the π and the σ mode divided by the beam-beam parameter ξ is referred to as the Meller factor [48] or the Yokoya factor [49]. This factor is plotted for all points of our computation for which both the π and the σ mode indicate stable motion. In Fig. 4.8, one can see that this factor is always above 1.25 in our Gaussian flat beam model.

There are only a few points close to $\nu = 0.25$ and $\nu = 0.75$ since the $l = 2$ modes for these tunes are unstable for small ξ.

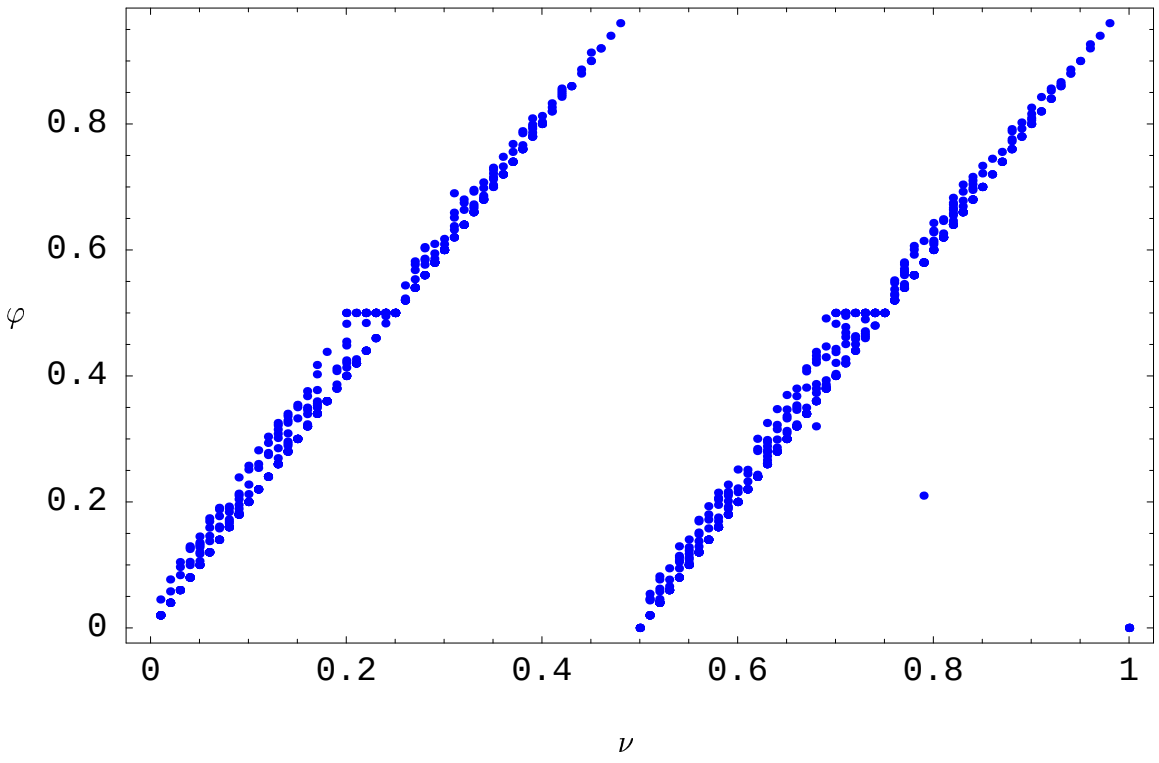

Figure 4.6: Phase vs. perturbed tune for $n = 0 \ldots 1$, $l = \pm 2$ modes (π-mode only).

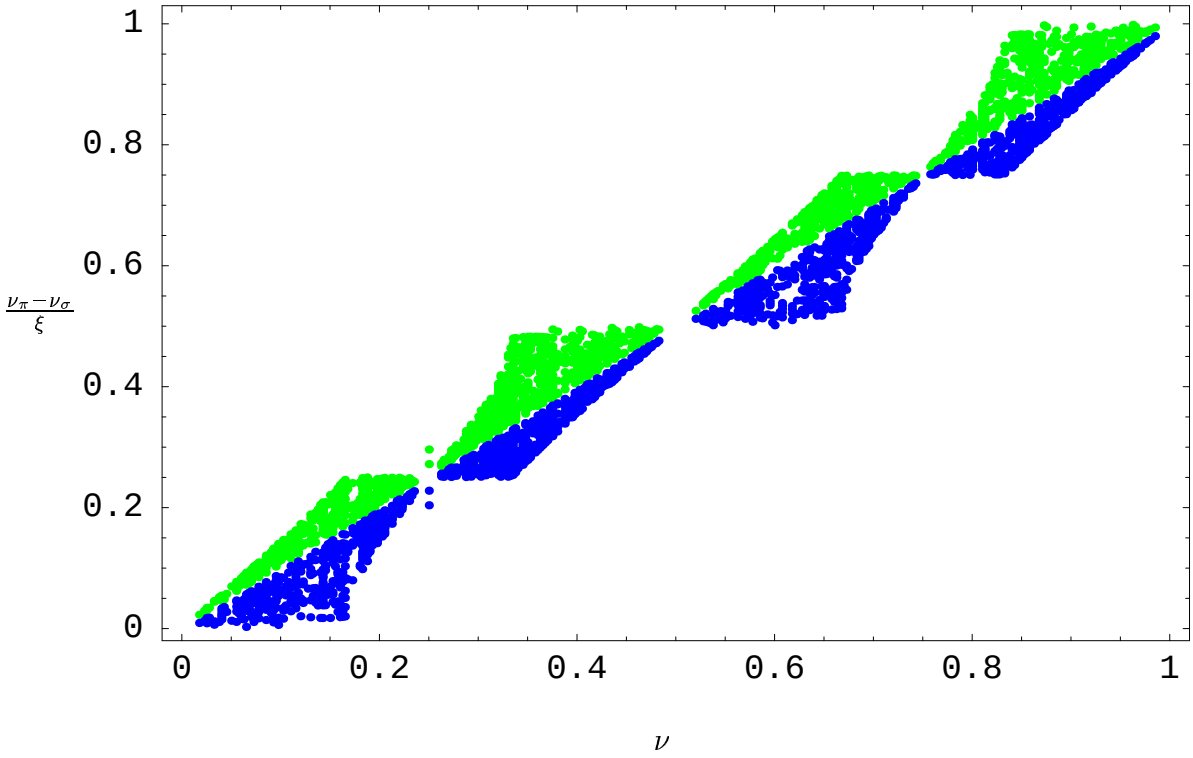

Figure 4.7: The dipole oscillation frequencies are plotted gray for the f_+ distribution and black for the f_- distribution with $\xi = 0$ to 0.2 for $n = 0$, $l = \pm 1$ modes.

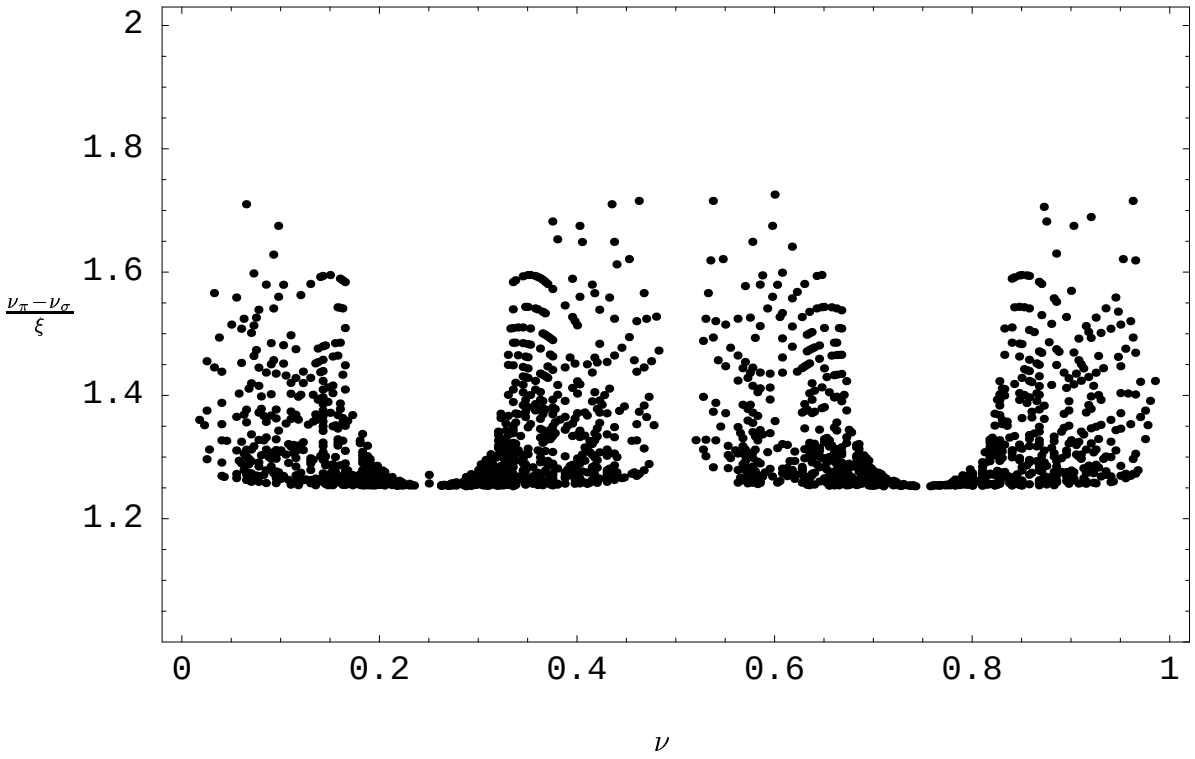

Figure 4.8: The Meller factor for stable motion in the region $\xi = 0$ to 0.2 for $n = 0$, $l = \pm 1$ modes.

4.7 Possible Extensions

4.7.1 Higher Order Resonances

In order to study resonances of order higher than 2 Eq. (4.2) must not be linearized, but rather the double integral has to be expanded about $y = 0$ to orders higher than 1. The expansion to 2nd order contains $y^2 \int_{-\infty}^{\infty} d\bar{y}' \frac{d}{dy} f(\bar{y}, \bar{y}', s)|_{\bar{y}=0}$. Inserting the expansion in Eq. (4.15) for f and writing $\frac{d}{dy}$ in terms of J and ϕ allows the evaluation of the integral. The resulting term $\frac{\partial \psi_0}{\partial y'} y^2 = -\frac{1}{2\pi\epsilon^2} (2\beta J)^{\frac{3}{2}} e^{-\frac{J}{\epsilon}} \sin\phi \cos^2\phi$ in Eq. (4.5) needs to be expanded in Laguerre polynomials and gives rise to higher orders in radial modes. The n-th order term can be written in terms of powers of $\sqrt{J}$, $\cos n\phi$, $\sin n\phi$ and lower frequency parts. Since the beam-beam force acts only at a single point, its contribution is not averaged out in the limit of a large number of turns if the tune matches the frequency of one of the sine or cosine functions. This is the case if the tune is a rational number, so higher order resonances would appear in Fig. 4.2. Without truncating the series the model would result in an infinite number of resonances since one can always find a rational number between two irrational numbers. However, this procedure is complicated by the fact that Eq. (4.13) is not an equilibrium distribution anymore when nonlinear terms are included.

When the length of the bunch and its longitudinal motion is included, synchro-betatron resonances can occur [50] when the bunch length is in the order of the betatron function. Including these resonances would require and extension of our treatment from two to four dimensional phase space. This would be a worthwhile but tedious continuation of our work.

4.7.2 Damping by Synchrotron Radiation

One can extend the presented model to account for damping by synchrotron radiation. In order to obtain the equilibrium distribution in Eq. (4.13) quantum excitation must be included as well. This turns Eq. (4.3) into the Fokker-Planck equation (4.34). In preliminary computations we found that the graphs we presented above remain unchanged for realistic values of the damping and excitation coefficients. To simplify the Fokker-Planck equation, we averaged over the phases in the damping and excitation terms but not in the beam-beam interaction term. This can be justified since the betatron phases in the terms for damping and quantum excitation change during one turn while the phase in the interaction term changes only once per turn. In Eq. (4.34) λ is the energy loss per turn due to synchrotron radiation divided by the energy of the particle, η is the dispersion and D is the quantum excitation coefficient.

$$\frac{\partial \psi_{1,2}}{\partial s} + y' \frac{\partial \psi_{1,2}}{\partial y} - \left(\frac{\lambda}{C} y' + K(s) y + \frac{4\pi N r_e}{\gamma} \delta_p(s) I_{\psi_{2,1}}(y,s) \right) \frac{\partial \psi_{1,2}}{\partial y'} = \frac{\lambda}{C} \psi_{1,2} + D \left(\eta \frac{\partial}{\partial y} + \eta' \frac{\partial}{\partial y'} \right)^2 \psi_{1,2} \qquad (4.34)$$

4.7.3 Different Tunes

If the two beams have different tunes, Eq. (4.10) cannot be used anymore to decouple the system. It is easier to work with the uncoupled system and solve for the g_{nl} of the two beams separately. Introducing the column vector G which contains the g_{nl} for both beams, one can proceed as before and describe the beam transport for each turn by a matrix multiplication with a matrix T. Introducing

$$\tilde{R} = \begin{pmatrix} R(\nu_1) & 0 \\ 0 & R(\nu_2) \end{pmatrix} \qquad (4.35)$$

where $R(\nu)$ is a diagonal matrix which has the components $e^{-2\pi i l \nu}$ we can write the matrix T as

$$T = \tilde{R} \left[\mathbb{1} + \xi \begin{pmatrix} 0 & M \\ M & 0 \end{pmatrix} \right] \tag{4.36}$$

Chapter 5

Coherent Synchrotron Radiation[†]

5.1 Introduction

The high brightness temperatures of the radio emission of pulsars ($T_B \gg 10^{12}$K) implies a coherent emission mechanism [52, 53, 20, 54, 55] and some part of the radio emission of extragalactic jets may be coherent [56]. Recently, coherent synchrotron radiation (CSR) has been observed in bunch compressors [17, 23, 18] which are a crucial part of future particle accelerators. When a relativistic beam of electrons interacts with its own synchrotron radiation the beam may become modulated. If the wavelength of the modulation is less than the wavelength of the emitted radiation, a linear instability may occur which leads to exponential growth of the modulation amplitude. The coherent synchrotron instability of relativistic electron rings and beams has been investigated theoretically by [20, 21, 22, 57, 58]. Goldreich and Keeley analyzed the stability of a ring of monoenergetic relativistic electrons which were assumed to move on a circle of fixed radius. Electrons of the ring gain or lose energy owing to the tangential electromagnetic force and at the same time generate the electromagnetic field. [19] analyzed the stability of a relativistic electron ring enclosed by a conducting beam pipe in an external betatron magnetic field. A distribution function with a spread in the canonical momentum was chosen for their analysis. For simplicity the effect of the betatron oscillations was not included in their treatment. They find a resistive wall instability and a negative mass instability. Furthermore, they find an instability which can perturb

[†]This chapter appeared as a journal article [51]. Reprinted in modified form with kind permission from the American Physical Society.

the surface of the beam. [57] analyzed the stability of a ring of relativistic electrons in free space including a small energy spread which gives a range of radii such that particles on the inner orbits can pass particles on outer orbits. [58] has developed a similar model which includes the effects of the conducting beam pipe. Numerical simulations by [59] show the burst-like nature of the coherent synchrotron radiation.

The present work analyzes the linear stability of a cylindrical, collisionless, relativistic electron (or positron) layer or E-layer [60]. Particle densities in pulsar magnetospheres are very low, of order the Goldreich-Julian charge density $n_{GJ} = \mathbf{\Omega} \cdot \mathbf{B}/2\pi ce \sim 10^{11}\,\mathrm{cm}^{-3}(B/10^{12}\,\mathrm{G})(R/r)^3[P(\mathrm{sec})]^{-1}$ at radius $r > R$, where R is the stellar radius, $B = 10^{12}B_{12}\,\mathrm{G}$ is the surface field strength, and P is the rotational period; thus, the magnetospheric plasma is collisionless to an excellent approximation [27]. The particles in the layer have a finite 'temperature' and thus a range of radii so that the limitation of the Goldreich and Keeley model is overcome. Although we allow a spread in energies, we assume that it is small, so the charge layer is also thin; efficient radiation losses are probably sufficient to maintain rather low energy spreads in a pulsar magnetosphere, although the precise size of the spread is still not entirely certain. Viewed from a moving frame the E-layer is a rotating beam. The system is sufficiently simple that it is relevant to electron flows in pulsar magnetospheres (cf. [61]). The analysis involves solving the relativistic Vlasov equation using the full set of Maxwell's equations and computing the saturation amplitude due to trapping. The latter allows us to calculate the energy loss due to coherent radiation.

In §5.2 we describe the considered Vlasov equilibria. The first type of equilibrium (a) is formed by electrons (or positrons) moving perpendicular to a uniform

magnetic field in the $z-$direction so as to form a thin cylindrical layer referred to as an E-layer. The second type of equilibrium (b) is formed by electrons moving almost parallel to an external toroidal magnetic field and also forming a cylindrical layer. §5.3 describes the method of solving the linearized Vlasov equation which involves integrating the perturbation force along the unperturbed orbits of the equilibrium. In §5.4, we derive the dispersion relation for linear perturbations for the case of a radially thin E-layer and zero wavenumber in the axial direction, $k_z = 0$. We find that there is in general a short wavelength instability. In §5.5 we analyze the nonlinear saturation of the wave growth due to trapping of the electrons in the potential wells of the wave. This saturation allows the calculation of the actual spectrum of coherent synchrotron radiation. In §5.6, we derive the dispersion relation for linear perturbations of a thin E-layer including a finite axial wavenumber. The linear growth is found to occur only for small values of the axial wavenumber. The nonlinear saturation due to trapping is similar to that for the case where $k_z = 0$. In §5.7 we consider the effect of the thickness of the layer more thoroughly and include the betatron oscillations. §5.8 discusses the apparent brightness temperatures for the saturated coherent synchrotron emission. §5.9 discusses some implications on particle accelerator physics. §5.10 gives conclusions of this work.

5.2 Equilibrium Configuration

5.2.1 Configuration a

We first discuss the Vlasov equilibrium for an axisymmetric, long, thin cylindrical layer of relativistic electrons where the electron motion is almost perpendicular to

the magnetic field. This is shown in Fig. 5.1. The case where the electron motion is almost parallel to the magnetic field is discussed below. The equilibrium has $\partial/\partial t = 0,\ \partial/\partial\phi = 0,$ and $\partial/\partial z = 0$. The configuration is close to the non-neutral Astron E-layer of [60]. The equilibrium distribution function f^0 can be taken to be an arbitrary non-negative function of the constants of motion, the Hamiltonian,

$$H \equiv \left(m_e^2 + p_r^2 + p_\phi^2 + p_z^2\right)^{1/2} - e\Phi^s(r)\ , \tag{5.1}$$

and the canonical angular momentum,

$$P_\phi \equiv rp_\phi - erA_\phi(r)\ , \tag{5.2}$$

where $A_\phi = A_\phi^e + A_\phi^s$ is the total (external plus self) vector potential, Φ^s is the self electrostatic potential, m_e is the electron rest mass, $-e$ is its charge, and the units are such that $c = 1$. Here, the external magnetic field is assumed to be uniform, $\mathbf{B}^e = B_z^e\hat{\mathbf{z}}$, with $A_\phi^e = rB_z^e/2$, and $B_z^e > 0$. Thus we have $f^0 = f^0(H, P_\phi)$. We consider the distribution function

$$f^0 = K\delta(P_\phi - P_0)\exp\left[-H/T\right]\ , \tag{5.3}$$

where K, P_0, and T are constants (see for example [62]). The temperature T in energy units is assumed sufficiently small that the fractional radial thickness of the layer is small compared with unity. Note that a Lorentz transformation in the $z-$direction gives a rotating electron beam.

The equations for the self-fields are

$$\frac{1}{r}\frac{d}{dr}\left(r\frac{d\Phi^s}{dr}\right) = 4\pi e\int d^3p\ f^0(H, P_\phi)\ , \tag{5.4}$$

$$\frac{d}{dr}\left(\frac{1}{r}\frac{d(rA_\phi^s)}{dr}\right) = 4\pi e\int d^3p\ v_\phi\ f^0(H, P_\phi)\ , \tag{5.5}$$

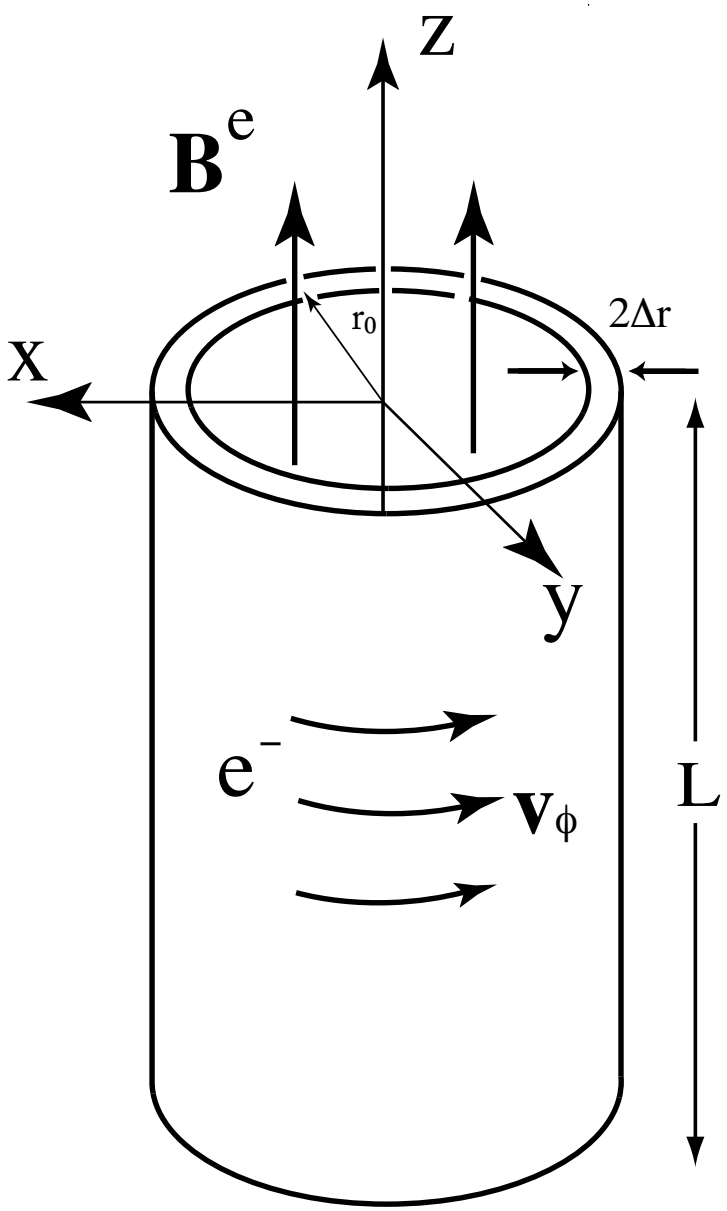

Figure 5.1: Geometry of relativistic E-layer for the case of a uniform external axial magnetic field.

where $v_\phi = (P_\phi/r + eA_\phi)/H$.

Owing to the small radial thickness of the layer, we can expand radially near r_0

$$\left[\frac{P_\phi}{r} + eA_\phi(r)\right]^2 = \left[\frac{P_\phi}{r_0} + eA_\phi(r_0)\right]^2 + \delta r D_1 + \frac{1}{2}\delta r^2 D_2, \tag{5.6}$$

where D_1, D_2 are the derivatives evaluated at r_0, and $\delta r \equiv r - r_0$ with $(\delta r/r_0)^2 \ll 1$. We choose r_0 so as to eliminate the term linear in δr. Thus,

$$H = H_0 - e\Phi^s(r_0) + \frac{1}{2H_0}\left(p_r^2 + p_z^2 + H_0^2\ \omega_{\beta r}^2\ \delta r^2\right)\ , \tag{5.7}$$

where $\omega_{\beta r}$ is the radial betatron frequency, and

$$\begin{aligned} H_0 &\equiv m_e\left\{1 + \left[\frac{P_\phi}{r_0} + eA_\phi(r_0)\right]^2\right\}^{1/2}\ , \\ \gamma_0 &\equiv \frac{H_0}{m_e}\ , \\ v_{\phi 0} &\equiv \frac{1}{H_0}\left[\frac{P_\phi}{r_0} + eA_\phi(r_0)\right]\ . \end{aligned} \tag{5.8}$$

We assume $\gamma_0^2 \gg 1$ and $v_{\phi 0} > 0$ so that $v_{\phi 0} = 1 - 1/(2\gamma_0^2)$ to a good approximation. The "median radius" r_0 is determined by the condition

$$\frac{D_1}{2H_0} - e\left.\frac{d\Phi^s}{dr}\right|_{r_0} = 0\ ,$$

or

$$\frac{1}{H_0}\left(\frac{P_\phi}{r_0} + eA_\phi\right)\left(-\frac{P_\phi}{r_0^2} + e\left.\frac{dA_\phi}{dr}\right)\right|_{r_0} = e\left.\frac{d\Phi^s}{dr}\right|_{r_0}. \tag{5.9}$$

To a good approximation,

$$\begin{aligned} r_0 = \frac{m_e\gamma_0 v_{\phi 0}}{(1-2\zeta)eB_z^e} &\approx \frac{m_e\gamma_0}{eB_z^e}(1+2\zeta) \quad \text{or} \\ r_0^2 &= \frac{2P_\phi}{eB_z^e}[1 + 3\zeta + \mathcal{O}(\zeta^2)]\ . \end{aligned} \tag{5.10}$$

Here,

$$\zeta \equiv -\frac{B_z^s(r_0)}{B_z^e}\ , \qquad \text{with} \qquad \zeta^2 \ll 1\ , \tag{5.11}$$

is the field-reversal parameter of Christofilos. For a radially thin E-layer of axial length L consisting of a total number of electrons N, the surface density of electrons is $\sigma = N/(2\pi r_0 L)$ and the surface current density is $-ev_\phi\sigma$. Because $B_z^s(r_0)$ is one-half the full change of the self-magnetic field across the layer, we have $\zeta = r_e N/(\gamma L)$, where $r_e = e^2/(mc^2)$ is the classical electron radius. Notice that N, ζ, and γL are invariants under a Lorentz transform in the $z-$direction.

The radial betatron frequency $\omega_{\beta r}$ is given by

$$H_0^2\ \omega_{\beta r}^2 = \frac{D_2}{2} - \frac{D_1^2}{4H_0^2} - H_0 e\frac{d^2\Phi^s}{dr^2}\ . \tag{5.12}$$

Using Eq. (5.9) gives

$$\begin{aligned}\omega_{\beta r}^2 &= \frac{1-4\zeta}{1-2\zeta}\ \frac{v_{\phi 0}^2}{r_0^2}\ + \frac{ev_{\phi 0}}{\gamma_0 m_e}\ \left.\frac{d^2A_\phi}{dr^2}\right|_{r_0} - \frac{e}{\gamma_0 m_e}\ \left.\frac{d^2\Phi^s}{dr^2}\right|_{r_0} \\ &\approx \frac{1-2\zeta}{r_0^2} - \frac{\sqrt{2/\pi}\ \zeta}{r_0\Delta r\gamma^2}\ .\end{aligned} \tag{5.13}$$

The term $\propto 1/\Delta r$ is the sum of the defocusing self-electric force and the smaller focusing self-magnetic force. For the layer to be radially confined we need to have $\zeta < \sqrt{\pi/2}\ \gamma^2(\Delta r/r_0)$. For $\zeta \ll \gamma^2(\Delta r/r_0)$ and $\zeta^2 \ll 1$, we have $\omega_{\beta r} = 1/r_0$ to a good approximation.

The number density follows from Eq. (5.3),

$$\begin{aligned} n &\approx n_0 \exp\left(-\frac{\delta r^2}{2\Delta r^2}\right) \quad \text{where} \quad \Delta r \equiv \left(\frac{T}{H_0\omega_{\beta r}^2}\right)^{1/2} \\ \text{or} \quad \frac{\Delta r^2}{r_0^2} &\simeq \frac{v_{th}^2}{1-2\zeta-\sqrt{2/\pi}\ \zeta(r_0/\Delta r)/\gamma^2}\end{aligned} \tag{5.14}$$

where

$$v_{th} \equiv \left(\frac{T}{\gamma_0 m_e}\right)^{1/2} \tag{5.15}$$

and

$$n_0 = 2\pi K H_0 T r_0^{-1} \exp\left(-\frac{H_0 - e\Phi^s(r_0)}{T}\right) \ . \tag{5.16}$$

As mentioned we assume the layer to be radially thin with $(\Delta r/r_0)^2 \ll 1$. Consequently, Eqs. (5.4) and (5.5) become

$$\begin{aligned} \frac{d^2\Phi^s}{dr^2} &\approx 4\pi e n_0 \ \exp\left(-\frac{\delta r^2}{2\Delta r^2}\right) \ , \\ \frac{d^2 A_\phi^s}{dr^2} &\approx 4\pi e n_0 \ v_{\phi 0} \ \exp\left(-\frac{\delta r^2}{2\Delta r^2}\right) \ . \end{aligned} \tag{5.17}$$

Thus we obtain

$$\zeta = \frac{-B_z^s(r_0)}{B_z^e} = \frac{4\pi e n_0 v_{\phi 0} \Delta r \sqrt{\pi/2}}{B_z^e} \tag{5.18}$$

The equilibrium is thus seen to be determined by three parameters,

$$\zeta^2 \ , \quad v_{th}^2 \ , \quad \text{and} \quad 1/\gamma_0^2 \ , \tag{5.19}$$

which are all small compared with unity.

5.2.2 Equilibrium Orbits

From the Hamiltonian of Eq. (5.7) we have

$$\frac{d^2\delta r}{dt^2} = -\omega_{\beta r}^2 \delta r, \ \ \rightarrow \ \delta r(t') = \delta r_i \sin[\omega_{\beta r}(t' - t) + \varphi] \ , \tag{5.20}$$

where $r - r_0 = \delta r_i \sin\varphi$. For future use we express the orbit so that $\mathbf{r}(t' = t) = \mathbf{r}$, where $(\mathbf{r}, t)$ is the point of observation. Also, we have

$$\frac{d\phi}{dt} = \frac{P_\phi + erA_\phi(r)}{m_e \gamma r^2} = \dot{\phi}(r_0) + \left.\frac{d\dot{\phi}}{dr}\right|_{r_0} \delta r + .. \ , \tag{5.21}$$

so that

$$\phi(t') = \phi + (t'-t)\dot{\phi}_0 + \frac{1}{\omega_{\beta r}}\frac{\partial\dot{\phi}_0}{\partial r}\bigg|_{r_0} \times$$
$$\left\{ -\delta r_i \cos[\omega_{\beta r}(t'-t)+\varphi] + \delta r_i \cos(\varphi) \right\}, \tag{5.22}$$

where $\partial\dot{\phi}/\partial r|_{r_0} = -\dot{\phi}_0/r_0$. For $\zeta \ll \gamma^2(\Delta r/r_0)$ and $\zeta^2 \ll 1$, we have $\partial\dot{\phi}/\partial r|_{r_0}/\omega_{\beta r} = -1/r_0$ to a good approximation. Because the E-layer is uniform in the $z-$direction,

$$z(t') = z + (t'-t)v_z \ . \tag{5.23}$$

The orbits are necessary for the stability analysis.

5.2.3 Configuration b

Here, we describe a Vlasov equilibrium for an axisymmetric, long, thin cylindrical layer of relativistic electrons where the electron motion is almost parallel to the magnetic field. The equilibrium distribution function f^0 is again taken to be given by Eq. (5.3) in terms of the Hamiltonian, H, and the canonical angular momentum, $P_\phi \equiv rp_\phi - erA_\phi(r)$, where $A_\phi = A^s_\phi$. We make the same assumptions as above, $\gamma^2 \gg 1$, $T/(m_e\gamma) \ll 1$, and $\Delta r^2/r_0^2 \ll 1$. In this case there is no external B_z field. Instead, we include an external toroidal magnetic field B^e_ϕ with corresponding vector potential A^e_z and an external electric field $\mathbf{E}^e$ with potential Φ^e. The fields $\mathbf{B}^e$ and $\mathbf{E}^e$ correspond to the magnetic and electric fields of a distant, charged, current-carrying flow along the axis. Thus, $|E^e_r| < |B^e_\phi|$. The considered external field is of course just one of a variety of fields which give electron motion almost parallel with the magnetic field. Note also that the distribution function is restricted in the respect that it does not include a dependence on the canonical momentum in the $z-$direction $P_z = m_e\gamma v_z - eA_z$.

The distribution function (5.3) gives $J_z = 0$ so that there is no toroidal self magnetic field. Thus the self-potentials in this case are also given by Eqs. (5.4) and (5.5). Eqs. (5.6) - (5.9) are also applicable with the replacement of Φ^s by the total potential Φ. In place of Eq. (5.10) we find

$$r_0 = \frac{m_e \gamma v_\phi^2}{(1-2\zeta) e E_r^e(r_0)} \approx \frac{m_e \gamma}{e E_r^e(r_0)}(1+2\zeta) \ , \tag{5.24}$$

where $\zeta \equiv B_z^s(r_0)/E_r^s(r_0)$. We again have $\zeta = r_e N/(\gamma L)$, where $r_e = e^2/(mc^2)$ is the classical electron radius and L is the axial length of the layer. Because $d^2\Phi^e/dr^2 = -(1/r)d\Phi^e/dr$, the radial betatron frequency is again given by Eq. (5.13) (with Φ now the total potential) so that the equilibrium orbits given in §5.2.2 also apply in this case. The electron motion is almost parallel to the magnetic field in that $(B_z^s/B_\phi^e)^2 = \zeta^2 (E_r^e/B_\phi^e)^2 < \zeta^2 \ll 1$. Notice that Eq. (5.24) for r_0 is formal in the respect that $E_r^e \propto 1/r$. Therefore, r_0 is in fact arbitrary in this case. Because the wavelengths of the unstable modes are found to be small compared with r_0, it may be interpreted as local radius of curvature of the magnetic field.

5.3 Linear Perturbation

We now consider a general perturbation of the Vlasov equation with $f(\mathbf{r}, \mathbf{p}, t) = f^0(\mathbf{r}, \mathbf{p}) + \delta f(\mathbf{r}, \mathbf{p}, t)$. To first order in the perturbation amplitude δf obeys

$$\left(\frac{\partial}{\partial t} + \mathbf{v} \cdot \frac{\partial}{\partial \mathbf{r}} + \frac{d\mathbf{p}}{dt} \cdot \frac{\partial}{\partial \mathbf{p}} \right) \delta f \equiv \frac{D\delta f}{Dt} = e(\delta \mathbf{E} + \mathbf{v} \times \delta \mathbf{B}) \cdot \frac{\partial f^0}{\partial \mathbf{p}} \ , \tag{5.25}$$

where $\delta \mathbf{E}$ and $\delta \mathbf{B}$ are the perturbations in the electric and magnetic fields. All scalar perturbation quantities are considered to have the dependencies

$$F(r) \exp(im\phi + ik_z z - i\omega t) \ , \tag{5.26}$$

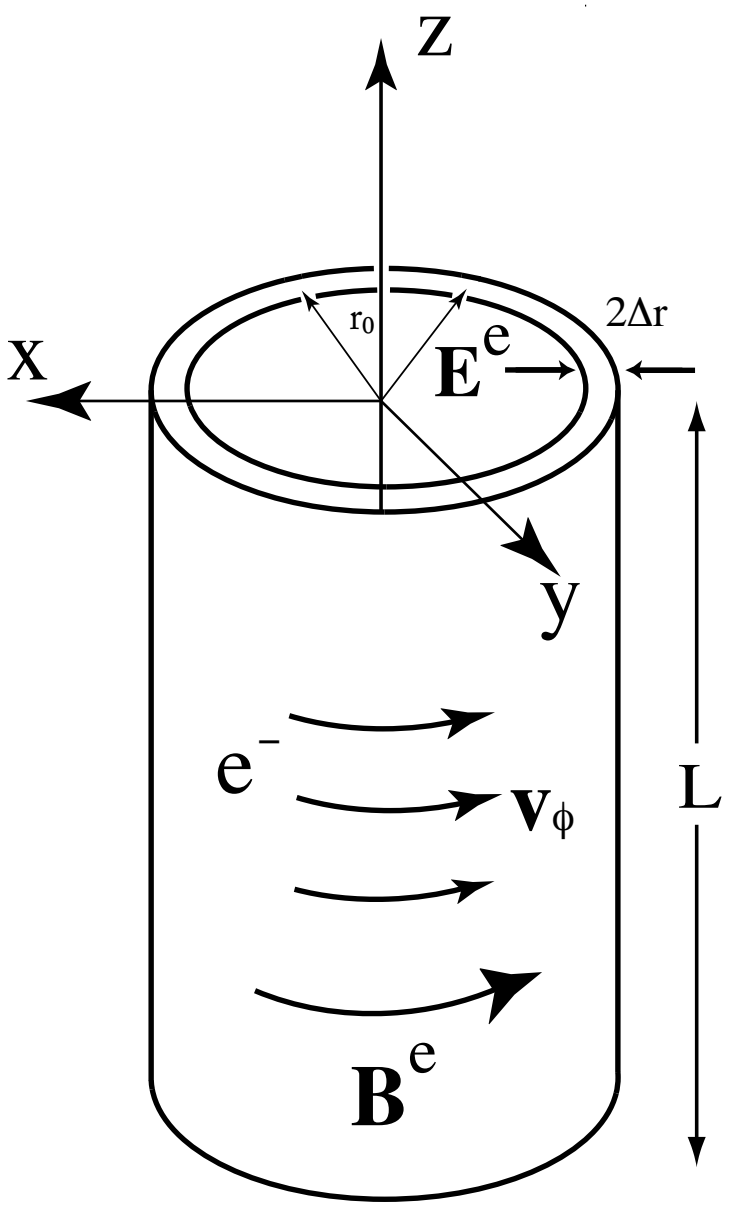

Figure 5.2: Geometry of relativistic E-layer for the case of an external toroidal magnetic field with an external radial electric field.

where the angular frequency ω is taken to have at least a small positive imaginary part which corresponds to a growing perturbation. This allows for a correct initial value treatment of the problem [63]. For a perturbation taken to vanish as $t \to -\infty$,

$$\delta f(\mathbf{r},\mathbf{p},t) = e\int_{-\infty}^{t} dt' \Big\{ \delta\mathbf{E}[\mathbf{r}(t'),t'] + \mathbf{v}(t')\times\delta\mathbf{B}[\mathbf{r}(t'),t'] \Big\} \cdot \frac{\partial f^0}{\partial \mathbf{p}} \ , \tag{5.27}$$

where the integration follows the orbit $[\mathbf{r}(t'),\mathbf{p}(t')]$ which passes through the phase-space point $[\mathbf{r},\mathbf{p}]$ at time t. For the considered axisymmetric equilibria,

$$\frac{\partial H}{\partial \mathbf{p}} = \frac{\mathbf{p}}{H} \tag{5.28}$$

$$\frac{\partial}{\partial \mathbf{p}} = \frac{\mathbf{p}}{H}\frac{\partial}{\partial H} = \frac{\mathbf{p}}{H}\frac{\partial P_\phi}{\partial H}\frac{\partial}{\partial P_\phi} \tag{5.29}$$

$$\frac{\partial f}{\partial \mathbf{p}} = \frac{\mathbf{p}}{H}\frac{\partial P_\phi}{\partial H}\left(\left.\frac{\partial f}{\partial P_\phi}\right|_H + \frac{\partial H}{\partial P_\phi}\left.\frac{\partial f}{\partial H}\right|_{P_\phi} \right) \tag{5.30}$$

since $f \equiv f(H,P_\phi)$ and $H \equiv H(P_\phi,\ldots)$

$$\frac{\partial}{\partial \mathbf{p}} = \mathbf{v}\left.\frac{\partial}{\partial H}\right|_{P_\phi} + r\hat{e}_\phi \left.\frac{\partial}{\partial P_\phi}\right|_H \tag{5.31}$$

$$\frac{\partial f^0}{\partial \mathbf{p}} = \frac{\mathbf{p}}{H}\left.\frac{\partial f^0}{\partial H}\right|_{P_\phi} + r\hat{\boldsymbol{\phi}}\left.\frac{\partial f^0}{\partial P_\phi}\right|_H \ , \tag{5.32}$$

where the partial derivatives are to be evaluated at constant P_ϕ and H, respectively. Thus, the right-hand side of Eq. (5.25) becomes

$$\begin{aligned} &e\left(-\frac{d\delta\Phi}{dt} + i\omega(\dot{\phi}\ \delta\Psi - \delta\Phi) + i\omega\mathbf{v}_\perp\cdot\delta\mathbf{A} \right)\frac{\partial f^0}{\partial H} + \\ &e\left(-\frac{d\delta\Psi}{dt} + im(\dot{\phi}\ \delta\Psi - \delta\Phi) + im\mathbf{v}_\perp\cdot\delta\mathbf{A} \right)\frac{\partial f^0}{\partial P_\phi} \ , \end{aligned} \tag{5.33}$$

where $\delta\mathbf{E} = -\nabla\delta\Phi - \partial\delta\mathbf{A}/\partial t$ and $\delta\mathbf{B} = \nabla\times\delta\mathbf{A}$, $\delta\Psi \equiv r\delta A_\phi$ is the perturbation in the flux function, $\mathbf{v}_\perp = (v_r, v_z)$, and $d/dt = \partial/\partial t + \mathbf{v}\cdot\nabla$. We assume the Lorentz gauge $\nabla\cdot\delta\mathbf{A} + \partial\delta\Phi/\partial t = 0$.

Evaluating Eq. (5.27) gives

$$\delta f = e \frac{\partial f^0}{\partial H}\left[-\delta\Phi + i\omega\int_{-\infty}^{t} dt'\left(\dot{\phi}'\delta\Psi' - \delta\Phi' + \mathbf{v}'_\perp\cdot\delta\mathbf{A}'\right)\right] \tag{5.34}$$

$$+ e\frac{\partial f^0}{\partial P_\phi}\left[-\delta\Psi + im\int_{-\infty}^{t} dt'\ \left(\dot{\phi}'\delta\Psi' - \delta\Phi' + \mathbf{v}'_\perp\cdot\delta\mathbf{A}'\right)\right]\ , \tag{5.35}$$

where the prime indicates evaluation at $[\mathbf{r}(t'), t']$. The integration is along the unperturbed particle orbit so that $\partial f^0/\partial H$ and $\partial f^0/\partial P_\phi$ are constants and can be taken outside the integrals. Note also that d/dt acting on a function of $(\mathbf{r}, t)$ is the same as D/Dt.

5.4 First Approximation

As a starting approximation we neglect (i) the radial oscillations in the orbits $[(\Delta r/r_0)^2 \ll 1]$, (ii) the self-field corrections to orbits proportional to ζ, (iii) the terms in δf proportional to $v_\perp^2$ ($v_{th}^2 \approx (\Delta r/r_0)^2 \ll 1$), (iv) we take $k_z = 0$ and (v) we assume the layer is very thin. Owing to approximation (iii), we can neglect the terms $\propto \mathbf{v}_\perp\cdot\delta\mathbf{A}$ in Eq. (5.35) in the evaluation of $\delta\rho$ and δJ_ϕ. This is because these terms give contributions to δf which are odd functions of v_r and v_z. Therefore, their average contribution can be neglected.

Evaluation of Eq. (5.35) gives

$$\delta f = -e\frac{\partial f^0}{\partial H}\bigg|_{P_\phi}\frac{\dot{\phi}(\omega\delta\Psi - m\delta\Phi)}{\omega - m\dot{\phi}} - e\frac{\partial f^0}{\partial P_\phi}\bigg|_{H}\frac{\omega\delta\Psi - m\delta\Phi}{\omega - m\dot{\phi}}\ , \tag{5.36}$$

where $\dot{\phi} = \dot{\phi}(r_0)$. The approximations lead to a closed system with potentials $(\delta\Phi,\ \delta\Psi)$ and sources $(\delta\rho,\ \delta J_\phi)$.

We have

$$\delta\rho = -e\int d^3p\ \delta f = -\frac{e}{r_0}\int dp_r dp_z dP_\phi\ \delta f\ ,$$

$$\delta J_\phi = -e\int d^3p\ v_\phi\delta f = -\frac{e}{r_0}\int dp_r dp_z dP_\phi\ v_\phi\delta f\ . \tag{5.37}$$

For the considered distribution function, Eq. (5.3), $\partial f^0/\partial H = -f^0/T$. The $\partial f^0/\partial P_\phi$ term in Eq. (5.36) can be integrated by parts. Furthermore, note that $\partial H/\partial P_\phi = \dot{\phi}$ and $\partial\dot{\phi}/\partial P_\phi = -(\dot{\phi})^2/H$, which corresponds to an effective "negative mass" for the particle's azimuthal motion [64, 5, 65]. From the partial integration the small term proportional to $\partial v_\phi/\partial P_\phi = v_\phi/(r_0 H^3)$ is neglected. Also note that H is not a constant when performing the integration over momenta. Evaluating this term by an integration by parts with a general function $g(P_\phi)$ in the integrand gives

$$\begin{aligned} & \int dP_\phi \left.\frac{\partial f^0}{\partial P_\phi}\right|_H g(P_\phi) = \\ - \quad & K \int dP_\phi \delta(P_\phi - P_0) \frac{\partial}{\partial P_\phi} \left[g(P_\phi) e^{-H/T} \right] = \\ - \quad & K \int dP_\phi \delta(P_\phi - P_0) \frac{\partial}{\partial P_\phi} \left[g(P_\phi) \right] e^{-H/T} \\ + \quad & \frac{K}{T} \int dP_\phi \delta(P_\phi - P_0) g(P_\phi) e^{-H/T} \frac{\partial H}{\partial P_\phi} \ . \end{aligned} \tag{5.38}$$

That is, the integration produces an additional term which cancels the $1/T$-term. Thus,

$$\int dP_\phi \delta f = -e \int dP_\phi \frac{f^0}{H} \ \frac{m\dot{\phi}^2(\omega\delta\Psi - m\delta\Phi)}{(\Delta\omega)^2} \ , \tag{5.39}$$

where $\Delta\omega \equiv \omega - m\dot{\phi}$. Integrating over the remaining momenta gives

$$(\delta\rho, \ \delta J_\phi) = (1, v_\phi) \ e^2 \ n(r) \frac{m\dot{\phi}^2}{H} \cdot \frac{(\omega\delta\Psi - m\delta\Phi)}{(\Delta\omega)^2} \ . \tag{5.40}$$

For a radially thin E-layer we may take

$$n(r) = n_0 \exp(-\delta r^2/2\Delta r^2) \rightarrow n_0 \sqrt{2\pi} \Delta r \ \delta(\delta r). \tag{5.41}$$

We comment on this approximation below in more detail when we include the radial wavenumber k_r of the perturbation. Then Eqs. (A.4) and (A.5) can be

written as

$$[\delta\Phi(r_0),\ \delta\Psi(r_0)] = \left[1,\ r_0 v_\phi(1+\Delta\tilde{\omega})\right]\ 2\pi^2 r_0\ Z \int dr\ \delta\rho(r)\ , \tag{5.42}$$

where $Z \equiv iJ_m(\omega r_0)H_m^{(1)}(\omega r_0)$, $\tilde{\omega} \equiv \omega/(m\dot{\phi})$ and $\Delta\tilde{\omega} \equiv \Delta\omega/(m\dot{\phi})$. Integrating Eq. (5.40) over the radial extent of the E-layer and canceling out the field amplitudes gives the dispersion relation

$$1 = 2\pi^2 r_0\ [n_0 e^2\sqrt{2\pi}\Delta r]\ Z\frac{m\dot{\phi}^2}{H}\cdot\frac{\omega r_0 v_\phi(1+\Delta\tilde{\omega}) - m}{(\Delta\omega)^2}\ . \tag{5.43}$$

In terms of dimensionless variables this becomes

$$1 = \pi\ \zeta\ Z\ \left(2\Delta\tilde{\omega} - \frac{1}{\gamma^2}\right)\frac{1}{(\Delta\tilde{\omega})^2}\ , \tag{5.44}$$

where $Z = iJ_m(m\tilde{\omega}v_\phi)H_m^{(1)}(m\tilde{\omega}v_\phi)$, $H_m^{(1)} = J_m + iY_m$, and the field-reversal parameter $\zeta = 4\pi e n_0 v_\phi \Delta r\sqrt{\pi/2}/B_z^e$ as given by Eq. (5.11).

For $m \gg 1$ approximation (B.2) can be used to give

$$\begin{aligned} J_m(m\tilde{\omega}v_\phi) &\approx (2/m)^{1/3}\mathrm{Ai}(w) \\ Y_m(m\tilde{\omega}v_\phi) &\approx -(2/m)^{1/3}\mathrm{Bi}(w), \end{aligned} \tag{5.45}$$

where

$$w = (m/2)^{2/3}(\gamma^{-2} - 2\Delta\tilde{\omega}). \tag{5.46}$$

Thus we have

$$Z = iJ_m H_m^{(1)} \approx (2/m)^{2/3}[\mathrm{Ai}(w)\,\mathrm{Bi}(w) + i\mathrm{Ai}^2(w)]. \tag{5.47}$$

Occasionally, $Z_m(w)$ is denoted by Z. For $|w|^2 \gg 1$ using (B.3)

$$Z \approx (2/m)^{2/3}/(2\pi|w|^{1/2}). \tag{5.48}$$

and for $|w|^2 \lesssim 0.5$ using (B.4)

$$Z \approx (2/m)^{2/3}[\sqrt{3}(c_1^2 - c_2^2 w^2) + i(c_1 - c_2 w)^2]. \tag{5.49}$$

For $|w|^2 \ll 1$,

$$Z \approx (0.347 + 0.200\ i)/m^{2/3}. \tag{5.50}$$

5.4.1 Range of Validity

We are interested in the regime where the wavelength of the emitted radiation is comparable to the "bunch length", i.e. $\omega \approx m$ or equivalently $\Delta\tilde{\omega} \ll 1$. However, Eq. (5.44) is only valid if $\Delta\tilde{\omega} \ll \gamma^{-2}$. Since we neglected δJ_r and δJ_z we obtain from the continuity equation $\delta J_\phi = \frac{\omega r_0}{m}\delta\rho$. Due to this approximation the factor on the right hand side can become bigger than the speed of light if $\Delta\tilde{\omega} > \gamma^{-2}$ which leads to unphysical results. In the latter case $\delta J_\phi = v_\phi \delta\rho$ is a better approximation. Fortunately, $\Delta\tilde{\omega} \ll \gamma^{-2}$ is the most interesting case and in the remainder of this paper we will always work in this limit. Furthermore, for the continuum approximation to be valid the mean particle distance has to be much smaller than the wavelength.

5.4.2 Growth Rates

It will prove useful to define two characteristic values of m: $m_1 \equiv \zeta^{3/2}\gamma^3$ and $m_2 = 2\gamma^3$, and therefore $m_1 = \zeta^{3/2} m_2/2$. We can obtain approximate solutions to Eq. (5.44) in two different cases. There may be solutions with small values of $\gamma^2\Delta\tilde{\omega}$, so that $w \simeq (m/m_2)^{2/3}$. In this case, Eq. (5.44) becomes a simple quadratic equation, which can be solved for $\Delta\tilde{\omega}$. We can simplify the solution somewhat by

changing variables to $\sigma \equiv \gamma^2 \Delta\tilde{\omega}$ in which case Eq. (5.44) can be written in the form

$$1 = \frac{\pi\zeta Z_m \gamma^2}{\sigma^2}(\sigma - 1) \approx -\frac{\pi\zeta Z_m \gamma^2}{\sigma^2},$$

where we have neglected σ compared to one in the approximate version of this equation. We find that

$$\sigma \simeq \sqrt{-\pi\zeta Z_m \gamma^2}\ . \tag{5.51}$$

For case I let us assume that $m \ll m_2$, in which case Eq. (5.51) implies

$$\sigma \simeq \pm 1.121 (m_1/m)^{1/3}\ e^{i(7\pi/12)}$$

$$= 1.121(m_1/m)^{1/3}(-0.2588 + 0.9659i)\ . \tag{5.52}$$

so $|\sigma| \ll 1$ for $m \gg m_1$. The growth rate of the unstable mode is

$$\omega_i \simeq \frac{1.083\zeta^{1/2} m^{2/3}\dot{\phi}}{\gamma} \tag{5.53}$$

in this regime. For case II we assume that $m \gg m_2$, in which case Eq. (5.51) implies

$$\sigma = \pm\frac{i\zeta^{1/2}\gamma^{3/2}}{m^{1/2}} = \pm i\zeta^{1/2}(m_2/2m)^{1/2}$$

$$\omega_i \simeq \frac{\zeta^{1/2} m^{1/2}\dot{\phi}}{\gamma^{1/2}}\ ; \tag{5.54}$$

note that the growth rates in cases I and II match almost exactly at $m = m_2$, where $|\sigma| \approx \zeta^{1/2}$.

Note that $m_2\dot{\phi}$ is the approximate frequency of the peak of the single particle synchrotron radiation spectrum. For more accurate results we employ a numerical method for solving Eq. (5.44) outlined in [66]. This method also allows us to count the number of roots which are enclosed by a contour. The basic idea is that for a

null-homotopic cycle Γ which does not cross any poles or roots and a meromorphic function f which is not constant [67]

$$N(0) = \frac{1}{2\pi i}\int_{\Gamma}\frac{f'(\zeta)}{f(\zeta)}d\zeta \tag{5.55}$$

where $N(0)$ is the number of roots minus the number of poles enclosed by Γ (an n-th order root or pole counts as n roots or n poles, respectively). So far we have no numerical evidence of the existence of more than one solution with a positive real part. The numerical results agree very well with our approximations even if $m < m_1$ and are shown in Fig. 5.3.

5.4.3 Comparison with Goldreich and Keeley

Goldreich and Keeley [20] find a radiation instability in a thin ring of relativistic, monoenergetic, zero temperature electrons constrained to move in a circle of fixed radius. Under the condition $1 \ll m^{1/3} \ll \gamma$ their growth rate is $\omega_i \approx 1.16\dot{\phi}\, m^{2/3}[r_e N/(\gamma^3 r_0)]^{1/2}$ which is close to our growth rate with L replaced by r_0.

5.5 Nonlinear Saturation

Clearly the rapid exponential growth of the linear perturbation can continue only for a finite time. We analyze this by studying the trapping of electrons in the moving potential wells of the perturbation. For $(\Delta r/r_0)^2 \ll 1$, the electron orbits can be treated as circular. The equation of motion is

$$\frac{dP_\phi}{dt} = r\delta F_\phi\ , \quad \delta F_\phi = -e[\delta E_\phi + (\mathbf{v}\times\delta\mathbf{B})_\phi]\ , \tag{5.56}$$

where P_ϕ is the canonical angular momentum, where

$$\delta F_\phi = -e\delta E_{\phi 0}\exp(\omega_i t)\cos(m\phi - \omega_r t)\ , \tag{5.57}$$

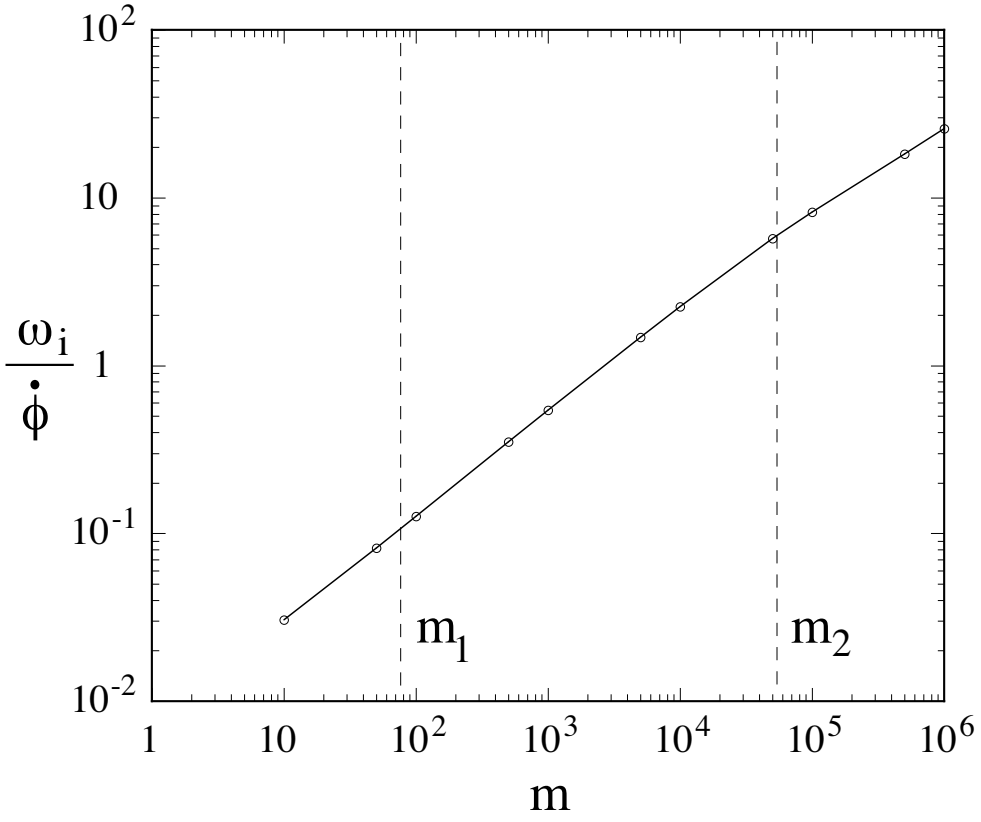

Figure 5.3: The graph shows the frequency dependence of the growth rate for a sample case where $\gamma = 30$ and $\zeta = 0.02$ obtained from our approximations for Eq. (5.44). For these parameters, $m_1 \approx 10^2$ and $m_2 \approx 2.7 \times 10^4$.

where $\delta E_{\phi 0}$ is the initial value of the potential, $\omega_r \equiv \mathrm{Re}(\omega)$, and $\omega_i \equiv \mathrm{Im}(\omega)$.

For a relativistic particle in a circular orbit,

$$\delta P_\phi = m_{e*} r_0^2 \delta\dot{\phi}, \quad \text{where } m_{e*} = \frac{-m_e\gamma^3}{\gamma^2 - 1} \approx -m_e\gamma, \tag{5.58}$$

where m_{e*} is the "effective mass," which is negative, for the azimuthal motion of the electron ([64, 5] or [65], p.68). Combining Eqs. (5.56) and (5.58) gives

$$\frac{d^2\varphi}{dt^2} = -\omega_T^2(t)\sin\varphi\ , \tag{5.59}$$

where $\varphi \equiv m\phi - \omega_t t + \frac{3}{2}\pi$, $\omega_T \equiv \omega_{T0}\exp(\omega_i t/2)$, and $\omega_{T0} \equiv [em\delta E_{\phi 0}/(m_e\gamma r_0)]^{1/2}$, where ω_T is termed the "trapping frequency." At the "bottom" of the potential well of the wave, $\sin\varphi \approx \varphi$. An electron oscillates about the bottom of the well with an angular frequency $\sim \omega_T$. This is of course a nonlinear effect of the finite wave amplitude. A WKBJ solution of Eq. (5.58) gives

$$\varphi \propto \omega_{T0}^{-1/2}\exp(-\omega_i t/4)\sin\left\{(2\omega_{T0}/\omega_i)[\exp(\omega_i t/2) - 1]\right\}\ . \tag{5.60}$$

The exponential growth of the linear perturbation will cease at the time t_{sat} when the particle is turned around in the potential well. This condition corresponds to $\omega_T(t_{sat}) \approx \omega_i$. Thus, the saturation amplitude is

$$\left|\delta E_{sat}\right|^2 = \left(\frac{m_e\gamma}{er_0 m}\right)^2\left(\frac{\omega_i(m)}{\dot{\phi}}\right)^4\ , \tag{5.61}$$

where $|\delta E_{sat}| \equiv |\delta E(t_{sat})| = |\delta E_0|\exp(\omega_i t_{sat})$.

5.6 First Approximation with $k_z \neq 0$

Here, we consider $k_z \neq 0$ but keep the other approximations. Our ansatz for δf is general enough to handle this case since it retains the biggest contribution to the

Lorentz force in the z-direction which is of the order $v_\phi B_r$. In place of Eq. (5.39) we obtain

$$\int dP_\phi \delta f = -e \int dP_\phi \frac{f^0}{H} \frac{m\dot{\phi}^2(\omega\delta\Psi - m\delta\Phi)}{(\omega - m\dot{\phi} - k_z v_z)^2} , \tag{5.62}$$

where we assume without loss of generality $k_z > 0$ and $k_z \ll m/r_0, \omega$. In place of Eq. (5.44) we find

$$\varepsilon(\omega, k_z) = 1 + k_z A(\omega, k_z) \int_{-\infty}^{\infty} dv_z \frac{\exp(-v_z^2/2v_{th}^2)}{\sqrt{2\pi}\, v_{th}} [...] = 0, \tag{5.63}$$

where

$$[...] \equiv -\frac{m\dot{\phi}}{(\omega - m\dot{\phi} - k_z v_z)^2} .$$

Here, ε acts as an effective dielectric constant for the E-layer, and

$$A(\omega, k_z) \equiv \pi\ \zeta\ Z(\omega, k_z)\ \left(u - \frac{k_\phi}{k_z \gamma^2}\right), \quad u \equiv \frac{\omega - m\dot{\phi}}{k_z} ,$$

$$Z \equiv i J_m[r_0(\omega^2 - k_z^2)^{1/2}]\ H_m^{(1)}[r_0(\omega^2 - k_z^2)^{1/2}] , \tag{5.64}$$

and $k_\phi = m/r_0$ is the azimuthal wavenumber. The expression for Z is from §5.4. An integration by parts gives

$$\varepsilon(u) = 1 + A(\omega) \int dv_z \frac{\exp(-v_z^2/2v_{th}^2)}{\sqrt{2\pi}\, v_{th}^3} \frac{m\dot{\phi} v_z/k_z}{v_z - u} , \tag{5.65}$$

where the k_z dependence of ε and A is henceforth implicit. We can also write this equation as

$$\varepsilon(u) = 1 + B(u) \left[1 + \frac{u}{v_{th}} F\left(\frac{u}{v_{th}}\right)\right] , \tag{5.66}$$

where

$$B(u) \equiv \frac{\pi}{v_{th}^2}\ \zeta\ Z\ \frac{k_\phi}{k_z}\left(u - \frac{k_\phi}{k_z \gamma^2}\right) , \tag{5.67}$$

and

$$F(z) \equiv \frac{1}{\sqrt{2\pi}} \int_{-\infty}^{\infty} dx \; \frac{\exp(-x^2/2)}{x - z} \; ,$$

for $\mathrm{Im}(z) > 0$, and

$$F(z) \equiv \frac{1}{\sqrt{2\pi}} \int_{-\infty}^{\infty} dx \; \frac{\exp(-x^2/2)}{x - z} + i\sqrt{2\pi} \exp\left(-\frac{z^2}{2}\right) \; ,$$

for $\mathrm{Im}(z) < 0$. The second expression for $F(z)$ is the analytic continuation of the first expression to $\mathrm{Im}(z) < 0$ which corresponds to wave damping (see, e.g., [68], ch. 5). Note that terms of order $\Delta\tilde{\omega}$ have been omitted.

For $m \gg 1$, the factor $Z = iJ_m(J_m + iY_m)$ can be expressed in terms of Airy functions in a way similar to that done in §5.5. One finds $J_m[r_0(\omega^2 - k_z^2)^{1/2}] \approx (2/m)^{1/3}\mathrm{Ai}(w)$, $Y_m[r_0(\omega^2 - k_z^2)^{1/2}] \approx -(2/m)^{1/3}\mathrm{Bi}(w)$,

$$Z_r \approx \left(\frac{2}{m}\right)^{2/3} \mathrm{Ai}(w)\mathrm{Bi}(w) \; , \; Z_i \approx \left(\frac{2}{m}\right)^{2/3} \mathrm{Ai}^2(w) \; , \tag{5.68}$$

where

$$\tan\psi \equiv \frac{k_z}{k_\phi} \; , \; w \equiv \left(\frac{m}{2}\right)^{2/3} \left(\frac{1}{\gamma^2} + \tan^2\psi - 2u\tan\psi\right) \; .$$

It is clear that ε has in general a rather complicated dependence on $u = u_r + iu_i$ and $\tan\psi$. Note that the expression for w goes over to our earlier w for $\psi = 0$ noting that $u\tan\psi \to \Delta\tilde{\omega}$.

A limit where Eq. (5.66) can be solved analytically is for $|u|^2 = |\Delta\tilde{\omega}|^2/\tan^2\psi \gg v_{th}^2$, that is, for sufficiently small $\tan\psi$. In this limit Eq. (5.66) can be expanded as an asymptotic series $F(z) = -1/z - 1/z^3 - 3/z^5 - ...$ Keeping just the first three terms of the expansion gives

$$\varepsilon = 1 + \pi\zeta Z \left(1 + \frac{3v_{th}^2 \tan^2\psi}{(\Delta\tilde{\omega})^2}\right) \frac{\gamma^{-2}}{(\Delta\tilde{\omega})^2} = 0. \tag{5.69}$$

For $\tan\psi \to 0$ and $\Delta\tilde{\omega} \ll \gamma^{-2}$, this is the same as Eq. (5.44) as it should be. In general Eq. (5.69) will have more than one unstable mode. In the remainder of this

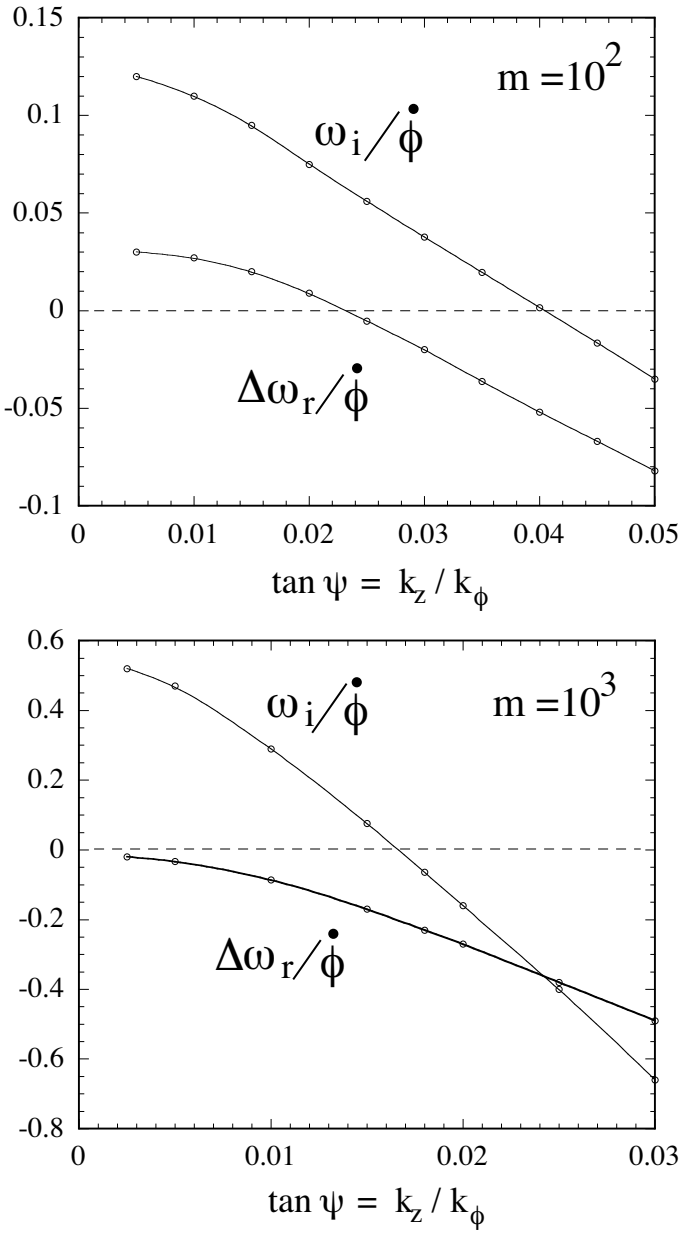

Figure 5.4: The figure shows the growth / damping rate ω_i and real part of the frequency $\Delta\omega_r = \omega - m\dot{\phi}$ in units of $\dot{\phi}$ as a function of $\tan\psi = k_z/k_\phi$ for $m = 100$ and $m = 1000$ for an E-layers with $\gamma = 30$, $\zeta = 0.02$ and $v_{th} = 30/\gamma^2$. In the region of damping $\omega_i < 0$, the second expression for $F(z)$ in Eq. (5.66) is used.

paragraph we will only study the largest unstable solution for which we recover the growth rates found in §5.4 in the limit $\tan\psi \to 0$. Fig. 5.4 shows some sample solutions. For the case shown the u dependence of Z is negligible.

General solutions of Eq. (5.66) can be obtained using the Newton-Raphson method ([69], ch. 9) where an initial guess of (u_r, u_i) gives (ϵ_r, ϵ_i). This guess is incremented by an amount

$$\begin{bmatrix} \delta u_r \\ \\ \delta u_i \end{bmatrix} = \begin{bmatrix} \partial\epsilon_r/\partial u_r & \partial\epsilon_r/\partial u_i \\ \\ \partial\epsilon_i/\partial u_r & \partial\epsilon_i/\partial u_i \end{bmatrix}^{-1} \begin{bmatrix} -\epsilon_r \\ \\ -\epsilon_i \end{bmatrix} , \tag{5.70}$$

and the process is repeated until $\varepsilon_r = 0$ and $\varepsilon_i = 0$. Fortunately, the convergence is very rapid and gives $|\varepsilon| < 10^{-10}$ after a few iterations.

Fig. 5.4 shows the dependence of the complex wave frequency on the tangent of the propagation angle, $\tan\psi = k_z/k_\phi$, for a sample cases. The maximum growth rate is for $\psi = 0$ or $k_z = 0$. With increasing ψ the growth rate decreases, and for ψ larger than a critical angle ψ_{cr} there is damping. For the damping the second expression for F in Eq. (5.66) must be used. Roughly, we find that the critical angle corresponds to having the wave phase velocity in the $z-$direction of the order of the thermal spread in this direction, that is, $u_r = \Delta\omega_r/k_z \sim v_{th}$. This gives

$$\tan\psi_{cr} \sim \frac{\sqrt{\zeta}}{v_{th}\gamma\ m^{1/3}} = \left(\frac{r_e N}{v_{th}^2\gamma^3 L}\right)^{1/2} \frac{1}{m^{1/3}} \leq \frac{1}{\gamma^2 v_{th}} , \tag{5.71}$$

for $m_1 < m < m_2$. Note that the dimensionless parameter which determines the cut-off at $\tan\psi_{cr}$ is $\gamma^2 v_{th}$. Our numerical calculations of ψ_{cr} give a slightly faster dependence, $\tan\psi_{cr} \propto 1/m^{0.40}$ for this range of m. Fig. 5.5 shows the m-dependence of the critical angle. It is reasonable to assume that in a particle accelerator the weak focusing in the z-direction sets a low limit on k_z.

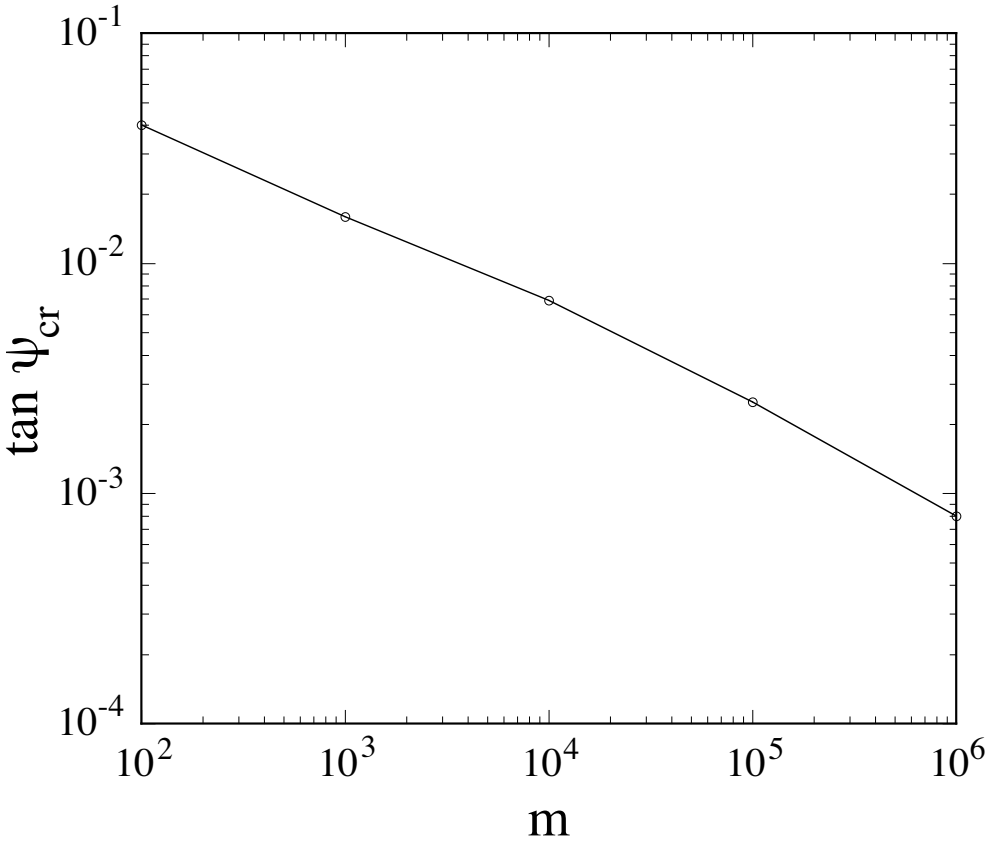

Figure 5.5: Critical angle for $\gamma = 30$, $\zeta = 0.02$ and $v_{th} = 30/\gamma^2$.

5.7 Nonlinear Saturation for $k_z \neq 0$

We generalize the results of §5.6 by including the axial as well as the azimuthal motion of the electrons in the wave. The axial equation of motion is

$$\begin{aligned} m_e\gamma\frac{d^2z}{dt^2} &= -e\left[\delta E_z + (\mathbf{v}\times\delta\mathbf{B})_z\right] \\ &\approx -e\delta E_{z0}\exp(\omega_i t)\cos(m\phi + k_z z - \omega t)\ . \end{aligned} \tag{5.72}$$

The approximation involves neglecting the force $\propto v_r\delta B_\phi$ which is valid for a radially thin layer ($\Delta r^2/r_0^2 \ll 1$). Following the development of §5.6, the azimuthal equation of motion is

$$m_e\gamma r_0\frac{d^2\phi}{dt^2} = -e\delta E_{z0}\cos(m\phi + k_z z - \omega t)\ . \tag{5.73}$$

Combining Eqs. (5.72) and (5.73) gives

$$\frac{d^2\varphi}{dt^2} = -\ \frac{e\ m\delta E_{\phi 0}}{m_e\gamma r_0}\left(1+\tan^2\psi\right)\sin\varphi\ , \tag{5.74}$$

where $\varphi \equiv m\phi + k_z z - \omega t + \frac{3}{2}\pi$ and $\tan\psi = k_z/k_\phi$. Because $\psi^2 \ll 1$ for wave growth (Eq. (5.71)), the saturation wave amplitude δE_{sat} is again given by Eq. (5.61).

5.8 Thick Layers Including Radial Betatron Oscillations

5.8.1 The Limit $k_r\Delta r \gg 1$

In this section we include the small but finite radial thickness of the E-layer. We keep the other approximations mentioned at the beginning of §5.4. In particular we consider $k_z = 0$. In order to include the layer's radial thickness, we consider the wave equations within the E-layer,

$$\begin{aligned} (\nabla^2 + \omega^2)\delta\Phi &= -4\pi\delta\rho\ , \\ (\tilde{\nabla}^2 + \omega^2)\delta\Psi &= -4\pi r\delta J_\phi\ , \end{aligned} \tag{5.75}$$

where

$$\tilde{\nabla}^2 \equiv \frac{\partial^2}{\partial r^2} - \frac{1}{r}\frac{\partial}{\partial r} - \frac{m^2}{r^2} + \frac{\partial^2}{\partial z^2} \ , \tag{5.76}$$

is the adjoint Laplacian operator.

Within the E-layer, we assume that the potentials can be written in a WKBJ expansion as

$$(\delta\Phi,\ \delta\Psi) = (K_\Phi,\ K_\Psi) \exp\left[im\phi + ik_r(r - r_0) - i\omega t\right] \ , \tag{5.77}$$

where k_r is the radial wavenumber with $(k_r \Delta r)^2 \gg 1$ (K_Φ, K_Ψ) are constants. This is equivalent to assuming that the charge density is constant between $r_0 - \Delta r$ and $r_0 + \Delta r$ and zero elsewhere. Evaluation of the time integrals in Eq. (5.35) for $r = r_0$ gives

$$e^{-iz\sin t} = \sum_{n=-\infty}^{\infty} e^{-int} J_n(z) \tag{5.78}$$

$$\begin{aligned}
&\int_{-\infty}^{t} dt' \delta\Phi e^{-i\omega t' + im\phi' + ik_r r'} = \\
&\int_{-\infty}^{t} dt' \delta\Phi \exp\left\{-i\omega t' + im\left[\phi + (t'-t)\dot{\phi}_0 - \right.\right. \\
&\left.\left.\frac{\delta r_i}{r_0}\left(-\cos[\omega_{\beta r}(t'-t)] + 1\right)\right] + ik_r \delta r_i \sin(\omega_{\beta r}(t'-t)) + ik_r r_0\right\} \\
&= \int_{-\infty}^{t} dt' \delta\Phi e^{-i\omega t' + im\dot{\phi}_0 + ik_r r_0 - im\frac{\delta r_i}{r_0}} \sum_{n=-\infty}^{\infty} e^{-in\omega_{\beta r} t'} J_n(-k_r \delta r_i)
\end{aligned} \tag{5.79}$$

$$\int_{-\infty}^{t} dt' \delta\Phi' = \delta\Phi(r_0, t) \sum_{n=-\infty}^{\infty} \frac{J_n(k\delta r_i) i^n \exp(-ik_\phi \delta r_i - in\psi)}{i(m\dot{\phi} + n\omega_{\beta r} - \omega)} \ , \tag{5.80}$$

where n is an integer, $k \equiv (k_r^2 + k_\phi^2)^{1/2}$, with $k_\phi = m/r_0$, and $\tan\psi \equiv k_r/k_\phi$. There is an analogous expression for the integral of $\delta\Psi$. We have used Eq. (5.20) for the

radial motion with $\varphi = 0$ assuming $\zeta^2 \ll 1$ and $\zeta \ll \gamma^2(\Delta r/r_0)$ so that $\omega_{\beta r} = 1/r_0$, and Eq. (5.22) for the ϕ-motion with $\partial\dot{\phi}_0/\partial r|_{r_0}/\omega_{\beta r} = -1/r_0$. Using Eqs. (5.35) and (5.80), the momentum space integrals (5.37) can be done to give

$$\left(eKe^{-H/T}\right)^{-1}\int dP_\phi \delta f = -\frac{m\dot{\phi}^2}{H}\frac{\omega K_\Psi - mK_\Phi}{(m\dot{\phi}-\omega)^2} +$$
$$\frac{1}{T}(K_\Psi\dot{\phi}-K_\Phi)\left\{J_0(k\delta r_i) - 1 + (m\dot{\phi}-\omega)\sum_{n=-\infty}^{\infty}{}' \frac{i^n e^{-in\psi - ik_\phi \delta r_i} J_n(k\delta r_i)}{m\dot{\phi}+n\omega_{\beta r}-\omega}\right\} -$$
$$\frac{m\dot{\phi}^2}{H}m(K_\Psi\dot{\phi}-K_\Phi)\left\{\frac{J_0(k\delta r_i)-1}{(m\dot{\phi}-\omega)^2} + \sum_{n=-\infty}^{\infty}{}' \frac{i^n e^{-in\psi - ik_\phi \delta r_i} J_n(k\delta r_i)}{(m\dot{\phi}+n\omega_{\beta r}-\omega)^2}\right\}, \quad (5.81)$$

and finally if $\Delta\tilde{\omega} \ll \gamma^{-2}$

$$\delta\rho \approx \frac{e^2 n_0 m\dot{\phi}^2 K_\Phi}{H}\left(\frac{r_0^2\dot{\phi}\omega - m[1-(1-F_0)/\gamma^2]}{(\omega - m\dot{\phi})^2} - \frac{m}{\gamma^2}\sum_{n=-\infty}^{\infty}{}' \frac{F_n}{(m\dot{\phi}+n\omega_{\beta r}-\omega)^2}\right). \quad (5.82)$$

The prime on the sums indicate that the $n = 0$ term is omitted. Here,

$$F_n \equiv \frac{i^n \exp(-in\psi)}{\sqrt{2\pi}\chi}\int_{-\infty}^{\infty} d\xi\ J_n(\xi)\exp\left(-\frac{\xi^2}{2\chi^2} - i\frac{k_\phi \xi}{k}\right), \quad (5.83)$$

with

$$\chi \equiv k\Delta r\ . \quad (5.84)$$

The $1/T$ terms in Eq. (5.82) do not cancel exactly. They may be neglected if

$$|\Delta\tilde{\omega}|^2 \ll F_0 v_{th}^2 \quad (5.85)$$

for the $n = 0$ term or if

$$|\Delta\tilde{\omega}||n/m - \Delta\tilde{\omega}| \ll v_{th}^2 \quad (5.86)$$

for the $n \neq 0$ terms.

For weak E-layers we have for $\chi \to 0$, $F_0 \to 1$ and $F_{n\neq 0} \to 0$. In this limit we recover the results of §5.4. For $\chi \gg 1$ and $1 \ll k_r r_0 \ll k_\phi r_0$, the Gaussian factor

in the integrand of F_n can be neglected so that one obtains

$$F_n \approx i^n e^{-in\psi} \frac{1}{\sqrt{2\pi}\chi} \frac{2k}{|k_r|} \cos\left(\frac{n\pi}{2}\right) \ , \quad \text{even } n \ ,$$

$$F_n \approx -i^n e^{-in\psi} \frac{1}{\sqrt{2\pi}\chi} \frac{2ik}{|k_r|} \sin\left(\frac{n\pi}{2}\right) \ , \quad \text{odd } n \ . \tag{5.87}$$

An alternative approximation for F_n can be obtained by using the integral representation of the Bessel function. The remaining integral can then be computed numerically more easily. In this way we find

$$F_n = \frac{i^n e^{-in\psi}}{2\pi} \int_{-\pi}^{\pi} d\theta \exp\left[-in\theta - (\chi^2/2)(k_\phi/k - \sin\theta)^2\right] \ . \tag{5.88}$$

For $\chi \gg 1$, $1 \ll (k_\phi/k_r)^2$ and $|n| < \sqrt{\chi}$ we can approximate $\sin\theta$ in the exponent by a parabola at its maximum. We obtain

$$F_n \approx \frac{i^n e^{-in\psi}}{2^{3/4}\Gamma\left(\frac{3}{4}\right)\sqrt{\chi}} \ . \tag{5.89}$$

In general $F_n/(i^n e^{-in\psi})$ decreases as χ and n increase. This acts to prevent the unlimited increase of the growth rate as $m \longrightarrow \infty$, and it ensures that the sums over n converge. Fig. 5.6 shows a plot of F_0 obtained by numerical evaluation of Eq. (5.88).

Within the E-layer, Eq. (5.75) gives

$$k_r^2 = \omega^2 - \frac{m^2}{r_0^2} + \frac{4\pi e^2 n_0 m \dot{\phi}^2}{H}$$
$$\times \left(\frac{r_0^2 \dot{\phi}\omega - m[1-(1-F_0)/\gamma^2]}{(\omega - m\dot{\phi})^2} - \frac{m}{\gamma^2} {\sum_n}' \frac{F_n}{(m\dot{\phi} + n\omega_{\beta r} - \omega)^2} \right) \ . \tag{5.90}$$

In terms of dimensionless variables this equation becomes

$$\bar{k}_r^2 = 2m^2 \Delta\tilde{\omega} - \frac{m^2}{\gamma^2} + \frac{\zeta\sqrt{2}}{v_\phi v_{th}\sqrt{\pi}}$$
$$\times \left(\frac{(1+\Delta\tilde{\omega})(1-\gamma^{-2}) - [1+(F_0-1)/\gamma^2]}{(\Delta\tilde{\omega})^2} - \frac{1}{\gamma^2} {\sum_n}' \frac{F_n}{(v_\phi^{-1} n/m - \Delta\tilde{\omega})^2} \right) \ , \tag{5.91}$$

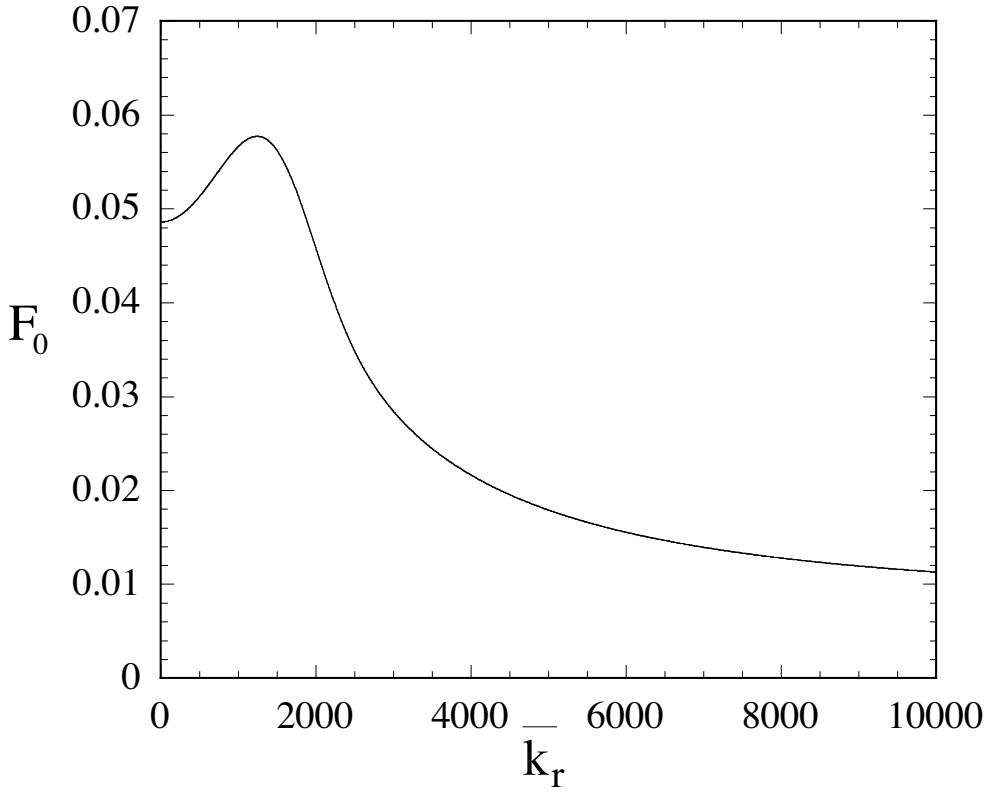

Figure 5.6: F_0 for $v_{th} = 0.01$ and $k_\phi r_0 = 10^4$

where $\bar{k}_r \equiv r_0 k_r$, $\bar{k}_\phi \equiv r_0 k_\phi$, $\bar{k} \equiv r_0 k$, and $\chi = \bar{k} v_{th}$.

Notice that Eq. (5.77) can also be written as

$$\delta\Phi = C_2 \sin\left[k_r(r - r_0)\right] + C_3 \cos\left[k_r(r - r_0)\right] \ , \tag{5.92}$$

for $r_0 - \Delta r \leq r \leq r_0 + \Delta r$. For $r \leq r_0 - \Delta r$, we have

$$\delta\Phi = C_1 J_m(\omega r) \ , \tag{5.93}$$

since the potential must be well behaved as $r \to 0$. For $r \geq r_0 + \Delta r$, we must have

$$\delta\Phi = C_4\left[J_m(\omega r) + iY_m(\omega r)\right] \ . \tag{5.94}$$

This combination of Bessel functions gives $\delta\Phi(r \to \infty) \to 0$ for the assumed conditions where $\mathrm{Im}(\omega) > 0$. Note that these potentials are just the solutions of Eq. (5.75) in our approximation for $\delta\rho$. The eigenvalue problem can now be solved by matching the boundary conditions. However, we have not solved the full eigenvalue problem. Instead we consider unstable solutions with the restriction that $k_r \Delta r \gg 1$. Under this condition we can interpret Eq. (5.91) as a local dispersion relation. Unstable modes found from Eq. (5.91) will need a slight correction in order to satisfy the boundary conditions.

We expect that Eq. (5.91) has solutions near each betatron resonance at $\Delta\tilde{\omega} = \pm n/m$. This is a familiar concept in the treatment of resonances in storage rings (cf. [16] or [39]). We extract each solution by summing over a single value of n and $-n$ only and obtain from Eq. (5.91) for the case $n \neq 0$ and $\Delta\tilde{\omega} \ll \gamma^{-2}$

$$\Xi \equiv -\frac{\gamma^2 v_{th}\sqrt{\pi}\left(\bar{k}_r^2 + m^2\gamma^{-2}\right)}{\zeta\sqrt{2}} = \frac{F_{-n}}{\left(\frac{n}{m} + \Delta\tilde{\omega}\right)^2} + \frac{F_n}{\left(\frac{n}{m} - \Delta\tilde{\omega}\right)^2} \ .$$

Thus,

$$\Delta\tilde{\omega} \approx \frac{F_{-n} - F_n}{\Xi} \pm \frac{n}{m} \tag{5.95}$$

for sufficiently big Ξ, i.e. we expect the imaginary part of $\Delta\tilde{\omega}$ to be negligible for the $n \neq 0$ modes. Despite a lot of effort we were not able to prove this statement under more relaxed conditions.

We can easily find an analytic solution of Eq. (5.91) for the case where the $n = 0$ term is dominant. If $|\Delta\tilde{\omega}| \ll 1/\gamma^2$ and $|\Delta\tilde{\omega}| \ll F_0/\gamma^2$, we obtain

$$\Delta\tilde{\omega} = \pm\frac{2^{1/4}\sqrt{-\zeta F_0}}{\pi^{1/4}\sqrt{v_{th}(m^2 + \gamma^2\bar{k}_r^2)}} \tag{5.96}$$

The dependence of the growth rate on k_r becomes significant when $\gamma^2\bar{k}_r^2/m^2$ is comparable to unity. For $m \sim m_2 \sim \gamma^3$, we see that this happens when $(k_r\Delta r)^2/\gamma^4 v_{th}^2 \sim 1$, which involves the combination $\gamma^2 v_{th}$ again.

The growth rate of Eq. (5.96) is proportional to $\sqrt{\zeta}$. This implies from §5.5 that the emitted power scales as the square of the number of particles in the E-layer which corresponds to coherent radiation. Sample results are shown in Fig. 5.7. We conclude that the main effect of the betatron oscillations is an indirect one. The radial motion itself is unimportant for the interaction. However, the influence of the radial motion on the time dependence of the azimuthal angle ϕ of a particle is important since a shift in ϕ can take the particle out of coherence with the wave. This effect is accounted for by F_0.

5.8.2 Qualitative Analysis of the Effect of the Betatron Motion

Let us suppose that $v_{th} \gg 1/\gamma^2$, and that $|\Delta\tilde{\omega}|$ is not necessarily small compared with v_{th} (We can still assume $|\Delta\tilde{\omega}| \ll 1$ without requiring the more restrictive condition $\gamma^2|\Delta\tilde{\omega}| \ll 1$.). The key effect of the betatron oscillations is to "wash out" the phase coherence of the response within the layer; for a cold layer, all

orbiting particles move in "lock step", which is particularly favorable for a bunching instability. Let us suppose that $|\Delta\tilde{\omega}|$ has a real part that is substantially larger than $1/\gamma^2$. The response in the layer scales as an Airy function with argument $w(1+\xi)$ where $|\xi| < v_{th}$. The phase accumulated across the layer thickness $\sim v_{th} r_0$ is $\eta \sim m v_{th}^{3/2}$ if $\Delta\tilde{\omega}_r \ll v_{th}$ and $\eta \sim m v_{th}^{3/2}(\Delta\tilde{\omega}_r/v_{th})^{1/2}$ if $\Delta\tilde{\omega}_r \gg v_{th}$. Large η ought to imply substantial decoherence of the response in the layer. We see that this is likely irrespective of the value of $\Delta\tilde{\omega}_r/v_{th}$ provided that $m \gg v_{th}^{-3/2}$, i.e. for $m/\gamma^3 \gg (\gamma^2 v_{th})^{-3/2}$. At large values of $\gamma^2 v_{th}$, phase smearing should suffice to suppress - if not eliminate - the bunching instability at frequencies near the synchrotron peak. Moreover, if $\gamma^2 v_{th} \gtrsim \zeta^{-1}$, the instability should be suppressed over the entire range $m \gtrsim \zeta^{3/2}\gamma^3$ for which we found unstable modes in §5.4. Large $\Delta\tilde{\omega}_r/v_{th}$ would merely accentuate the smearing. At a given value of m, we see that $\Delta\tilde{\omega}_r \gtrsim (m^2 v_{th}^2)^{-1}$, i.e. $\gamma^2\Delta\tilde{\omega}_r \gtrsim (m/\gamma^3)^{-1}(\gamma^2 v_{th})^{-2}$ suffices for large phase decoherence in the layer.

5.8.3 The Limit $k_r\Delta r \ll 1$

In order to determine the lowest allowed value for k_r and the highest possible growth rate the full eigenvalue problem has to be solved. We estimate the result by evaluating Eq. (A.4) in the thin approximation again. Looking at Eq. (A.4) and replacing the Bessel functions by their Airy function approximations for the case $m \gg m_1$ and $m \ll m_2$ we see that the thin approximation is justified if $\bar{k}_r v_{th} \ll 1$ and $m^{2/3} v_{th} \ll 1$. It starts to fail completely if $m^{2/3} v_{th} \gtrsim 1$, i.e. once we start integrating over the oscillating and/or the exponentially damped/increasing part of the Airy function, which implies we would like to have $m^{2/3}|\Delta\tilde{\omega}| \ll \sqrt{F_0}$ with $|\Delta\tilde{\omega}|^2 \ll F_0 v_{th}^2$ from the previous paragraph. However, for real values of k_r we

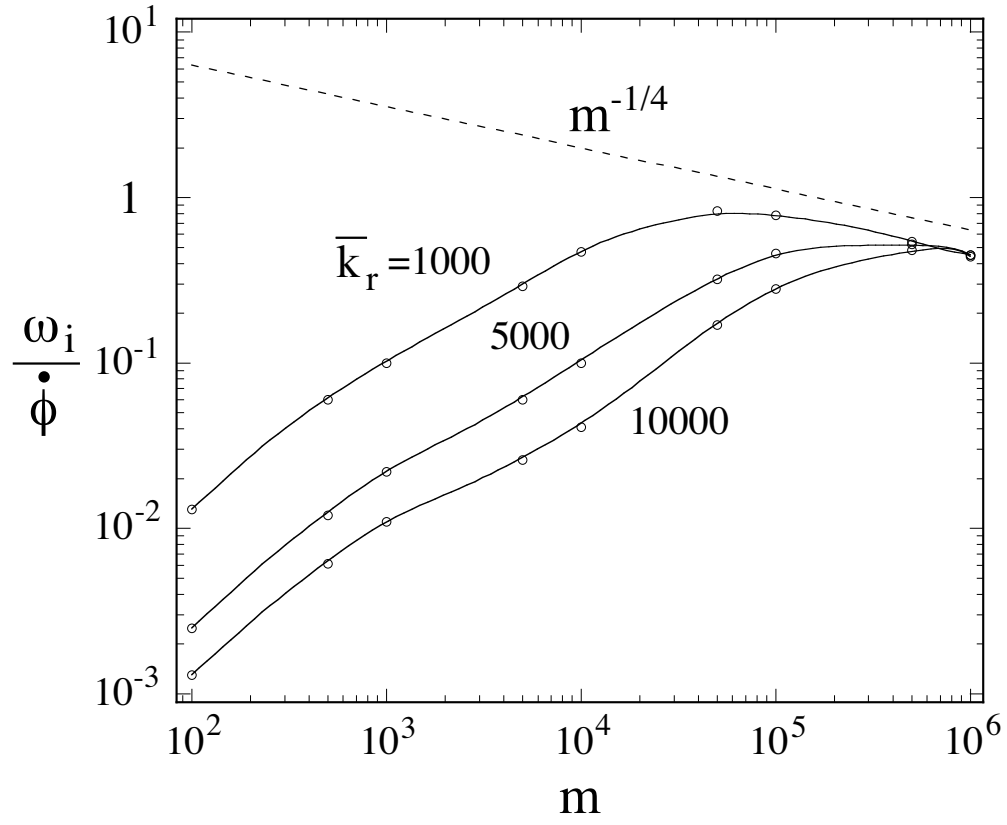

Figure 5.7: Growth rates in the limit $\bar{k}_r v_{th} \gg 1$ for our reference case $\gamma = 30$, $\zeta = 0.02$ and $v_{th} = 1/\gamma^2$ and various values of $\bar{k}_r$. The line proportional to $m^{-1/4}$ is shown for comparison.

expect that the thin approximation will still give us an upper bound of the growth rate because it is easier to maintain coherence if all the radiation is emitted from the same orbit. With Eq. (5.82) we obtain in the limit $\Delta\tilde{\omega} \ll \gamma^{-2}$

$$1 = -\pi\ \zeta\ Z\ \frac{F_0\gamma^{-2}}{(\Delta\tilde{\omega})^2}\ , \tag{5.97}$$

The growth rates can be found as before. For $m \gg m_1$ we obtain

$$\omega_i \simeq \frac{1.083\zeta^{1/2}m^{2/3}\dot{\phi}}{\gamma}\sqrt{F_0} \tag{5.98}$$

and

$$\omega_i \simeq \frac{\zeta^{1/2}m^{1/2}\dot{\phi}}{\gamma^{1/2}}\sqrt{F_0}$$

for $m \gg m_2$, i.e. there is an additional factor of $\sqrt{F_0}$. The results for our reference case are plotted in Fig. 5.8 which were computed numerically. In Fig. 5.9 the function F_0 is plotted which we compare with the squared ratio of our new growth rates to the ones evaluated previously without betatron oscillations.

We could also study the effect of the non-zero thickness alone without betatron oscillations setting $F_0 = 1$ and $F_{n\neq 0} = 0$ and solving the full eigenvalue problem. Due to the complicated nature of the dispersion relation we have not done this yet. Note that the thin approximation will suppress certain modes, e.g. the negative mass instability cannot be expected to be present with the fields having been evaluated at one radius only, cf. [6].

5.9 Spectrum of Coherent Radiation

Having computed the growth rate and the saturation amplitude, the radiated power can now be calculated. Starting from Eq. (A.10) we now have

$$P_m = \frac{\pi}{2}L\omega r_0^4\ \left|\delta J_{\phi 0}\right|^2 \left|\int \xi d\xi e^{i\bar{k}_r\xi}J_m'(\omega r_0\xi)\right|^2\ , \tag{5.99}$$

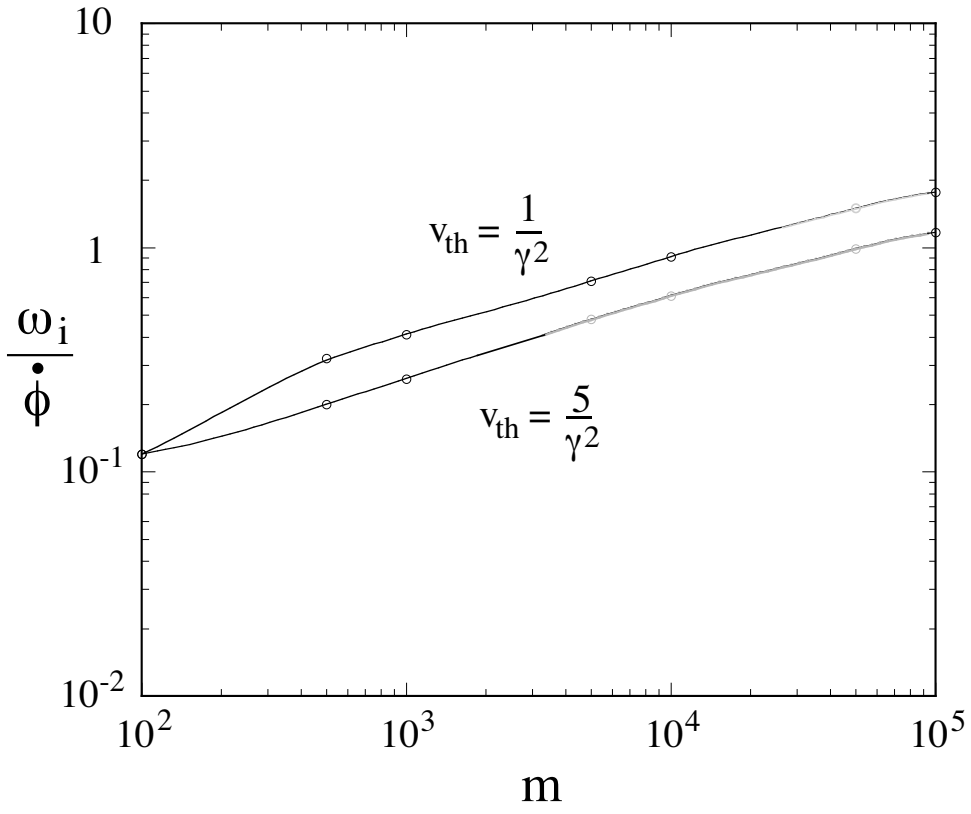

Figure 5.8: Solutions of the dispersion relation in the presence of betatron oscillations in the limit $\bar{k}_r v_{th} \ll 1$, $\gamma = 30$, $\zeta = 0.02$. Points which do not satisfy the inequalities $m \gg 1$, $m^{2/3} v_{th} < 1$ and $|\Delta\tilde{\omega}|^2 < F_0 v_{th}^2$ are plotted in gray.

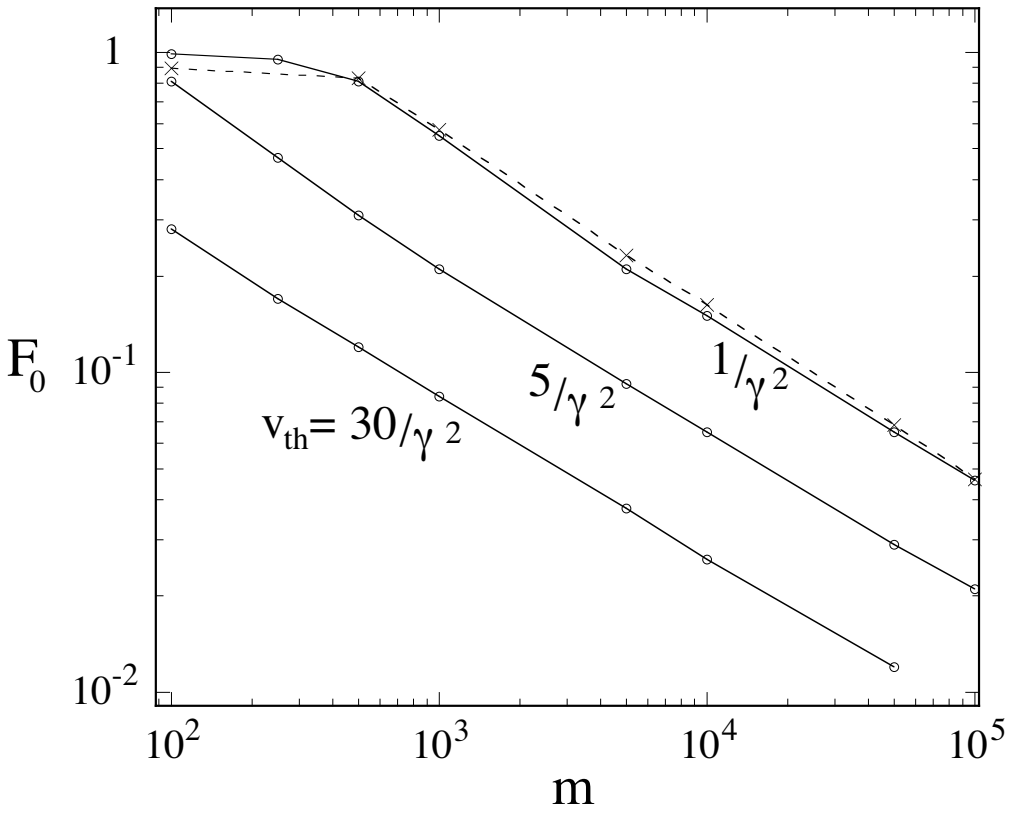

Figure 5.9: F_0 as a function of m for various values of v_{th} and the squared ratio of the growth rates from Fig. 5.3 and Fig. 5.8 (dashed line)

where $\xi \equiv r/r_0$ and the integration is over the thickness of the layer. The Bessel function can be expressed approximately in term of an Airy function as done before. We take the linear approximation to the Airy function as discussed previously, and this gives

$$P_m = \frac{\pi L \omega}{2} r_0^4 c_2^2 \left(\frac{2}{m}\right)^{4/3} \left|\delta J_{\phi 0}\right|^2 \left| \int_{1-v_{th}}^{1+v_{th}} \xi d\xi e^{i\bar{k}_r \xi} \right|^2 , \tag{5.100}$$

where $c_2 \approx 0.259$. This is valid for sufficiently big values of γ and low m. The largest values occur for $\bar{k}_r v_{th} \ll 1$, where this quantity is simply $4v_{th}^2$. This is enough motivation for us to work in this limit. Thus,

$$P_m \leq 2\pi L \omega r_0^4 c_2^2 v_{th}^2 \left|\delta J_{\phi 0}\right|^2 \left(\frac{2}{m}\right)^{4/3} . \tag{5.101}$$

Because we calculated our growth rates in the thin approximation for $k \approx k_\phi$ it is consistent to use $\delta\phi = 4\pi^2 v_{th} v_\phi^{-1} Z r_0 \delta J_{\phi 0}$. Furthermore, we set $\omega \to m\dot{\phi}$. This is consistent even for large growth rates since the exponential growth has stopped. With our expression for the saturation amplitude we obtain

$$P_m \leq \frac{L c_2^2 v_\phi^2 m_e^2}{8\pi^3 r_0 e^2} \frac{\gamma^6}{|Z|^2} \left(\frac{2}{m}\right)^{4/3} \frac{1}{m^3} \left(\frac{\omega_i(m)}{\dot{\phi}}\right)^4 . \tag{5.102}$$

Since the number of particles N is proportional to ζ and the growth rates are proportional to $\sqrt{\zeta}$ for $m > m_1$ the radiated power scales like N^2. This suggests that the emitted radiation is coherent. In Fig. 5.10 we plotted the radiated power in arbitrary units having evaluated F_0 numerically. For large m the curve scales as $m^{-5/3}$. Analytically we obtain with our second approximation for F_0 the scaling $m^{-3}(m^{2/3}/m^{1/4})^4 = m^{-4/3}$. With $|Z|^2 \approx 4c_1^4 (2/m)^{4/3}$ we obtain

$$P_m \lesssim 3.71 \times 10^{14} \gamma^6 m^{-3} \frac{L}{r_0} \left(\frac{\omega_i}{\dot{\phi}}\right)^4 \frac{\text{erg}}{\text{s}} . \tag{5.103}$$

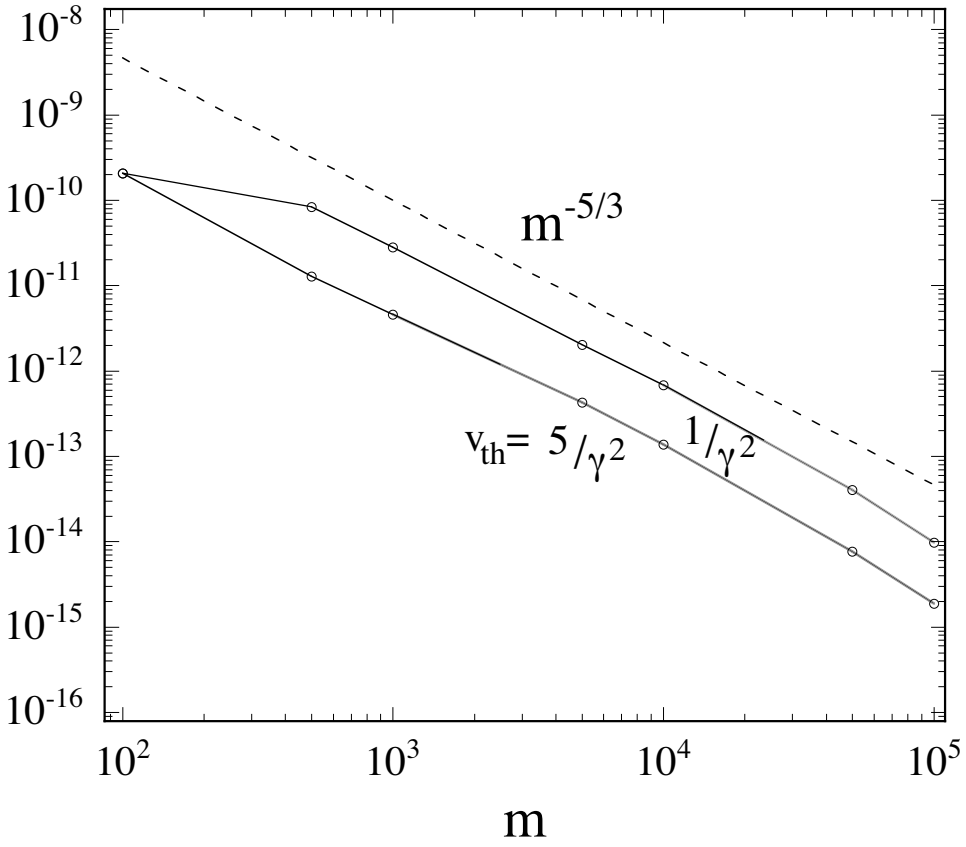

Figure 5.10: Radiated power $(m^{-3}(\omega_i/\dot{\phi})^4)$ for $\gamma = 30$ and $\zeta = 0.02$ in arbitrary units. The straight line is proportional to $m^{-5/3}$ and is shown for comparison. Points which do not satisfy the inequalities $m \gg 1$, $m^{2/3}v_{th} < 1$ and $|\Delta\tilde{\omega}|^2 < F_0 v_{th}^2$ are plotted in gray.

5.10 Brightness Temperatures

We consider the brightness temperatures T_B for conditions relevant to the radio emissions of pulsars. Using the Rayleigh-Jeans formula $B_\nu = 2k_B T_B(\nu/c)^2$ for the radiated power per unit area per sterradian at a frequency $\nu = m\dot{\phi}/2\pi$ gives

$$2k_B T_B(\nu/c)^2 \mathcal{A}\Delta\Omega = 2\pi P_m/\dot{\phi}$$
$$T_B \lesssim 4.5 \times 10^{21} \frac{\mathrm{K}}{\mathrm{m}} \cdot L\gamma^6 m^{-4} \left(\frac{\omega_i}{\dot{\phi}}\right)^4 \tag{5.104}$$

where k_B is Boltzmann's constant and $\mathcal{A} = 2\pi r_0 L$ is the area of the E-layer. The solid angle of the source seen by a distant observer has been computed in appendix A and its value is $\Delta\Omega = 4\pi^2 r_0/(mL)$. It is assumed that the angular size of the source is small such that that radiation from the top and the bottom emitted at an angle θ with respect to the normal is received by the observer at the same position. For the sample values $\gamma = 1000$, $\zeta = 0.08$, $v_{th} = 0.04\gamma^{-2}$, $L = 100$ km and $m = m_1$ our model predicts a maximum brightness temperature of $T_B \approx 2 \times 10^{20}$K. According to our results from previous sections there may be degeneracy from modes with non-zero axial wavenumbers k_z. It is reasonable to assume that this will increase the brightness temperature by a factor in the order of $m \tan\psi_{cr}$. Beaming along the z-axis may increase the brightness temperature and the observed frequency even further.

5.11 Applications in Accelerator Physics

The next-generation linear collider requires a beam with very short bunches and low emittance. That is, the beam must occupy a very small volume in phase space. The emittance of the pre-accelerated beam is reduced in a damping ring which is operated with longer bunches to avoid certain instabilities. The bunch length has

to be decreased in a so-called bunch compressor before the beam can be injected into the linear collider. A bunch compressor consists of an accelerating part and an arc section. Since the bunch lengths of the proposed linear colliders are in the order of the wavelength of the synchrotron radiation which is being radiated in the arc section, instabilities due to coherent synchrotron have to be taken seriously. For a design energy of 2 GeV and 7×10^{11} electrons per 100 μm our dimensionless quantities become $\gamma = 4000$ and $\zeta = 0.08$ [70]. Our qualitative analysis of the betatron motion suggests that CSR is suppressed for a minimum energy spread of $v_{th} > \zeta^{-1}\gamma^{-2} = 12.5\gamma^{-2}$.

5.12 Discussion and Conclusions

This work has studied the stability of a collisionless, relativistic, finite-strength, cylindrical electron (or positron) layer by solving the Vlasov and Maxwell equations. This system is of interest to understanding the high brightness temperature coherent synchrotron radio emission of pulsars and the coherent synchrotron radiation observed in particle accelerators. The considered equilibrium layers have a finite 'temperature' and therefore a finite radial thickness. The electrons are considered to move either almost perpendicular to a uniform external magnetic field or almost parallel to an external toroidal magnetic field. A short wavelength instability is found which causes an exponential growth an initial perturbation of the charge and current densities. The periodicity of these enhancements can lead to coherent emission of synchrotron radiation. Neglecting betatron oscillations we obtain an expression for the growth rate which is similar to the one found by Goldreich and Keeley [20] if the thermal energy spread is sufficiently small. The growth rate increases monotonically approximately as $m^{1/2}$, where m is the

azimuthal mode number which is proportional to the frequency of the radiation. With the radial betatron oscillations included, the growth rate varies as $m^{1/3}$ over a significant range before it begins to decrease.

We argue that the growth of the unstable perturbation saturates when the trapping frequency of electrons in the wave becomes comparable to the growth rate. Owing to this saturation we can predict the radiation spectrum for a given set of parameters. For the realistic case including radial betatron oscillations we find a radiation spectrum proportional to $m^{-5/3}$. This result is in rough agreement with observations of radio pulsars [54, 28] (Fig. 3.2). The power is also proportional to the square of the number of particles which indicates that the radiation is coherent. Numerical simulations of electron rings based on the fully relativistic, electromagnetic particle-in-cell code OOPIC [71] recovers the main scalings found here.

Chapter 6

Particle in Cell Simulations[†]

6.1 Introduction

Attempts to extract the nonlinear evolution of a plasma are usually unsuccessful except in some very special cases and numerical methods have to be applied. Seeking a straightforward numerical solution of the Vlasov equation however is prohibitive except in lower dimensional models [3] because the dimensionality of the problem is doubled in a framework which makes use of phase space. A possible solution to this problem is MHD which condenses the full momentum space distribution to only a few macroscopic quantities like density and current. Numerical MHD is extremely popular and a vast amount of literature exists on this topic. Despite its popularity MHD has some shortcomings. First, the results are only as good as the used closing condition. Second, some important effects like Landau damping rely on the knowledge of the momentum distribution. Landau damping [72] is a stabilization mechanism which is crucial for the generation of stable beams in particle accelerators. Therefore, MHD is of limited use in particle accelerator physics. Particle tracking programs avoid both problems. The grid can be set up in position space and position and momentum can be stored for each particle. On contemporary computers this is efficient even for a large number of particles. Not working in the limit $N \longrightarrow \infty$ anymore the effect of changing the number of particles being tracked needs to be investigated. Even though the number of particles in a plasma is finite it is usually not possible to track that

[†]This chapter will appear as a journal article [71]. Reprinted in modified form with kind permission from the American Physical Society.

many and one resorts to tracking N_{mac} "macroparticles" with each macroparticle representing N/N_{mac} particles. One can only hope that the results obtained with N_{mac} macroparticles are sufficiently close to convergence, i.e. $N \longrightarrow \infty$, giving a reasonably good estimate of the behavior of the real system.

The objective in this chapter is to simulate the evolution of a particle distribution which resembles configuration a in chapter 5.

6.2 Particle-in-Cell Simulations with OOPIC

For the simulation the software package OOPIC [73] was used. OOPIC is a relativistic two-dimensional particle-in-cell code which supports both plain (x, y)-geometries and cylindrical (r, z)-geometries. Since the interesting dynamics takes places in the azimuthal direction one can only simulate a thin ring (instead of a cylinder) in the (x, y)-mode. Loading the initial circular particle distribution in the (x, y)-mode required modifying the source code (files load.cpp, diagn.cpp and c_utils.c) to allow the program to handle circular particle distributions. Some minor modifications were necessary in order to compile XOOPIC-2.5.1 with gcc 3.2.2 and the compiler compiler bison 1.28 under SunOS 5.9. The built-in function parser was extended to support elliptic integrals.

Since a thin ring of particles is simulated instead of a cylinder thereof all fields and charges were divided by the length L of the cylinder whereas the electron mass needs to be divided by L^2. $L = 10r_0$ is chosen unless noted otherwise. The electric and magnetic self-fields for a thin ring equilibrium differ from what was used in the model. The fields can be found in [74]. It is ensured that OOPIC uses these self-fields before the perturbation starts to build up. As it turns out choosing the correct self-fields is not too crucial. Leaving them out the system will build

them up itself. Once the self-fields are created the system shows no difference in behavior. The absence of the self-fields in the dispersion relation might help to understand this feature. As in [51] a Gaussian number density profile with RMS width v_{th} was chosen for the initial distribution. 5000 macro particles were tracked on a grid with resolution 512×512 unless noted otherwise. Once an energy for a particle has been chosen it is placed at the equilibrium radius $r_0 = m\gamma c(eB)^{-1}$, i.e. neglecting betatron oscillations particles on the same orbit have the same energy. This fixes the azimuthal component of the canonical angular momentum. The system can pick up transverse motion quickly. The grid represents a rectangular region 40m $\times$ 40m big where the ring with radius $r_0 = 10$m is centered.

In Fig. 6.1 the initial particle distribution (gray) and the particle distribution after $23ns$ are shown. The parameters are $\zeta = 0.010$, $\gamma = 30$, and $v_{th} = 0.002$. Qualitatively, a bunching of the particle distribution can be observed. An enlargement of a small section of Fig. 6.1 is also shown in the same figure. In Fig. 6.2, the bunching is shown for successively higher energy spreads. With increasing energy spread the bunches become fuzzier and the clean gaps between bunches that can be observed for small energy spreads are populated with "stray particles". This suggests that it may be harder to achieve complete coherence for larger values of v_{th}. The decoherence due to the non-zero width of the particle beam is investigated quantitatively later in the paper. These qualitative features are independent of γ.

Also note that during the evolution of the circular charge distribution both the radius and the width of the ring increase slightly. The former is due to a.) particles losing energy and b.) the perturbed magnetic field changing significantly. It tends to decrease for small energy spreads and increase for larger energy spreads. Starting with a larger radius the radius increases even further, i.e. this is not a relaxation

from a "false" to a true equilibrium. Since the non-zero mesh size imposes an upper limit on the azimuthal mode number m which can become unstable, it is expected that the distance between bunches decreases as the resolution increases. This is indeed the case. For larger energy spreads the bunching of the distribution becomes hardly visible, but it still can be observed in the z-component of the magnetic field (Fig. 6.5).

The bunches are slightly tilted and may be connected by a very thin inner ring of particles for sufficiently high beam currents. For these reasons it is not possible to Fourier transform the charge perturbations in order to compute the growth rates for each value of m. Since the resolutions used were low the range of m values is restricted. Therefore, only the radiated power is computed which can be obtained easily.

Estimates of the growth rate are two orders of magnitude higher than what would be expected. A possible explanation is that the ratio between the saturation amplitude and the electric self field

$$\left|\frac{\delta E_{sat}}{E_{self}}\right| = \frac{1}{m\zeta}\left(\frac{\Im(\omega)(m)}{\dot{\phi}}\right)^2 \tag{6.1}$$

is typically in the order of 10^{-3} for the given sample cases which is rather small. The initial perturbations due to discreteness, numerical noise etc. are usually in the same order of magnitude. Therefore, one cannot expect to see the regime covered by the linearized Vlasov equation. This is another reason for focusing entirely on the emitted power.

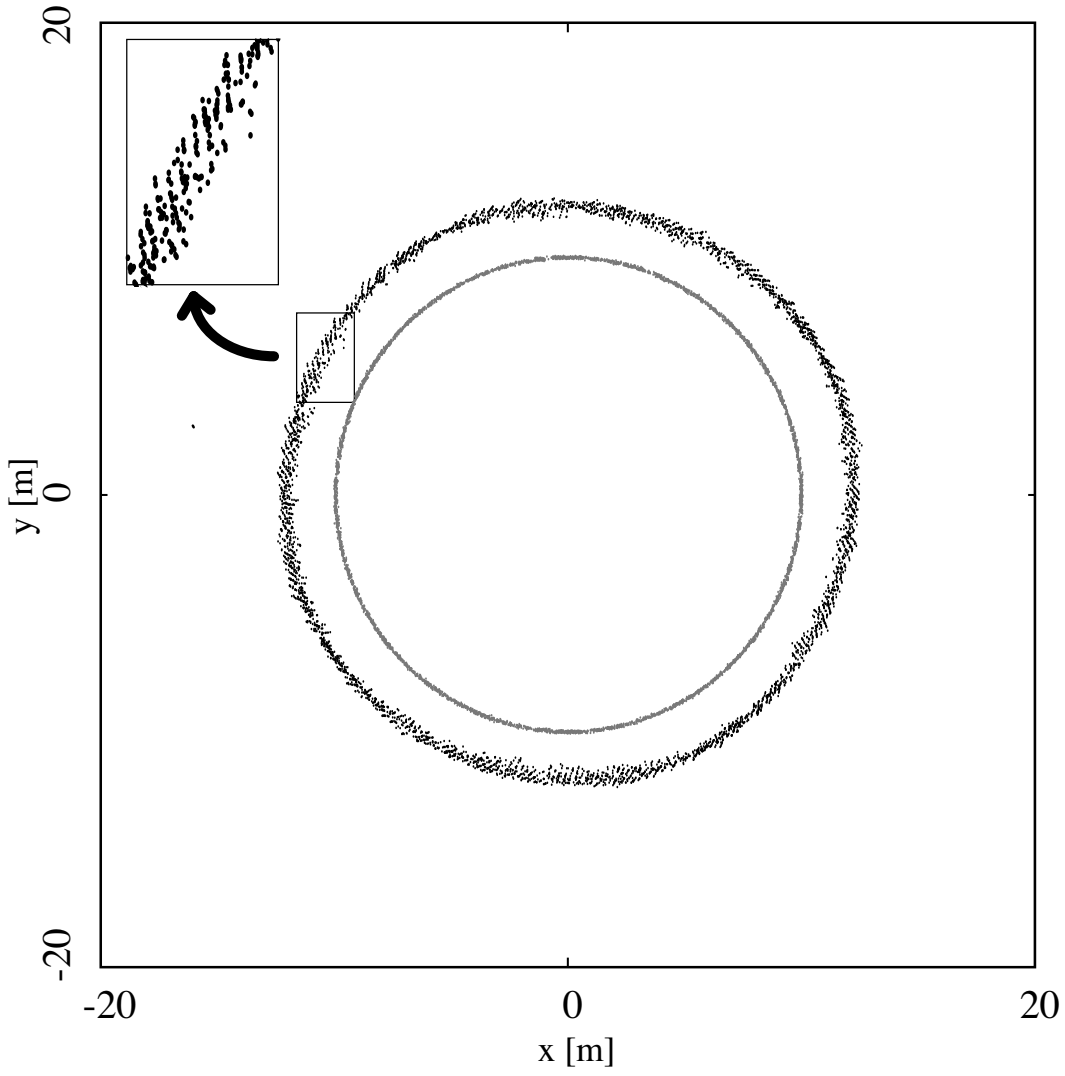

Figure 6.1: Initial particle distribution (gray) and the same distribution after 23ns have elapsed. Parameters: $\zeta = 0.010$, $\gamma = 30$ and $v_{th} = 0.002$

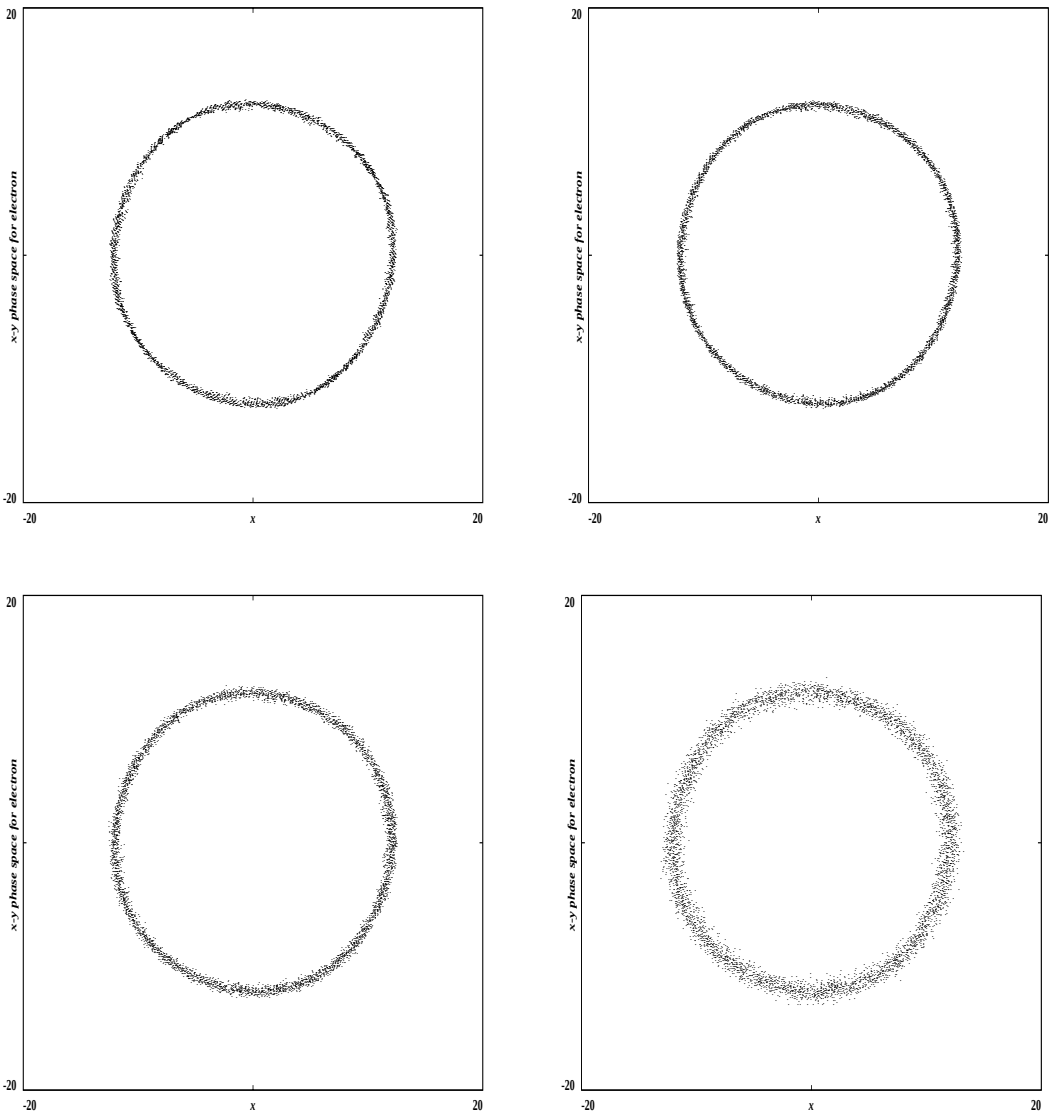

Figure 6.2: Particle distribution ($\gamma = 30$, $\zeta = 0.01$) after 23ns for $v_{th} = 0.002$, $v_{th} = 0.008$, $v_{th} = 0.015$ and $v_{th} = 0.033$ (from left to right, top to bottom). All lengths are measured in units of meters.

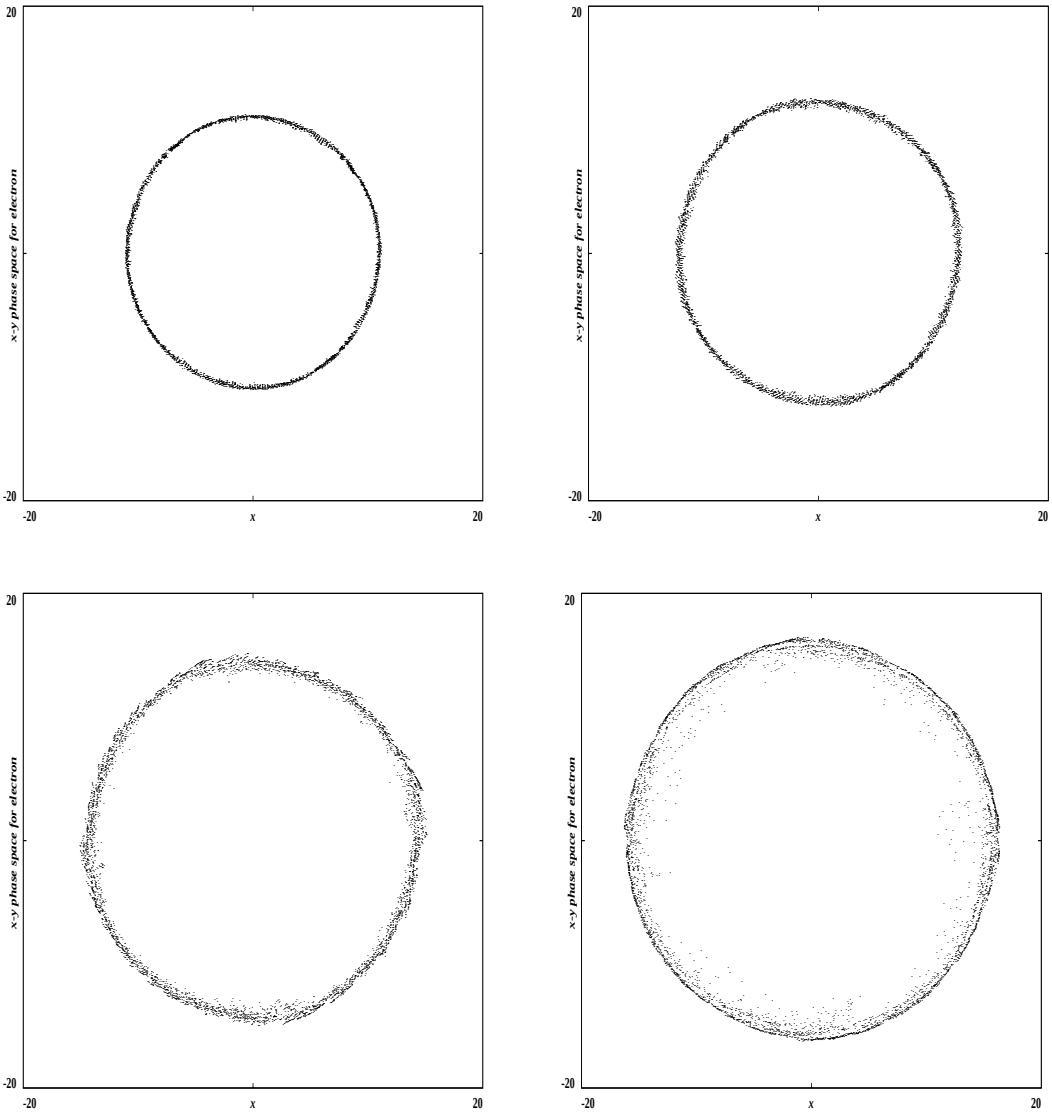

Figure 6.3: Particle distribution ($\gamma = 30$, $v_{th} = 0.002$) after 23ns for $\zeta = 0.005$, $\zeta = 0.010$, $\zeta = 0.020$ and $\zeta = 0.040$ (from left to right, top to bottom). All lengths are measured in units of meters.

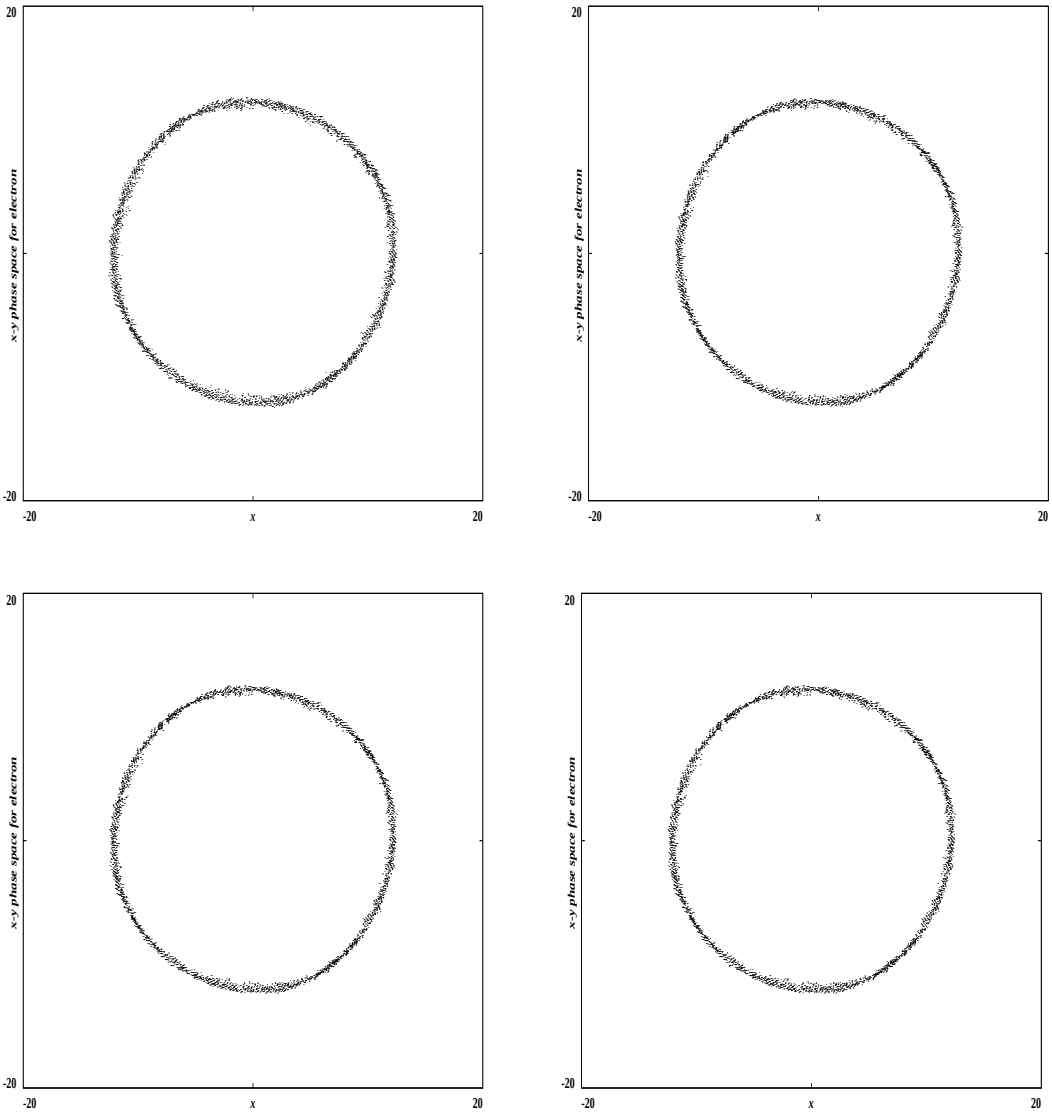

Figure 6.4: Particle distribution ($\zeta = 0.01$, $v_{th} = 0.002$) after 23ns for $\gamma = 10$, $\gamma = 30$, $\gamma = 75$ and $\gamma = 90$ (from left to right, top to bottom). All lengths are measured in units of meters.

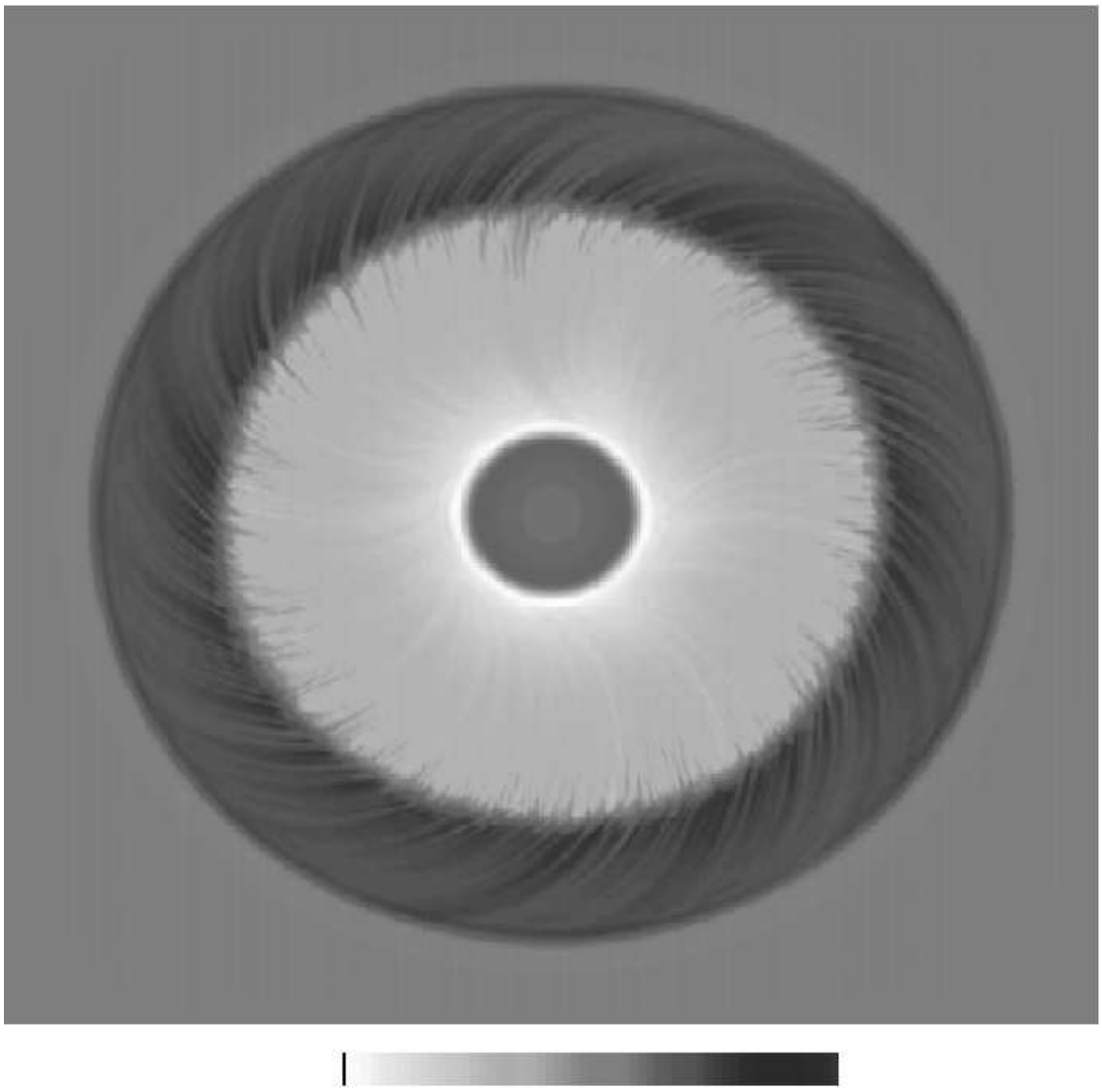

$-66.4\mu Tm^{-1}$ $158.0\mu Tm^{-1}$

Figure 6.5: z-component of the magnetic field (self-field plus perturbation without external magnetic field) after 23ns for $\zeta = 0.010$, $\gamma = 30$ and $v_{th} = 0.025$. The size of the area depicted is 40m $\times$ 40m.

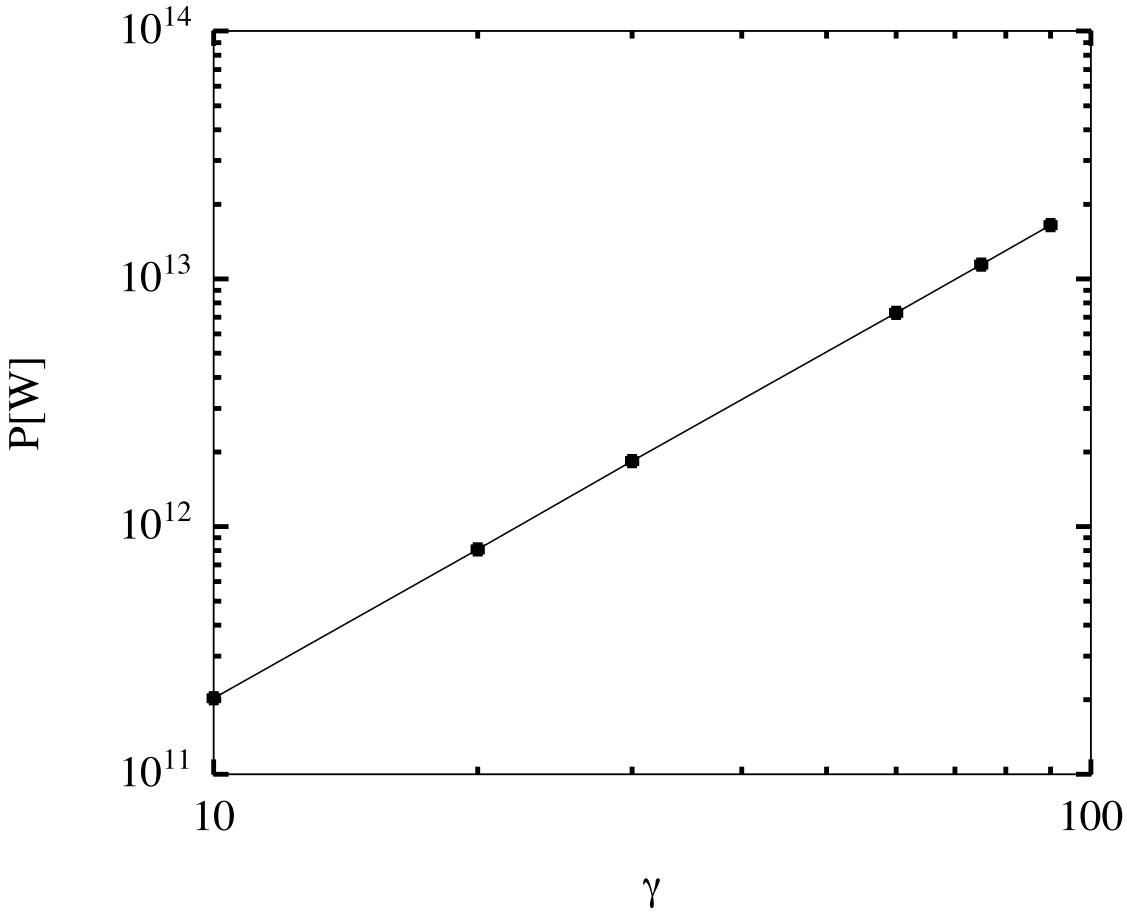

Figure 6.6: Loss of kinetic energy in W vs. γ for $\zeta = 0.01$ and $v_{th} = 0.002$.

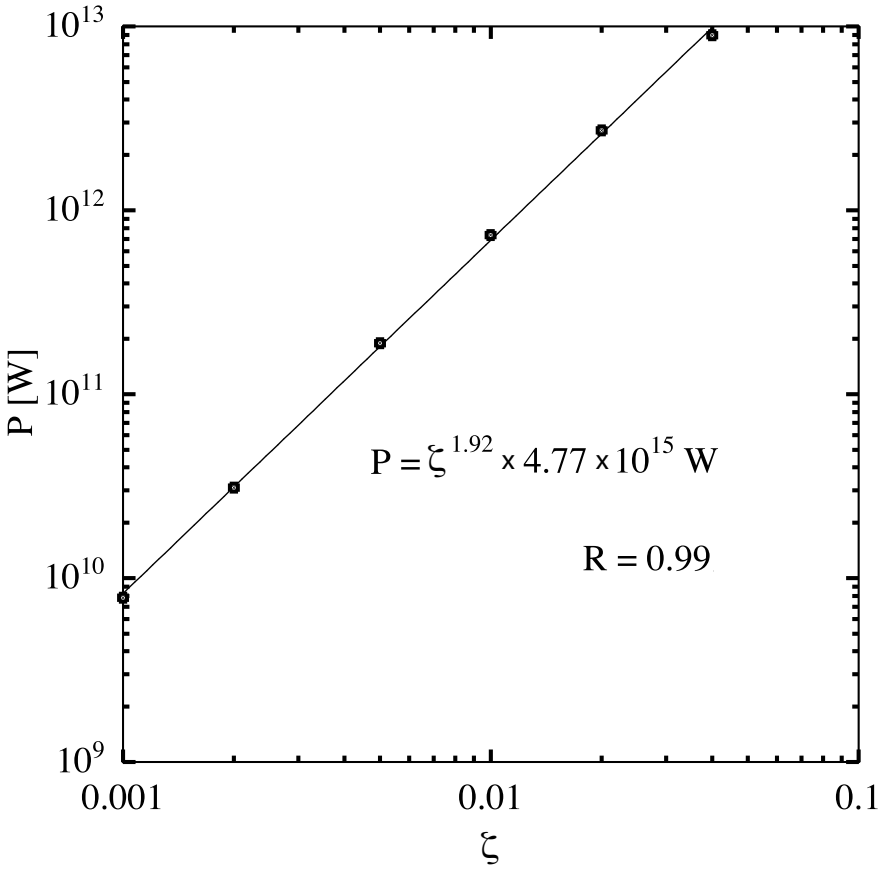

Figure 6.7: Loss of kinetic energy in W vs. ζ for $\gamma = 30$ and $v_{th} = 0.025$. The solid line shows the best fit.

6.3 Radiated Power

In Fig. 6.6 and Fig. 6.7 the radiated power determined by measuring the kinetic energy loss of the electron cloud after approximately 2.36 ns is plotted as a function of γ and ζ, respectively. After 0.24 ns the perturbations have saturated and the emitted power is fairly constant. A quadratic dependence can be established, i.e. the first two relevant scalings expected from the analytical model are recovered.

The simulation has been repeated at lower (256×256) and higher (1024×1024) resolution. No significant effect could be observed. This is consistent with the model which predicts that most power is emitted by modes with low m. The resolution is not high enough to resolve the path length difference of orbits with different radii at these low values of v_{th}. Also, decreasing the stepsize dt to 2.5 ps and increasing the number of macro particles to 50000 has a negligible effect.

Finally, the effect of the energy spread is investigated. With increasing v_{th} the power decreases which is due to the decoherence described by the factor F_0 defined in Eq. (5.88). The results are plotted in Fig. 6.8 for the parameters $\zeta = 0.01$, $\gamma = 30$ and $\zeta = 0.005$, $\gamma = 10$, respectively, and $L = r_0$. In the former case m_1 is 27 and in the latter case it is 0.4. Eq. (5.103) becomes

$$P \approx 3.71 \times 10^{14} \frac{\text{erg}}{\text{s}} \frac{L}{r_0} \gamma^2 \sum_m m \left[i\pi J_m(\omega r_0) H_m(\omega r_0) \right]^2 \tag{6.2}$$

Despite m_1 being much larger than 1 for the first set of parameters the slopes in Fig. 6.8 match exactly only if the summation starts at $m = 1$. This suggests that modes with $m < m_1$ do radiate and can be described by the same dispersion relation. Since the power scales as $m^{-5/3}$ these modes may actually be very important for computing the total energy loss. Note that while the simulation suggests $P \propto L^2$ Eq. (5.103) (which was derived under the assumption $L \gtrsim r_0$)

gives $P \propto L$. A 2D simulation cannot explain how the radiation from different axial positions on the cylinder interacts. In the thin ring case doubling L doubles the number of particles N and therefore quadruples P. Fortunately, as can be seen in the derivation of Eq. (5.103) in [51] the ζ, v_{th} and γ dependent part of P is independent of L. In Fig. 6.8 the overall factor matches if $r_0 = 100L$ whereas the growth rate for a perturbation of a cylinder and a thin ring coincide for $r_0 = L$ [51]. Also note that Fig. 6.1 suggests $k_r v_{th} r_0 \sim 1$, whereas Eq. (5.98) was derived under the assumption $k_r v_{th} r_0 \ll 1$.

6.4 Conclusions

The particle in cell code OOPIC was used to simulate the evolution of density perturbations in a thin ring of charged particles which move in relativistic almost circular motion in an external magnetic field. The results were compared with the model in [51]. Comparisons of the simulation with the model shows approximate agreement with the main predicted scaling relations. In particular the bunching effect could be observed very clearly and the emitted power is proportional to the square on the number density which implies coherent radiation. The dependence on the energy spread can be recovered exactly assuming all modes contribute to the observed energy loss suggesting that the model may apply even if $m < m_1$.

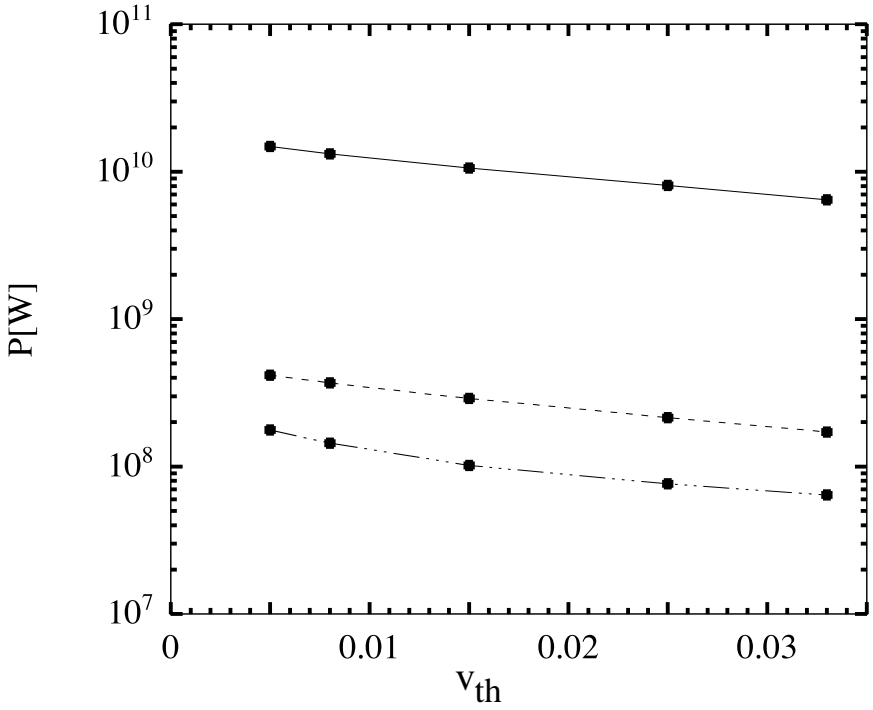

Figure 6.8: Total power radiated as obtained from OOPIC for the parameters $\zeta = 0.01$, $\gamma = 30$ (solid) and $\zeta = 0.005$, $\gamma = 10$ (dashed). The dash-dotted line is proportional to $\sum_{m=1}^{\infty} P_m$.

Chapter 7

MHD Approach for a Brillouin Flow

7.1 Theory

We consider a laminar Brillouin type equilibrium of a long, non-neutral, cylindrical relativistic electron (or positron) layer in a uniform external magnetic field $\mathbf{B}_e = B_e\hat{\mathbf{z}}$, where we use a non-rotating cylindrical (r, ϕ, z) coordinate system. The electron velocity is $\mathbf{v} = v_\phi(r)\hat{\boldsymbol{\phi}} = v(r)\hat{\boldsymbol{\phi}} = r\dot{\phi}(r)\hat{\boldsymbol{\phi}}$ The self-magnetic field is in the $z-$direction while the self-electric field is in the $r-$direction. The radial force balance of the equilibrium is

$$-\gamma\dot{\phi}^2 r = \frac{q}{m_e}(E + vB) \ , \tag{7.1}$$

where $\gamma = (1 - v^2)^{-1/2}$ is the Lorentz factor with velocities measured in units of the speed of light, $B = B_e + B_s$ is the total (self plus external) axial magnetic field, E is the total (= self) radial electric field, and q and m_e are the particle charge and rest mass. We have

$$\frac{1}{r}\frac{d(rE)}{dr} = 4\pi\rho_e \ , \quad \frac{dB}{dr} = -4\pi\rho_e v \ , \tag{7.2}$$

where $\rho_e(r)$ is the charge density of the electron layer.

We consider weak layers in the sense that the 'field reversal' parameter

$$\zeta \equiv -\frac{4\pi}{B_e}\int_{r_1}^{r_2} dr\rho_e v \tag{7.3}$$

is small compared with unity, $\zeta^2 \ll 1$. Under this condition Eq. (7.1) gives $\dot{\phi} = -qB_e/(m_e\gamma)$. Here, we have assumed that the layer exists between r_1 and r_2. We also consider that the Lorentz factor is appreciably larger than unity in the sense that $\gamma^2 \gg 1$.

We consider general electromagnetic perturbations of the electron layer with the perturbations proportional to

$$f_\alpha(r)\exp(im\phi - i\omega t)\ , \tag{7.4}$$

where $\alpha = 1, 2, ..$ for the different scalar quantities, $m =$ integer, and ω the angular frequency of the perturbation. Thus the perturbations give rise to field components δE_r, δE_ϕ, and δB_z. The perturbed equation of motion is

$$\left[\frac{\partial}{\partial t} + (\mathbf{v}+\delta\mathbf{v})\cdot\nabla\right]\left(\gamma\mathbf{v} + \mathbf{v}\delta\gamma + \gamma\delta\mathbf{v}\right)$$
$$= \frac{q}{m_e}\left(\delta\mathbf{E} + \mathbf{v}\times\delta\mathbf{B} + \delta\mathbf{v}\times\mathbf{B}\right)\ , \tag{7.5}$$

where the deltas indicate perturbation quantities. This equation can be simplified to give

$$\begin{bmatrix} -i\gamma\Delta\omega & -\gamma\dot\phi(1+\gamma^2) - \frac{q}{m_e}B \\ \gamma\dot\phi + (\gamma\dot\phi r)' + \frac{q}{m_e}B & -i\gamma^3\Delta\omega \end{bmatrix} \begin{bmatrix} \delta v_r \\ \delta v_\phi \end{bmatrix}$$

$$= \frac{q}{m_e}\begin{bmatrix} \delta E_r + v\delta B_z \\ \delta E_\phi \end{bmatrix}\ , \tag{7.6}$$

where the prime denotes a derivative with respect to r, and

$$\Delta\omega(r) \equiv \omega - m\dot\phi(r)$$

is the Doppler shifted frequency seen by a particle rotating at $\dot\phi$,

Using the equilibrium equation (7.1) and the condition $\zeta^2 \ll 1$, the matrix in Eq. (7.6) is approximately

$$\mathcal{D} = \begin{bmatrix} -i\gamma\Delta\omega & -\gamma^3\dot\phi \\ \gamma^3(\dot\phi r)' & -i\gamma^3\Delta\omega \end{bmatrix}\ , \tag{7.7}$$

We have used the fact that $(\gamma\dot{\phi}r)' = \gamma^3(\dot{\phi}r)'$. For $\zeta^2 \ll 1$ we have $(\dot{\phi}r)' = \dot{\phi}/\gamma^2$ and $\dot{\phi}' = -v^2\dot{\phi}/r$. Consequently

$$\det(\mathcal{D}) = \gamma^4(\dot{\phi}^2 - \Delta\omega^2) \ . \tag{7.8}$$

Inverting Eq. (7.6) gives

$$\delta v_r = \frac{q\gamma^3}{m_e \det(\mathcal{D})}\Big[- i\Delta\omega(\delta E_r + v\delta B_z) + \dot{\phi}\delta E_\phi\Big] \ , \tag{7.9}$$

and

$$\delta v_\phi = \frac{q\gamma^3}{m_e \det(\mathcal{D})}\Big[- i\Delta\omega\delta E_\phi - \dot{\phi}(\delta E_r + v\delta B_z)/\gamma^2\Big] \ , \tag{7.10}$$

7.2 Field Sources

The source terms due to the perturbation are

$$\delta J_r = \rho_e \delta v_r \ , \quad \text{and} \quad \delta J_\phi = \rho_e \delta v_\phi + \delta\rho_e v \ , \tag{7.11}$$

and from the continuity equation,

$$\delta\rho_e = \frac{1}{i\Delta\omega}\big[D_r(\rho_e\delta v_r) + ik_\phi\rho_e\delta v_\phi\big] \ , \tag{7.12}$$

where $D_r \equiv (1/r)[\partial/\partial r(r...)]$ and $k_\phi \equiv m/r$ is the azimuthal wavenumber. Expanding this equation gives

$$\delta\rho_e = \frac{1}{i\Delta\omega}\Bigg\{\frac{d\mathcal{F}}{dr}\delta E_\phi + \mathcal{F}\big[- ik_\phi(\delta E_r + v\delta B_z) + D_r(\delta E_\phi)\big]$$

$$-i\Delta\omega\Big[D_r\big[(\delta E_r + v\delta B_z)\mathcal{F}/\dot{\phi}\big] + ik_\phi\delta E_\phi\mathcal{F}/\dot{\phi}\Big]\Bigg\} \ . \tag{7.13}$$

Here,

$$\mathcal{F} \equiv \frac{q\rho_e\dot{\phi}\gamma^3}{m_e\det(\mathcal{D})} \ , \tag{7.14}$$

has the role of the distribution function of angular momentum [75].

7.3 The Limit $\Delta\omega \ll \gamma^{-1}\dot{\phi}$

For

$$\left|\frac{\Delta\omega}{\dot{\phi}}\right|^2 \ll 1 \tag{7.15}$$

the resonant term in $\delta\rho_e$ proportional to $1/\Delta\omega$ is dominant.

Thus we have

$$\delta J_r = \rho_e \delta v_r = \mathcal{F}\delta E_\phi + \mathcal{O}\left(\frac{\Delta\omega}{\dot{\phi}}\right) ,$$

$$\rho_e \delta v_\phi = -\frac{\mathcal{F}}{\gamma^2}(\delta E_r + v\delta B_z) + \mathcal{O}\left(\frac{\Delta\omega}{\dot{\phi}}\right) ,$$

$$\delta\rho_e v = \frac{r\dot{\phi}}{i\Delta\omega}\left[\frac{d\mathcal{F}}{dr}\delta E_\phi + ..\right] + \mathcal{O}\left(\left|\frac{\Delta\omega}{\dot{\phi}}\right|^0\right) ,$$

where the ellipsis indicates a term equal to the middle line of equation (7.13). To leading order in $|\dot{\phi}/\Delta\omega|$ we have

$$\begin{aligned} \delta J_r &= 0 , \\ \delta J_\phi &= \rho_e \delta v_\phi + \delta\rho_e v , \end{aligned}$$

or

$$\delta J_\phi = \frac{r\dot{\phi}}{i\Delta\omega}\left[\frac{d\mathcal{F}}{dr}\delta E_\phi + \mathcal{F}\big[-ik_\phi(\delta E_r + v\delta B_z) + D_r(\delta E_\phi)\big]\right]. \tag{7.16}$$

In this approximation we also have

$$\mathcal{F} = -\frac{\rho_e}{B} . \tag{7.17}$$

For an electron layer with $B_e > 0$, we have $\dot{\phi} > 0$ and $\mathcal{F} > 0$.

Thus,

$$\delta v_\phi = \frac{iq}{m_e\gamma\dot{\phi}}\left[-m\Delta\tilde{\omega} + \frac{1}{m\gamma^2\Delta\tilde{\omega}}\right]\delta E_\phi , \tag{7.18}$$

where $\Delta\tilde{\omega} \equiv \Delta\omega/(m\dot{\phi})$. Finally,

$$\delta v_\phi = \frac{iq}{m_e\gamma^3\Delta\omega}\delta E_\phi \tag{7.19}$$

The reason for the discrepancy from Eq. (5.40) is the difference in the used equilibrium. In chapter 5 the non-zero width was caused by betatron oscillations of particles with the same average angular velocity. In a Brillouin flow particles on different orbits have different angular velocities. This additional source of shear is reflected in the $(\gamma\dot{\phi}r)'$ term. Setting this term to zero one obtains the previous results from chapter 5 again (cf. Eq. (7.22)).

In the absence of radial currents the linearized continuity equation simply reads

$$\delta\rho = \frac{1}{\Delta\tilde{\omega}}\rho_0\delta v_\phi \tag{7.20}$$

Thus,

$$\delta\rho = \frac{-ie}{m_e\gamma^3 m\dot{\phi}}\frac{\rho_0}{(\Delta\tilde{\omega})^2}\delta E_\phi \tag{7.21}$$

7.4 The Limit $\Delta\omega \gg \dot{\phi}$

If we completly neglected radial motion as it was done in an earlier paragraph in chapter 5 Eq. (7.10) would read

$$\delta v_\phi = \frac{iq}{m_e\gamma\Delta\omega}\delta E_\phi \ . \tag{7.22}$$

In our two-dimensional MHD approach the motion is not constrained to a fixed radius and we are wondering under which conditions the radial motion in an unconstrained model can be neglected, i.e. when Eq. (7.22) and Eq. (7.10) coincide. $\delta v_r = 0$ implies that the forces due to δE_ϕ, δB_z and δE_r have to balance. Eq. (7.9) gives

$$\dot{\phi}\delta E_\phi = i\Delta\omega(\delta E_r + v\delta B_z) \tag{7.23}$$

Thus, Eq. (7.22) and Eq. (7.10) coincide if

$$\Delta\omega \gg \dot{\phi} \tag{7.24}$$

or if we choose an equilibrium distribution with zero average shear. In both cases the growth rates are given by Eq. (5.44).

7.5 Configuration b

In this section we are going to investigate the stability properties of an equilibrium with the same number density and velocity profile as before, but with different external fields. Instead of an external magnetic field in the z direction we consider an equilibrium with an azimuthal magnetic field acting as a guiding field and a radial electric field. The latter is included in the equilibrium condition and therefore does not enter the linearized Euler equation. B_ϕ^e would only enter if we considered motion in the axial direction and non-zero axial wavenumbers. Thus, we obtain the matrix $\mathcal{D}$ again without the B_0 terms, i.e. for $\gamma \gg 1$

$$\mathcal{D} = \begin{bmatrix} -i\gamma\Delta\omega & -\gamma^3\dot{\phi} \\ 2\gamma\dot{\phi} & -i\gamma^3\Delta\omega \end{bmatrix} , \tag{7.25}$$

with

$$\det(\mathcal{D}) = \gamma^4(2\dot{\phi}^2 - \Delta\omega^2) . \tag{7.26}$$

We obtain

$$\delta v_r = \frac{q\gamma^3}{m_e \det(\mathcal{D})}\Big[- i\Delta\omega(\delta E_r + v\delta B_z) + \dot{\phi}\delta E_\phi \Big] , \tag{7.27}$$

and

$$\delta v_\phi = \frac{q\gamma^3}{m_e \det(\mathcal{D})}\Big[- i\Delta\omega\delta E_\phi - 2\dot{\phi}(\delta E_r + v\delta B_z)/\gamma^2 \Big] , \tag{7.28}$$

In the limit $(\Delta\omega)^2 \gg 2\dot{\phi}^2$ the azimuthal current is given by Eq. (7.22) again and by Eq. (7.19) for $(\Delta\omega)^2 \ll 2\dot{\phi}^2$.

7.6 Two Cylinder Model

Instead of solving the full two-dimensional problem we solve it for two concentric cylinders, i.e. for the number density we have

$$n(r) = \frac{1}{2} n_0 \sqrt{2\pi} v_{th} r_0 \left(\delta(r - r_1) + \delta(r - r_2)\right) \tag{7.29}$$

Some interesting results can be obtained in that limit assuming zero average shear. The linearized continuity equation becomes

$$-i\omega\delta\rho + \frac{1}{r}\frac{\partial}{\partial r}\left(r\rho_0\delta v_r + r v_{0r}\delta\rho\right) + \frac{im}{r}\left(\rho_0\delta v_\phi + v_{0\phi}\delta\rho\right) = 0 \tag{7.30}$$

We drop all radial derivatives in the continuity equation which is consistent with our previous approximation. Thus,

$$\delta\rho = \frac{i}{2} e^2 n_0 \sqrt{2\pi} v_{th} r_0^2 \left(\delta(r - r_1) + \delta(r - r_2)\right) \frac{m^{-1}}{m_e \gamma} \frac{\delta E_\phi}{(\Delta\tilde{\omega})^2} \tag{7.31}$$

The Green function is

$$\delta\Phi(r_1) = 2\pi^2 i \left(r_1 J_m(\omega r_1) H_m^{(1)}(\omega r_1)\delta\rho_1 + r_2 J_m(\omega r_2) H_m^{(1)}(\omega r_1)\delta\rho_2\right) \tag{7.32}$$

$$\delta\Phi(r_2) = 2\pi^2 i \left(r_1 J_m(\omega r_2) H_m^{(1)}(\omega r_1)\delta\rho_1 + r_2 J_m(\omega r_2) H_m^{(1)}(\omega r_2)\delta\rho_2\right) \ , \tag{7.33}$$

so the problem can be written as a matrix

$$A \equiv -2\pi^2 i e^2 \frac{1}{2} n_0 \sqrt{2\pi} v_{th} r_0^2 \frac{1}{H} \gamma^{-2}$$
$$\cdot \begin{pmatrix} (\Delta\tilde{\omega}(r_1))^{-2} \frac{r_1}{r_0} J_m(\omega r_1) H_m(\omega r_1) & (\Delta\tilde{\omega}(r_2))^{-2} \frac{r_2}{r_0} J_m(\omega r_1) H_m(\omega r_2) \\ (\Delta\tilde{\omega}(r_1))^{-2} \frac{r_1}{r_0} J_m(\omega r_1) H_m(\omega r_2) & (\Delta\tilde{\omega}(r_2))^{-2} \frac{r_2}{r_0} J_m(\omega r_2) H_m(\omega r_2) \end{pmatrix} \tag{7.34}$$

acting on the column vector $(\delta\Phi(r_1)), \delta\Phi(r_2))^T$ which returns the same column vector. Nontrivial solutions can only exist if

$$\det(A - \mathbb{1}) = 0 \ . \tag{7.35}$$

Finally, this equation can be solved for $\Delta\tilde{\omega}$.

The coefficient in front of the matrix is equal to $-\frac{\pi}{2}i\zeta\gamma^{-2}$. We introduce the notation $\Delta\tilde{\omega} \equiv \Delta\tilde{\omega}(r_0)$, $\Delta\tilde{\omega}(r) = (1+\Delta\tilde{\omega})\frac{r}{r_0} - 1$ and solve the dispersion relation for $\Delta\tilde{\omega}$ approximating the Bessel functions by Airy functions

$$J_m(z) = \left(\frac{2}{m}\right)^{1/3} \mathrm{Ai}\left(-(2/m)^{1/3}(z-m)\right) \tag{7.36}$$

$$Y_m(z) = -\left(\frac{2}{m}\right)^{1/3} \mathrm{Bi}\left(-(2/m)^{1/3}(z-m)\right) \tag{7.37}$$

and neglecting terms proportional to $\Delta\tilde{\omega}$ which are assumed to be small compared with γ^{-2}. The growth rates for the parameters $\zeta = 0.02$, $\gamma = 30$, $m = 500$ are plotted in Fig. 7.1.

Numerically, we find that the drop occurs very roughly for $v_{th} = j\pi/m$ if j is an even integer, i.e. when the thickness of the layer is an integer multiple of 4 times the wavelength of the radiation. This periodicity is due to the Bessel functions. The drop in the growth rate is caused by the Coulomb term as can be seen by using the following approximation for the Airy functions

$$\mathrm{Ai}(w) \approx c_1 - c_2 w \tag{7.38}$$

$$\mathrm{Bi}(w) \approx \sqrt{3}[c_1 + c_2 w] \tag{7.39}$$

where $c_1 = 1/[3^{2/3}\Gamma(2/3)]$ and $c_2 = 1/[3^{1/3}\Gamma(1/3)]$ which is justified for $|w|^2 \lesssim 0.5$. This gives $Z_m(w) \equiv iJ_m(w)H_m(w) \approx (2/m)^{2/3}[\sqrt{3}(c_1^2 - c_2^2 w) + i(c_1 - c_2 w)^2]$. Evaluating the Green function at r_0 for $w = 0$ we just obtain the radiation term quoted by Goldreich and Keeley [20] and the two unstable modes shown in Fig. 7.1 become degenerate. Keeping the first order term in w we recover the Coulomb term as well. This approximation is valid in the shaded area of Fig. 7.1.

The dependence of the larger mode in Fig. 7.1 on v_{th} seems to be in rough agreement with the dependence obtained from including the decoherence due to